Effect of Carbodiimide Functionalization Chemistry on Alginate Structure and Hydrogel Properties

A thesis

submitted by

Mitchell Saeger

In partial fulfillment of the requirements

for the degree of

Master of Science

In

Chemical Engineering

Tufts University
May 2016

Committee Members:
Dr. Darryl Williams: Advisor
Dr. Ayşe Asatekin: Co-advisor
Dr. Catherine Kuo

Abstract

Designing scaffolds for regenerative tissue engineering relies upon creating a suitable microenvironment for directing biological responses. This work aims to further characterize functionalized alginate hydrogels designed to mimic the extracellular matrix. We investigated the effects of reactant concentrations, ligand loading density, and peptide spacer arm length on reaction efficiency, hydrogel mechanical properties, and gelation kinetics. Altering reactant concentrations had the greatest effect on both reaction yield and hydrogel performance. Low activation conditions resulted in over twice the yield relative to high activation chemistry while producing stiffer gels that possessed improved gelation kinetics. These results indicate that both the side reactions and structural modifications caused during functionalization affect hydrogel formation. This work provides deeper understanding into the interplay between alginate functionalization chemistry and hydrogel properties. These insights are important in creating 3D scaffolds that accurately mimic the desired microenvironments for supporting and directing key cellular processes.

Acknowledgements

I would like to thank Dr. David Wilbur from the Tufts University Department of Chemistry for his help with ^{1}H NMR, Dr. Benjamin Partlow for his help with designing mechanical property studies, and Dr. Hyunmin Yi from the Tufts University Department of Chemical and Biological Engineering for generously offering the use of his glove bag. Additional thanks goes to Jacob Gerace, Lily Corcoran, and Lindsey Jacobs for their help in synthesizing one of the conditions in this study as a part of their senior capstone project. I would also like to acknowledge the FRAC FRF award that funded this work.

I am grateful to my advisors and committee members for their mentorship and guidance throughout this work. I have learned much from your positive attitudes, multidisciplinary thinking, and critical mindsets. Finally, a special thank you to my family and friends for their support throughout this past year. I will forever be indebted to you all for the number of times that you have fed me.

Table of Contents

List of Figures

List of Tables

Effect of Carbodiimide Functionalization Chemistry on Alginate Structure and Hydrogel Properties

Chapter 1: Introduction

1.1 Overview

Effective tissue engineering strategies are based on proper interactions between a scaffold material and the human body. Scaffolds are responsible for generating a suitable microenvironment capable of directing cellular processes, such as adhesion, proliferation, migration, and differentiation [1,2]. Consequently, recent research has placed heavy focus on developing biomaterials that can mimic the microenvironments found within the extracellular matrices of native tissues [3]. Within the extracellular matrix, cells experience a complex barrage of soluble cues, such as growth factors, as well as insoluble cues, such as matrix stiffness [4]. These signals vary between organisms and specific tissue systems, and they continue to evolve throughout the aging process as they provide the context necessary to direct homeostatic cellular activity [5]. Therefore, having a well characterized system is paramount to properly engineering a synthetic extracellular matrix scaffolding material that is capable of supplying the proper cues, in the correct proportions and at the proper times, to engage cells in a specific and controlled manner.

Hydrogels are a popular scaffold of interest, as they are extremely hydrated three-dimensional environments composed of polymers that can be physically and chemically modified in order to be good representations of the natural extracellular matrices they are mimicking [6]. This creates the promise of designer

synthetic extracellular matrices that are synthesized in order to fit a niche purpose. Alginate is a naturally derived polymer from seaweed that has particular promise with respect to its biocompatibility, cost, and potential for material-tuning in terms of chemical modification and hydrogel mechanical properties [3].

Many of the studies that work with alginate characterize the biological response to a particular chemical modification without fully investigating the overarching material implications to that change. Yet to be able to further engineer biomaterials for targeted applications, we need a better understanding of the cause-and-effect relationships between the chemistry and properties of the material and how this influences the biological response. This is especially important as these two features are typically interdependent and hard to isolate. Yet many researchers in the field have not focused on the careful characterization of biomaterial chemistry, even after chemical modifications are introduced. This is highlighted by the fact that despite using similar carbodiimide chemistry for alginate functionalization, yields ranging from 2-90% have been reported in recent publications [7,8].

Therefore, this work proposes a more systematic characterization on how chemical modification of alginate with the cell-adhesion peptide G_nRGDSP affects alginate structure, mechanical properties, and gelation kinetics. The results from this study will aid in elucidating the interplay between structural changes due to carbodiimide chemistry and hydrogel performance. Ultimately, this has

implications on optimizing synthetic cellular microenvironments, which is a vital component in the design of biomaterials.

1.2 Background

1.2.1 Tissue Engineering

Introduction and Background

The field of tissue engineering is defined as a means to "*restore, maintain, or improve tissue functions that are defective or have been lost by different pathological conditions, either by developing biological substitutes or by reconstructing tissues* [9]." In order to achieve such paradigm-shifting advancements, tissue engineering is highly multi-disciplinary, serving as the intersection of chemistry, biology, materials science, medicine, and bioengineering [10]. Thus, the applications of tissue engineering are widespread, encompassing the full spectrum of organs found in the body and different treatment methodologies – ranging from 3D printing bionic ears to developing new materials that facilitate ligament healing [11,12]. Despite all of the complexities and differences among approaches, a few common themes emerge – particularly within the realm of biomaterials.

In particular, scaffold design has become a key field of interest, as the interface between a biomaterial and a living system is foundational to tissue engineering. For the majority of applications, a primary objective is to generate a material capable of replicating the extracellular matrix found in native tissue systems [13–15]. In order to accomplish this task, precise chemical and mechanical cues are necessary to promote cellular activity, and ultimately tissue regeneration, so they

are directly engineered into the material [10]. Numerous studies have demonstrated the importance of the local microenvironment for normal cell function, whether it be adhesion, migration, proliferation, or differentiation; therefore, developing a platform that can support the complexities found *in vivo* is not a trivial task [2,16]. Consequently, in the context of regenerative medicine, scaffolds are created around four primary design principles [17]. First, biomaterials must interact with cells in some capacity, stimulating cell adhesion and extracellular matrix (ECM) deposition. Second, scaffolds must facilitate proper nutrient and regulatory factor transport to ensure cell growth and survival. Third, the biomaterial degradation profile should approximate that of tissue regeneration in order to ensure proper support throughout the integration process. And fourth, the material must be biocompatible and not release toxic byproducts as it degrades.

Types of Scaffolds

In order to meet the aforementioned design criteria, a number of different polymer-based scaffolds have been developed and can be generally grouped into the following categories: porous scaffolds, hydrogels, fibrous scaffolds, microspheres, composite materials, and acellular scaffolds [9]. Each scaffold type possesses a unique set of advantages and disadvantages, which will be application specific. For example, porous scaffolds (e.g. foams and sponges) provide a significant porosity comparable to native ECM environments, yet they must develop a more interconnected structure to be suitable for applications, such as artificial blood vessel development [9]. With respect to fibrous scaffolds, such as

electrospun meshes, an ECM-like structure is capable of being fabricated on the micro- and nano-scale; but, due to high surface areas, it can be difficult to control mesh degradation properties [14].

Hydrogels, the primary focus of this work, consist of a crosslinked network of highly hydrophilic polymer chains that possess the ability to retain many times their dry weight in water content [13,18,19]. Below, Figure 1.1 shows the effect of hydration and dehydration on gel structure. Importantly, the hydrated gel network is comparable to that of the ECM. Therefore, hydrogels experience a unique advantage over alternative scaffold types, as cells can be added while the gel is still in its liquid state, they can often be gelled in mild, cell-compatible conditions, and they can be injected to gel *in situ* [20]. Additionally, many of the polymers used in hydrogels can be physically and chemically altered, creating a huge range of versatility with respect to the material's ability to crosslink, interact with cells, or degrade [21]. Additional molecules (e.g. cell signaling factors) can be engineered into hydrogels in order to generate a specific cellular response [18,22]. Ultimately, these tunable properties have dramatic implications on creating the proper cellular microenvironment for a desired application. For example, controlling scaffold stiffness has been shown to regulate stem cell differentiation, so by altering hydrogel crosslink density, the gel mechanical properties can be tuned accordingly [2,16,21]. Therefore, depending on the material used, these designer properties create a broad platform for functional application, ranging from soft contact lenses to drug delivery to regenerative tissue engineering [13].

Figure 1.1. Hydrogels can take many different sizes and shapes, adding to its diversity as a biomaterial. In the upper row, on the far left, a pre-gel powder is shown, followed by a hydrated powder before crosslinking. The middle image is a fully crosslinked hydrogel, while to its right is a dehydrated gel, showing that these gels often retain structural characteristics after drying. A mustard seed is shown to the far right for size comparison. On the bottom row, the effect of dehydration on hydrogel structure is shown from left to right [13].

Polymeric Materials

For a biomaterial, the intended application largely determines its desired material properties. It is difficult to find materials that have tunable mechanical properties that match that of native tissues while also remaining biocompatible and possessing a predictable degradation rate [22]. Due to their unique and often tailorable characteristics, polymers have become popular scaffold materials. Broadly, there are two primary types of polymers used: natural and synthetic, each with their own advantages and disadvantages.

A variety of natural polymers have been used to manufacture tissue engineering scaffolds, such as collagen, cellulose, hyaluronic acid, chitosan, and alginate [1,6,9,10,22]. A key advantage to these materials is their innate biocompatibility, as they naturally provide sites for cells to attach, proliferate, and differentiate while maintaining a low toxicity throughout degradation *in vivo* [6,23]. Yet due to their natural origins, these materials have a high degree of variability, which can be undesirable with respect to having a fully characterized system that performs in a reproducible manner [15,24]. Additionally, despite changing the degree of crosslinking, this class of polymers tends to have a relatively low elastic modulus, so depending on the tissue, it can be difficult to match native ECM stiffness [10,25].

On the other hand, synthetic polymeric materials are often more cost-effective, possess more reproducible properties, are capable of large-scale production, and can be designed to possess particular features, such as undergoing degradation at a particular pH [9,15]. A variety of synthetic polymers have been used, such as polyesters, polyurethanes, elastins, poly(ethylene oxide) and poly(ethylene glycol) for a diverse array of applications that include blood vessel regeneration and bone repair [10,18,22]. However, synthetic polymers often lack the cell-binding domains found in natural polymers. In order to circumvent this constraint, advances in synthesis techniques have allowed said sites to be engineered into the materials [26]. A greater concern is that some synthetic polymers (e.g. polyesters) degrade via a hydrolysis mechanism, resulting in acidic byproducts [10,22]. Additionally, many

synthetic polymers require harsh organic solvents during processing which severely limits the inclusion of cells or biological molecules [27].

Since it has proven to be difficult to generate materials that exhibit all of the desired characteristics for tissue engineering applications, researchers have begun to harness the advantageous properties of both natural and synthetic materials by creating composites and blends. For example, to maintain the bioactive domains found in natural polymers while benefitting from the cost effectiveness and reproducibility of synthetic polymers, some studies have blended naturally-derived molecules (e.g. collagens, silks) with synthetic polymers (e.g. elastin and poly(lactide-co-glycolide)) [22]. A similar strategy has also been explored for bone tissue engineering by combining synthetic and natural polymers with ceramics [28]. While studies have not necessarily found a universally "perfect" material, individual and composite material characterization studies have provided a wealth of knowledge with respect to the critical features of scaffold-cell interaction. This information enables researchers to select the optimal material, or material blend, for an intended application.

1.2.2 The Extracellular Matrix

Introduction and Background

The ECM consists of the secreted molecules present outside of cells within a tissue system [29]. The ECM was originally thought to be passive, providing merely structural support and a physical space for cells to grow, but research has

discovered it to be an incredibly dynamic environment that influences and drives many cellular processes [30–33]. Notably, it has been shown to regulate the growth factors and receptors available to cells, control hydration levels, and affect the local pH [30,33].

Additionally, the ECM is essential in imbuing tissues with their mechanical properties and providing cells with a medium to sense and respond to the mechanical loads they experience *in vivo* [34]. Furthermore, the ECM's stiffness has been shown to be a vital factor in controlling stem cell fate. For example, one study seeded human mesenchymal stem cells onto collagen-coated polyacrylamide gels of varying stiffness and found that soft gels (1 kPa) favored neuronal differentiation, mid-range matrix elasticity (10 kPa) favored the myoblast lineage, while rigid gels (100 kPa) encouraged the osteogenic phenotype [16]. This phenomenon has encouraged tissue engineering pursuits to become more holistic in their approaches, as cells depend on more than just the chemistry of the molecules present on a scaffold. A summary of different tissue elastic moduli is shown below in Figure 1.2. Ultimately, the ECM possesses a diverse portfolio of functions that create the complex microenvironment in which cells grow and respond to stimuli, and this has dramatic effects on regulating cell adhesion, migration, proliferation, apoptosis, and differentiation [31,32].

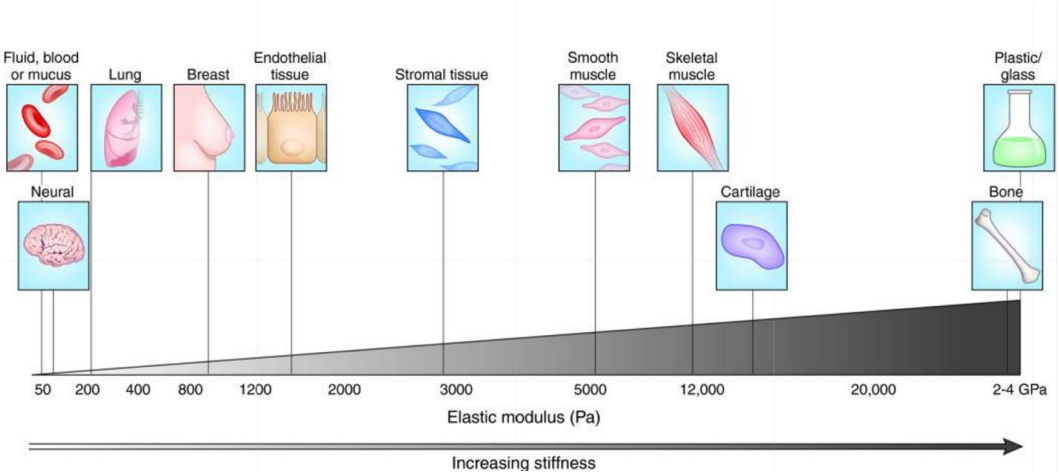

Figure 1.2. Matrix stiffness of different tissues varies over orders of magnitude, highlighting the need for biomaterials that can match the innate mechanical properties of the system of interest [35].

The ECM is established by cells during development and is continuously remodeled in order to adapt to aging, differences in tissues, disease, and mechanical forces in an attempt to maintain homeostasis [30–32]. Complex feedback mechanisms provide the means for cells to maintain a homeostatic environment, yet when these measures break down, pathology and disease result. For instance, with respect to mechanobiology, increases in matrix stiffness should trigger a negative feedback mechanism causing the matrix to become softer, yet if it results in further matrix stiffening, the result is fibrosis [31]. Therefore, the cell-ECM relationship is reciprocal, as cells establish and remodel the ECM while the ECM influences cellular function.

Structure and Function

The mammalian ECM is composed of over 300 proteins, 200 glycoproteins, and 30 proteoglycans, and it is this diverse array of molecules, and the resultant unique tissue architectures, that are able to create the incredible ECM tissue specificity seen *in vivo* [30,32,36]. Figure 1.3 shows a cartoon version of the ECM, highlighting its complex nature. Despite such a wide breadth of molecules, the majority of the ECM's mechanical properties come from 3 sources: fibrillar collagens, elastic fibers, and glycosaminoglycans (GAGs) [31].

The major component of most extracellular matrices is collagen and an incredible amount of variety exists within the different collagen proteins, 28 distinct forms of which have been discovered [37]. Structurally, collagen is a right-handed triple helix composed of either homo- or heterotrimers, and it is this specific structure that endows collagen with such unique mechanical properties. This is essential for matrix integrity, as collagen is responsible for setting matrix stiffness and strength [37,38]. Collagen fibril assembly is defined by four key, cell-mediated stages, and this generates a hierarchical structure that possesses the necessary binding sites for interacting with cells and other ECM molecules [33]. These interactions between ECM components are essential in the creation of proper microenvironments within a specific tissue system.

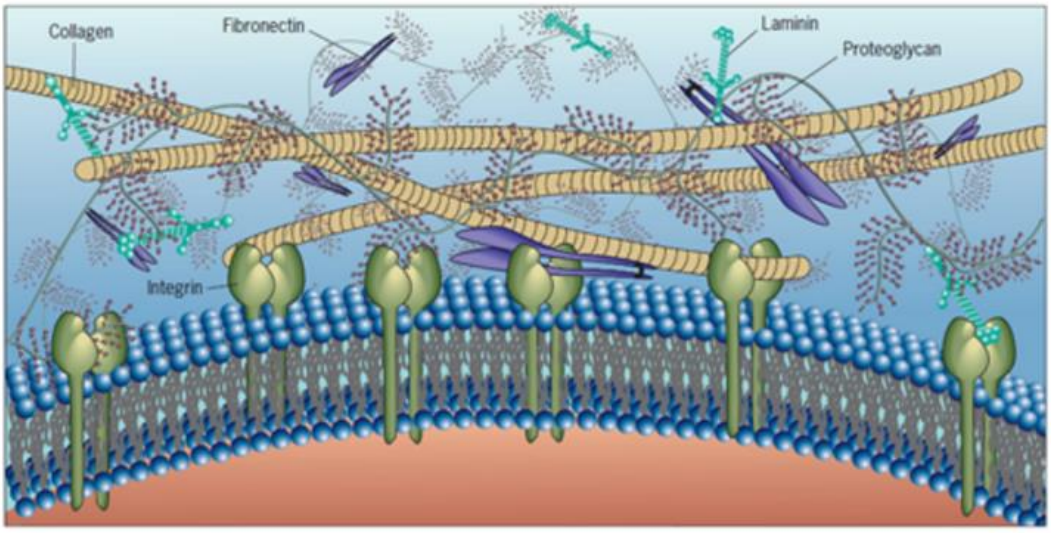

Figure 1.3. A cartoon diagram showing the complexity and interconnected nature of the extracellular matrix. Collagens typically serve as the major structural molecule, while fibronectin, laminin, and proteoglycans play a host of roles, including cell attachment sites and scaffolds for matrix deposition. These molecules interact with cells via membrane spanning proteins called integrins [39].

Elastic fibers follow a core-sheath structure with an elastin core and a sheath made of glycoprotein microfibrils. Notably, elastic fibers can stretch up to 150% before failure, giving tissues a significant source of pliability, yet they cannot be assembled in adulthood. Therefore, any damage sustained by the fibers will forever change a tissue's shape and properties, as evidenced through wrinkling of the skin [31,40]. GAGs are negatively-charged polysaccharides capable of attaching to a protein core, resulting in a proteoglycan. The negative charge of GAGs result in affiliations with water, and the resultant hydrated structure provides the ECM with compressive resistance [36,41]. Proteoglycans provide much of the higher order

ECM structure, and based on the GAG chain bound to it, they possess different binding affinities for molecules present within the matrix [33]. This behavior has major implications in growth factor sequestering, and thus regulation of cellular processes [42]

A common theme seen throughout biology is the relationship between structure and function, and the ECM does not deviate from this trend. This is seen acutely in tendon ECM, as the remarkable mechanical properties possessed by tendons originate from their unique structure. Tendons connect muscles to bones and are responsible for transmitting forces generated by muscles to the skeletal structure [43]. The primary component of tendon ECM is collagen type I (Col-I), and in mature tissue, Col-I is grouped hierarchically in order to form the tissue macrostructure, as shown in Figure 1.4 [44]. The individual collagen molecules are grouped together, forming fibrils. These fibrils bundle together to form collagen fibers which are aggregated into a larger structure termed fascicles. These fascicles are grouped in sections, called tertiary fiber bundles, which comprise the tendon macrostructure [33,45]. Tendon ECM composition changes throughout development, beginning with a high cell density and low amounts of collagen and ending relatively acellular with the highly organized collagen architecture described above [43,45]. This change in composition has been shown to correlate with dramatic changes in mechanical properties. The elastic modulus of day 5.5 chicken calcaneal tendon was shown to be 7 kPa, yet an 8 month old adult chicken tendon was shown to have an elastic modulus of 210 MPa [46].

To illustrate the differences between ECM in various tissues, ECM located in the brain is relatively amorphous and is primarily composed of hyaluronic acid, proteoglycans, and GAGs [47]. This is an interesting contrast to ECM composition in tendons, and yet it still provides the necessary support and regulation of neuronal cells. As an example of this, the ECM density and stiffness has been shown to regulate neuron growth at the end of development [33]. Thus the ECM, both in composition and structure, has been shown to be highly specific and localized to each tissue system in order to stimulate its diverse array of functions *in vivo*.

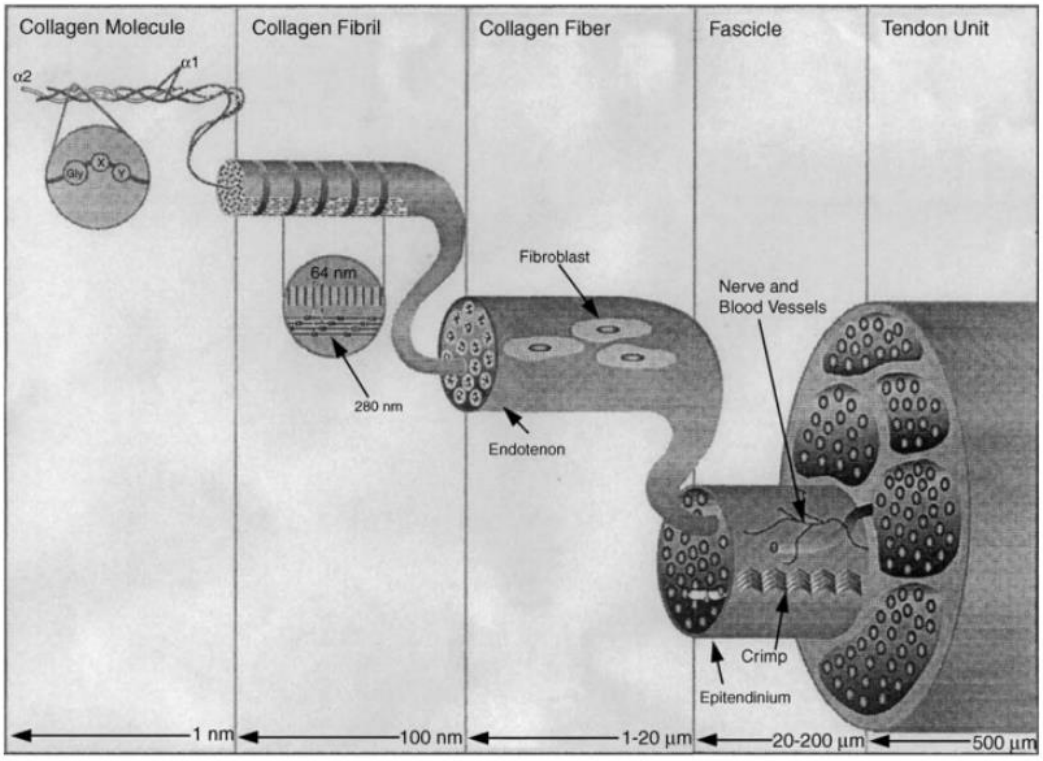

Figure 1.4. Tendon macrostructure is comprised of highly organized collagen type I. This unique structure begins on the molecular scale with collagen's characteristic triple helical structure and continues to organize into discrete higher order units, ultimately endowing the tendon with its remarkable mechanical strength [48].

Fibronectin and the RGD Cell Binding Motif

In addition to collagen, elastic fibers, and GAGs, there are a number of other molecules essential for ECM function. In particular, fibronectin has been shown to play a key role in a multitude of processes. It is a multi-domain protein that possesses different binding sites for a host of species [49]. As such, fibronectin plays the role of a bridge, connecting structural ECM components, secreted molecules, and cells to one another [33,50]. This ultimately gives cells a means of interacting with

the extracellular network, enabling regulation of cell adhesion, migration, and differentiation [33]. Yet even beyond this, fibronectin has been shown to be a vital component of ECM construction, playing roles in elastic fiber and collagen assembly [30,31]. Similarly, a number of molecules depend on fibronectin for incorporation into the matrix, including collagens, fibrillin, and tenascin-C [30]. Adding to its complexity *in vivo*, some molecules require individual fibronectin fibrils for incorporation, while others use the built-up fibronectin matrix as a scaffold for deposition [30]. Further, due to alternative exon splicing, fibronectin exists in 20 different isoforms in humans and possesses cryptic binding sites that are only unveiled after binding with certain proteins [50,51]. This creates a remarkable specificity and variety in its ability to interact with the extracellular matrix as a whole.

With such a prominent role in proper ECM formation and homeostatic function, fibronectin has become a target of tissue engineering efforts. It was discovered that cell attachment in fibronectin was mediated through the amino acid sequence arginine-glycine-aspartic acid (RGD, structure shown in Figure 1.5), and this finding spurred research into producing synthetic peptides that could subsequently mimic fibronectin activity [52]. The RGD motif has since been found in other ECM molecules, such as vitronectin, fibrinogen, osteopontin, laminin, and collagen, although depending on the molecular conformation, it may not be accessible in some of these molecules [53,54]. Cells interact with these binding motifs via membrane spanning proteins called integrins, which are heterodimeric

glycoproteins consisting of an α and a β subunit [53]. This interaction is summarized pictorially in Figure 1.6. In general, integrins bind to a ligand (i.e. the cell binding domain of ECM proteins) which can cause a cascade of responses, including integrin clustering, cytoskeletal activation (i.e. cell migration and cell spreading), differentiation, gene expression, and proliferation [55]. The type of response depends on the activated pathway. For example, fibronectin has been shown to bind to a multitude of integrins with high affinity, and this redundancy is indicative of the specialized roles that the different integrins play in directing cellular response [56].

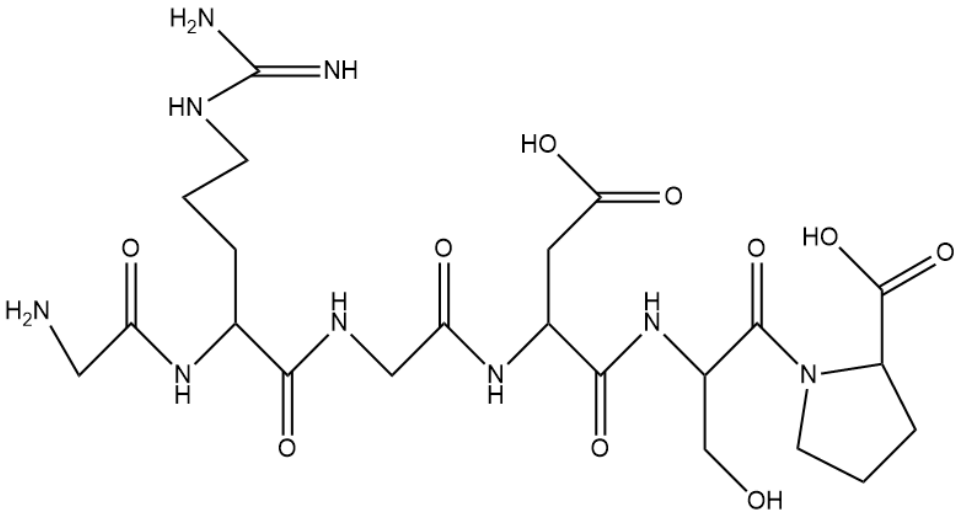

Figure 1.5. G_1RGDSP peptide structure. The flanking amino acids to the RGD sequence are derived from fibronectin to provide greater sequence specificity.

A major area of research within the field of synthetic cell-adhesion peptides has been devoted to generating a specific cellular response when modifying tissue engineering scaffolds. This becomes tricky when ubiquitous cell binding motifs -

such as the RGD sequence - are used, as they are present in numerous ECM molecules [55]. With that being said, researchers have found ways to increase binding specificity, thus promoting the desired signaling cascades and subsequent cellular responses. One route to accomplish this is by manipulating the amino acids flanking the RGD sequence, as this has been shown to affect the adhesive strength and integrin selectivity [57]. An alternative option is to control the 3-dimensional conformation of the RGD sequence, as cyclic peptides have been shown to have a much more potent, specific, and stable response than their linear counterparts [54]. In part, this has been confirmed by the fact that the synthetic peptide G_1RGDSP, derived from fibronectin, has been shown to have a 1000-fold lower activity than the native protein, although this is also due to a lack of cooperating domains in the synthetic peptide that enhance integrin signaling in the native fibronectin molecule [58].

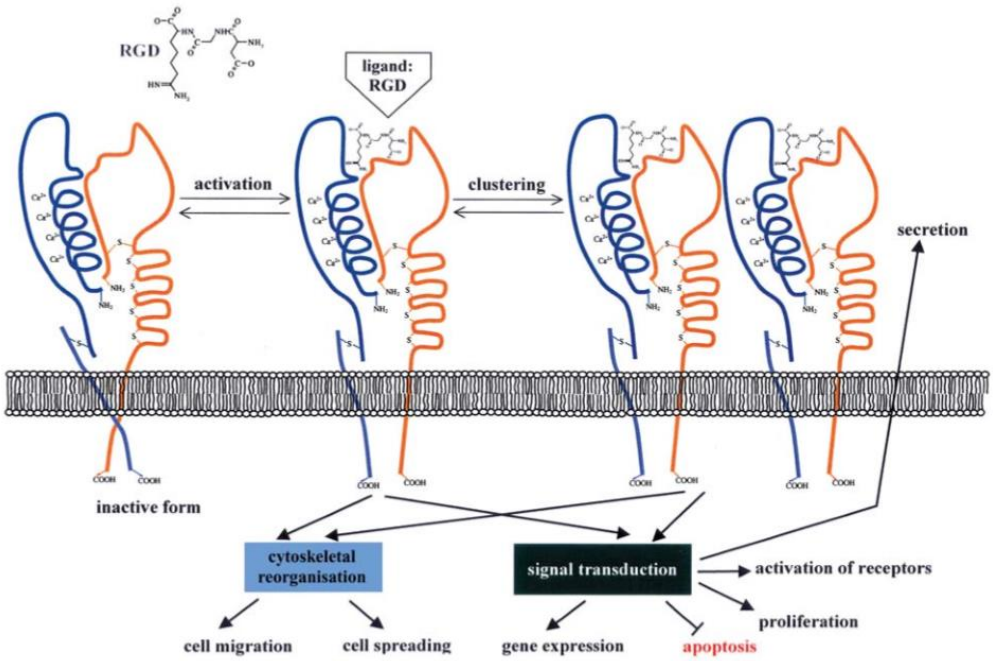

Figure 1.6. The RGD motif can interact with cells via integrins. Upon ligand binding, a host of intracellular pathways can be initiated depending on the specific integrin activated [55].

A considerable amount of research has gone into understanding what factors influence RGD binding and cellular response. In addition to the presentation of RGD, as dictated by stereochemistry, flanking amino acids, and 3-dimensional conformation, RGD density and patterning also affect integrin activation and cellular response [58,59]. For example, controlling the adhesion motif density has been shown to influence the efficiency of cell attachment, as well as proliferation and differentiation of multiple cell types [60,61]. Changing RGD patterning, as dictated through controlling the "island density" (number of RGD ligands in one location) or altering the spacing between RGD islands, has been shown to affect

the formation of focal adhesions and actin stress fibers, as well as cellular adhesion, proliferation and differentiation [58–60,62]. This island spacing can be changed independently of the bulk peptide density through mixing RGD functionalized polymer with unfunctionalized polymer, ultimately varying the distance between the polymer chains that possess peptides.

Additional research has shown the importance of how the adhesion motif is presented to cells. In particular, adding spacer molecules before the amino acid sequence of interest has been shown to enhance cellular response to the substrate [63–65]. It is hypothesized that these spacer arms, which can consist of amino acids, such as glycine, or polymers, such as PEG, enable integrins to bind properly to the adhesion molecule through enhanced accessibility. This phenomenon is shown pictorially in Figure 1.7. In one study, RGD peptides were synthesized with spacer arms ranging from 0 to 20 glycine units [64]. It was found that a minimum of 4 and a maximum of 12 glycine units proceeding the RGDSP motif were necessary to promote optimal levels of cell adhesion and growth. Additionally, this study showed that cells demonstrated reduced expression of key stress markers when presented with RGD peptides in the aforementioned spacer arm range, indicating that spacer arms can have a dramatic effect on cellular phenotype and environmental adaptation.

Other cell-binding peptide sequences have also been investigated, including YIGSR (laminin), DGEA (collagen), and GFOGRR (collagen). Thus, as adhesion motifs are characterized more extensively, more advanced biomaterials and ECM models will

be developed by incorporating a variety of these peptide sequences into scaffolds, in a particular patterning and presentation, with the goal of generating robust and specific cellular responses [4,66–69].

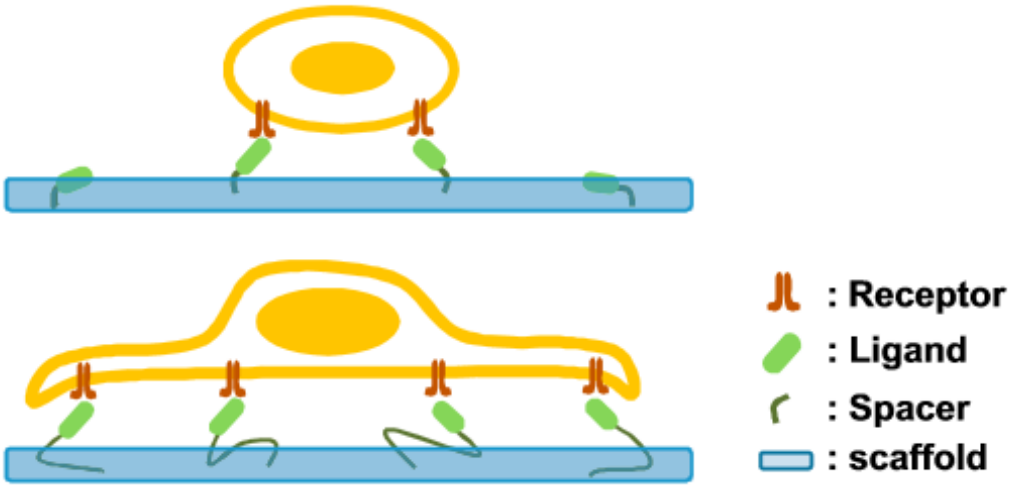

Figure 1.7. The hypothesized effect of utilizing cell adhesion motifs with a spacer arm. The top image shows the effect of a cell interacting with a scaffold imbued with an adhesion of minimal or no spacer arm. The bottom image uses a more significant spacer arm, allowing the cell to interact more effectively with the material [64].

1.2.3 Sodium Alginate as a Tissue Engineering Material

Introduction and Background

Sodium alginate has become a popular material for use in applications that range from emulsifying agents in the food industry to drug delivery vehicles. It is an anionic polysaccharide that is naturally-derived from algae and certain bacteria

[3,70]. Alginate consists of two epimers that comprise its copolymer structure: β-D-mannuronic acid (M) and its C-5 stereoisomer α-L-guluronic acid (G) [1,6,7,18,61]. As shown in Figure 1.8, the alginate polymer consists of M-blocks, G-blocks, and MG-blocks, and the relative length of these blocks, as well as the chain molecular weights, are dictated by the species that produces it and the harvest location [3,70–72]. For example, with respect to spatial variance within *Laminaria hyperborea*, a type of seaweed, alginate sourced from the plant stem possesses a M/G ratio of 0.45, while alginate sourced from the leaf possesses a ratio of 1.22 [73]. Certain research groups have even synthetically modified mannuronan with the appropriate enzymes to create alginate of a particular M/G ratio, ultimately providing more control over the structure, and thus properties of the material [7,74–77].

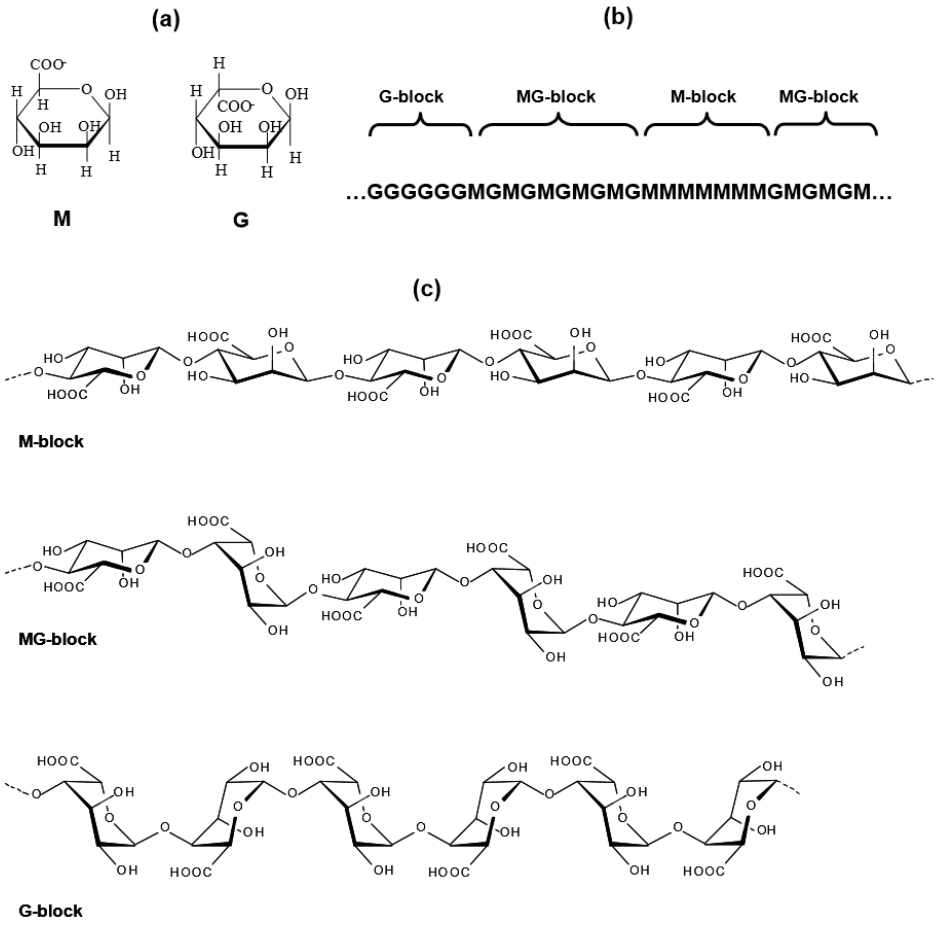

Figure 1.8. (A) Monomer units of alginate, β-D-mannnuronic acid and α-L-guluronic acid. (B) An example of alginate's block copolymer structure. Alginate is naturally derived, so the relative abundance of each component is subject to variation and is highly dependent on the species and location of collection. (C) Diagram of alginate's copolymer structure showing the steric component of each block configuration. Note the structural regularity and sterically exposed carboxylic acid groups in the G-block, allowing for easier coordination with divalent cations for gelling [78].

Alginate has found particular use in biomedical applications due to its natural abundance, low cost, biocompatibility, gentle gelling conditions, and tunable mechanical and chemical properties [1,6,19,79]. It is best known for its ability to form hydrogels in the presence of divalent cations, although it has been used to form other types of ECM scaffolds, such as sponges [19,80,81]. From a materials standpoint, alginate hydrogels have been coined a "blank slate," as mammalian cells lack the appropriate receptors to interact with alginate chains, and the hydrophilic nature of the polymer gels deters the adsorption of ECM proteins [71,79]. Despite this, the uronic acid monomers that comprise the alginate macrostructure possess carboxylic acid groups that can be chemically modified to contain peptides and other molecules that are capable of interacting with cells [61,71]. This creates a unique opportunity for tissue engineering in that a naturally derived material with established biocompatibility and low toxicity can be engineered with a high degree of specificity to elicit particular cellular responses.

Therefore, alginates have been extensively studied and characterized in order to understand the material properties necessary for generating a suitable cellular microenvironment [3,70]. As biomaterials have become more complex, researchers have also begun investigating the properties of, and biological responses to, chemically-modified alginate. For example, with respect to cell adhesion motifs, the effects of different peptides, bulk densities, ligand island patterning, and spacer arm length on cell proliferation, migration, adhesion, and differentiation have been investigated [4,7,8,61,62,64,74,82]. A similar functionalization chemistry has

even been used to attach different chemical groups (e.g. methacrylate) to the carboxylic acid moieties present on the uronic acid monomers in order to create photocrosslinkable gels with tunable mechanical properties [83]. Additionally, in order to imbue alginate with more appropriate material properties for particular applications, such as a positively charged exterior for drug delivery, blended alginate materials have been explored [84,85]. Thus the multifaceted nature of alginate has made it a ubiquitous material that is being used for a remarkable number of biomedical applications, such as sustained growth factor and drug delivery, as well as regenerative tissue engineering strategies involving muscles, nerves, bones, livers, blood vessels, and the pancreas [3].

Structural Analysis

A number of spectroscopic methods have been employed in characterizing alginate's structure, including NMR, FTIR, and Ramen, as well as chromatographic techniques, such as high-performance liquid chromatography (HPLC), gas chromatography (GC), and high-performance anion-exchange chromatography (HPAEC) [73,86–91]. This analysis provides key structural insights into alginate, such as the M/G ratio, fraction of diads (e.g. GG, MM, MG, GM) and triads (e.g. GGG, GGM, GMM, MMM, etc.) present, and the degree of polymerization. These factors play a significant role in determining the viscosity and mechanical properties of the alginate as a whole, as a higher molecular weight and a higher G-content have been shown to produce stiffer and more rigid hydrogels [3,72].

Each characterization method possesses a range of advantages and disadvantages, so the type of information needed ultimately motivates the technique of choice. For example, ^{1}H NMR provides a relatively simple and quick method of determining the aforementioned parameters, and if any derivatization chemistry is being studied, it provides a simultaneously qualitative, quantitative, and nondestructive structural analysis technique [7,92]. That being said, NMR tends to have a relatively high detection limit, and accurate peak integrations depend strongly on well-processed spectra [91]. Additionally, due to its high viscosity, and subsequent peak broadening, spectra need to be generated at elevated temperature (~65°C-80°C) [87,88,93,94]. In order to circumvent viscosity problems, select researchers have turned to a mild acid hydrolysis to slightly degrade the alginate [7]. Below, Figure 1.9 summarizes the relevant NMR peak analysis for alginate.

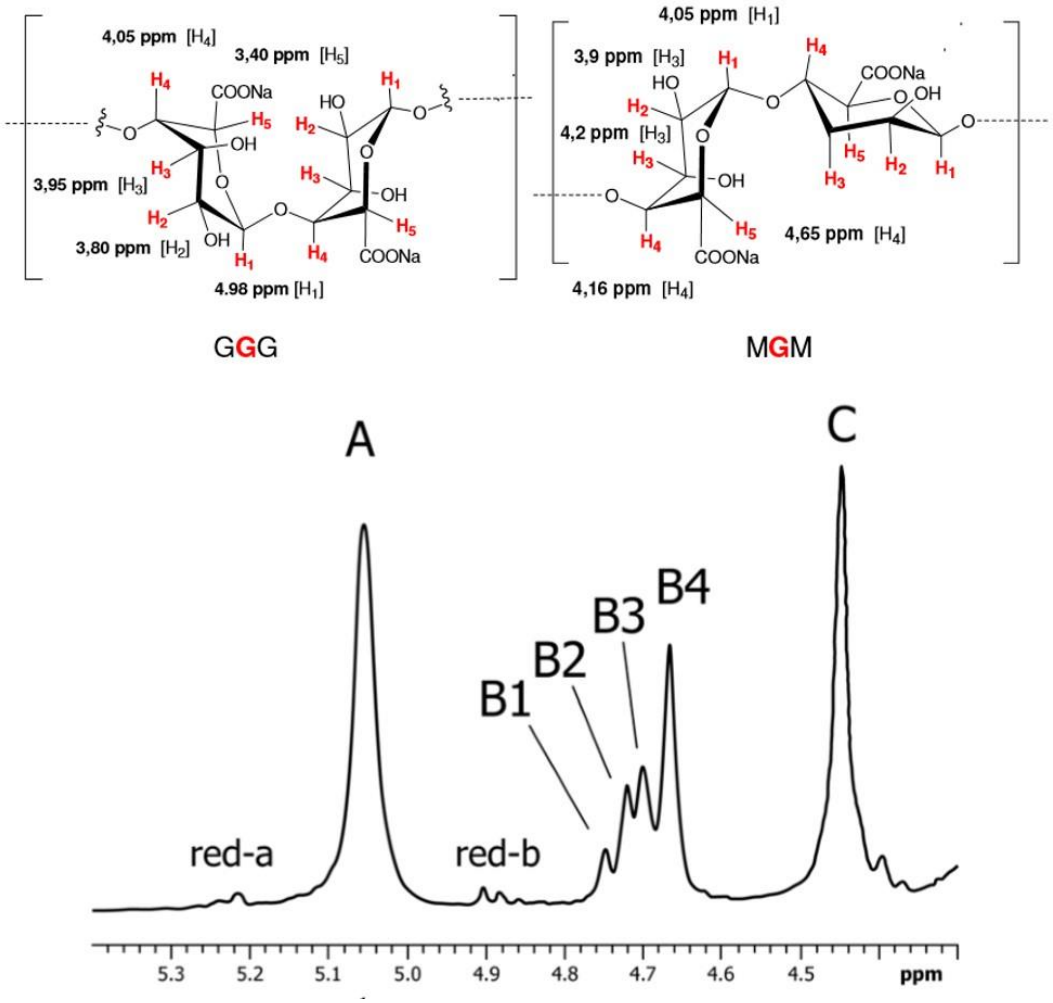

Figure 1.9. The upper picture labels the relevant protons for both alginate monomer units as a reference for the subsequent analysis. The lower picture provides the portion of the ^{1}H NMR spectrum for alginate that is used for quantitative structural information. Peak A corresponds to proton 1 on guluronate (G), while peak C corresponds to proton 5 of G in a GG diad. In the B-region, peak B1 refers to proton 5 of the middle G in a GGM triad. Peak B2 refers to proton 5 of the middle G in a MGM triad. Peak B3 refers to proton 1 of M (mannuronate) in a MG diad, while peak 4 corresponds with proton 1 of M in a MM diad. The red-a and red-b peaks refer to the alpha and beta polymer chain reducing ends,

respectively. Integration of these peaks can provide information such as fraction of G and M units, degree of polymerization, and abundance of diad and triad blocks present [87,88].

Gelation Mechanism

Alginate's unique structure lends itself to forming hydrogels in the presence of divalent cations, such as Ca^{2+} and Ba^{2+}. Carboxylate ion moieties present on the uronic acid monomers coordinate with free cations, generating an ionically crosslinked network. Sterically, guluronate is able to coordinate with divalent cations more readily than mannuronate, as shown in Figure 1.10, and this creates the rigid "egg-box" structure that is credited for providing alginate with its mechanical properties [3,18,72]. The structural integrity of the gels is also affected by the gelation rate. For example, rapid gelling in the presence of aqueous $CaCl_2$ can create non-homogenous gel beads of varying crosslink density and polymer concentration [1]. Therefore, different systems have been developed in order to slow down the gelation rate, ultimately creating more structurally uniform, and thus mechanically superior, hydrogels. One such system uses $CaCO_3$, a largely insoluble salt in water, and D-glucono-δ-lactone (GDL) to slowly release calcium ions from the salt through a proton releasing hydrolysis mechanism [1,8,18,95–98]. Importantly, cells can be encapsulated before gelation occurs, resulting in a homogenous cell-gel suspension. These gentle and cell amenable gelling conditions make alginate of particular interest in 3D culture studies [61]. In an aqueous environment, ionically crosslinked hydrogels often display a significant

degree of swelling, and the divalent cations that cause gelling can diffuse out of the gel, ultimately resulting in dissolution [18]. This can limit the long term feasibility of alginate-based materials, so some researchers have explored various methods of covalent crosslinking [3,83]. Additionally, partially oxidized alginates have been developed in order to promote more controlled degradation properties and renal clearance of high molecular weight chains [99,100].

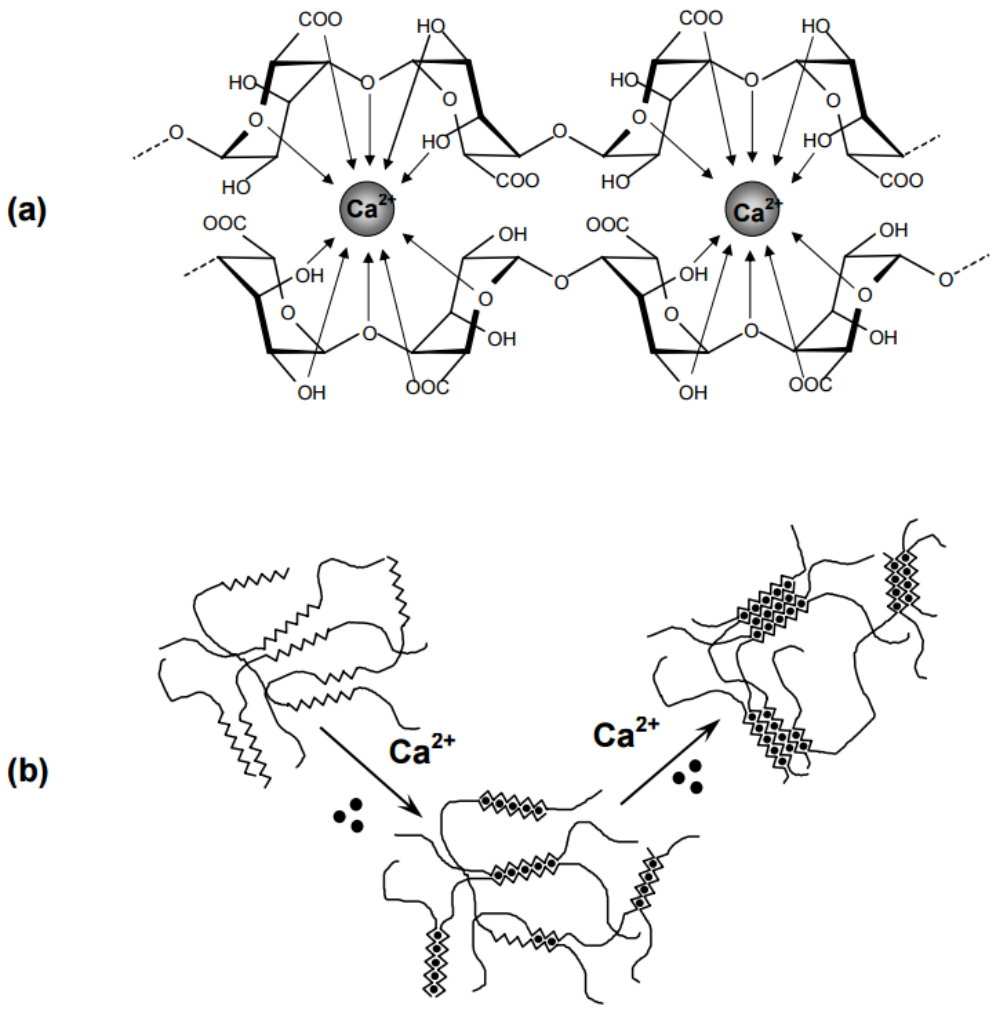

Figure 1.10. (A) The characteristic egg-box model found in alginate G-blocks. The regular structure and sterically accessible carboxylate groups provide a platform for ion chelation in order to create an ionically crosslinked network. (B) The association of different alginate chains upon addition of divalent calcium ions, forming a crosslinked gel network [78].

Alginate gels have been mechanically tested and extensively studied with respect to bulk tensile, compressive, and shear moduli, both in static and dynamic tests, as well as with and without cells [1,6,8,74,79,95]. These studies have revealed alginate's

versatile nature, with compressive moduli ranging from < 1 kPa to over 1,000 kPa and shear moduli ranging from 0.02 kPa to 40 kPa [1,6]. Changing factors such as M/G ratio, calcium content available for crosslinking, and crosslinking kinetics enable researchers to tune the moduli accordingly. These results have major implications in creating a synthetic extracellular network that possesses the proper mechanical properties for tuning degradation time and directing cellular processes, such as differentiation [16].

Many biological tissues (e.g. tendons and ligaments) are viscoelastic, so engineered scaffolds must be able to replicate these mechanical behaviors *in vivo* to provide the proper microenvironment for cells [101]. Viscoelastic materials possess both solid-like and liquid-like behavior, so traditional analyses assuming an elastic response do not necessarily hold for these materials. Therefore, analogous to a Young's Modulus, a complex modulus is defined, consisting of a storage modulus (G' in shear, E' in tensile or compressive testing), which corresponds to the material's elastic response, and a loss modulus (G" in shear, E" in tensile or compressive testing), which corresponds to a material's viscous response. In other words, the storage modulus gives a sense of material stiffness while the loss modulus is representative of a material's flow response [102]. Due to the viscous response of these materials, a phase lag exists between the stress and strain curves, termed "δ." A considerable number of reviews have been written on this topic, so for more information, the reader is referred to [102,103].

Small amplitude oscillatory rheometry provides a straightforward and established method for polymeric hydrogel viscoelastic property analysis [102–104]. This technique allows for *in situ* gelation and provides insight into kinetics, such as gelation time and time to fully crosslink, and the dependence of shear modulus on frequency and strain due to material viscoelasticity. Additionally, by making assumptions, or through a few simple experiments, more information vital to hydrogel performance can be calculated from rheometry, such as mesh size and Young's modulus [8,105]. Therefore, rheological analysis delivers the means for an extensive materials characterization that can also provide insight into tuning the crosslinking time, ultimately allowing biomaterial viscoelastic properties to match that of a native tissue system of interest. A representative time sweep curve, which indicates how a material performs over time at a constant frequency and strain, is shown below in Figure 1.11. These types of analyses are particularly useful in studies which characterize differences between a pre-gel solution and the resultant gelled material.

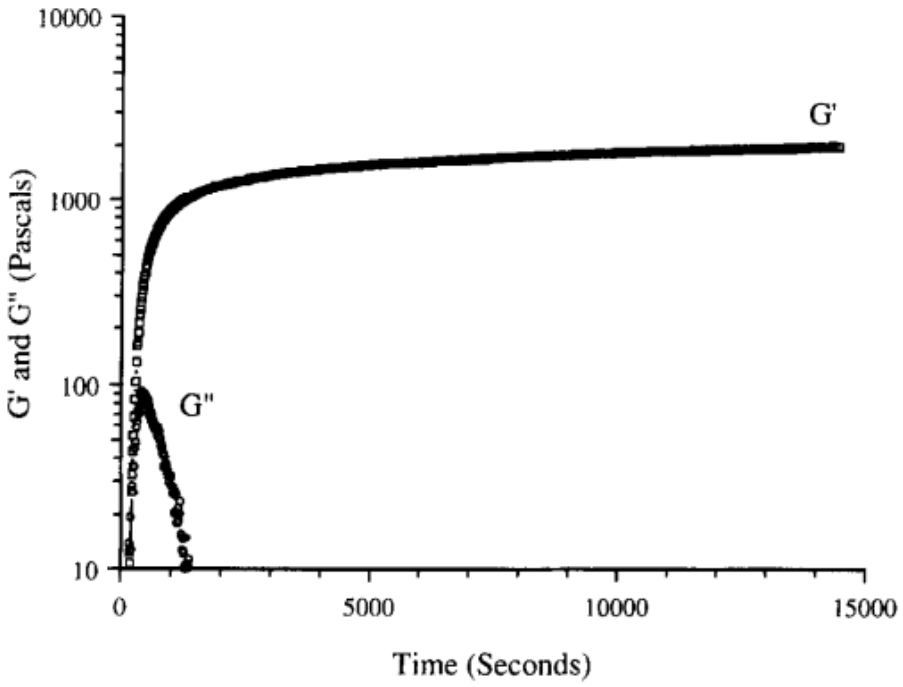

Figure 1.11. A typical time sweep curve performed in rheological studies. A constant frequency and strain percent are used for a predefined amount of time, showing material performance. Here, the G' curve refers to the storage modulus (elastic component), while the G" curve refers to the loss modulus (viscous component). These studies are particularly helpful during in situ *gelation studies, as the gel point can be identified, often by the crossover of the G' and G" curves.* [103].

Carbodiimide Peptide Coupling Chemistry

Using well-established carbodiimide chemistry, the carboxylic acid functional group on an alginate monomer can be modified to create an amide bond. In alginate, this chemistry was optimized by Rowley and Mooney with respect to

uronic acid activation, pH, and salt concentration using the RGD motif, ultimately providing a link for alginate, the "blank slate," to interact with cells in a controlled manner [61,71]. Various mechanisms have been proposed for this chemical modification, and the prevailing reaction schemes are summarized in Figures 1.12-1.14.

This reaction is performed in a slightly acidic buffer, such as 2-(N-morpholio)ethanesulfonic acid (MES) buffer, because MES does not contain any competing carboxylic acids that could reduce reaction efficiency [106,107]. Most commonly, for aqueous reactions, the water-soluble carbodiimide 1-ethyl-(dimethylaminopropyl) carbodiimide (EDC) is used to activate the carboxylic acid group [108]. In essence, the carbodiimide is thought to attack a proton in the buffer, creating a central electrophilic carbon (Figure 1.13, line A) [107,108]. Then, via nucleophilic attack by the carboxylate ion from the uronic acid monomers, a highly reactive intermediate called O-acylisourea is formed, which has a hydrolysis rate of approximately 2-3 s^{-1} at a pH of 4.75 (Figure 1.12, species 3; Figure 1.13, line A)[107,109–111]. It would be advantageous to prolong the life of this adduct, so N-hydroxysulfosuccinimide sodium salt (sulfo-NHS) can be added to stabilize O-acylisourea and prevent production of side products [110,111]. Thus, through a nucleophilic attack, the lone pairs present on an oxygen of sulfo-NHS can attack O-acylisourea and create a succinimidyl ester and a urea derivative side product (Figure 1.14, lines A and B). This urea derivative is thought to create the driving force for this reaction scheme [112]. Depending on solution pH, the activated ester

can prolong the reaction intermediate's lifetime to the order of hours, providing a greater chance of reacting with a primary amine [106]. Finally, a primary amine can attack the stabilized ester, creating an amide and regenerating sulfo-NHS (Figure 1.14, lines B and C) [107].

As shown in Figure 1.12, the sulfo-NHS step is not essential since amide formation can occur with just activation by EDC, although this can result in lower and more variable yields [111,112]. More practical mechanisms are shown in Figure 1.13, involving the formation of an acid anhydride intermediate, and Figure 1.14, involving the use of sulfo-NHS.

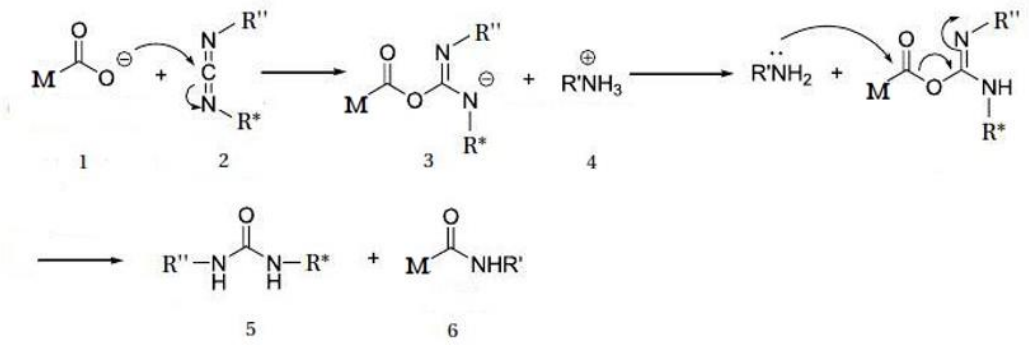

Figure 1.12. The basic reaction scheme for carbodiimde chemistry. The carboxylate ion on alginate monomers (1) attacks the carbodiimde (2) to create the unstable intermediate O-acylisourea (3). This intermediate is then attacked by a primary amine to create the desired amide compound (6) and a urea derivate side product (5) [107].

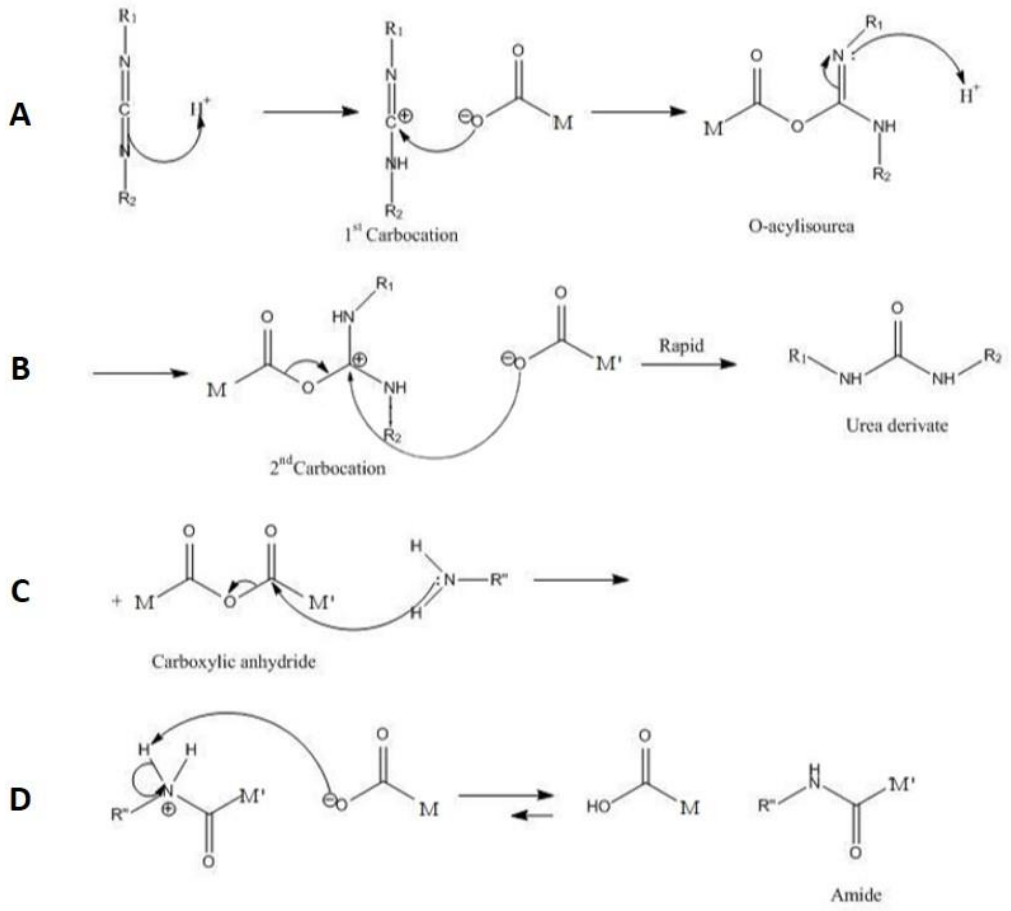

Figure 1.13. A more realistic mechanism for alginate carbodiimide chemistry that accounts for the fast reactivity of O-acylisourea by creating an acid anhydride intermediate before amide formation. (A) The carbodiimide first attacks an acidic proton from the reaction buffer, making the central carbon an electrophile that can be more readily attacked by the alginate carboxylate ion. This creates the unstable O-acylisourea intermediate, which proceeds to attack an acidic proton, creating an electrophilic carbon. (B) This electrophilic carbon is then attacked by another alginate carboxylate ion, expelling a urea based side product. (C, D) The acid anhydride is then attacked by a primary amine, creating the desired amide product and regenerating the other alginate carboxylate group [107].

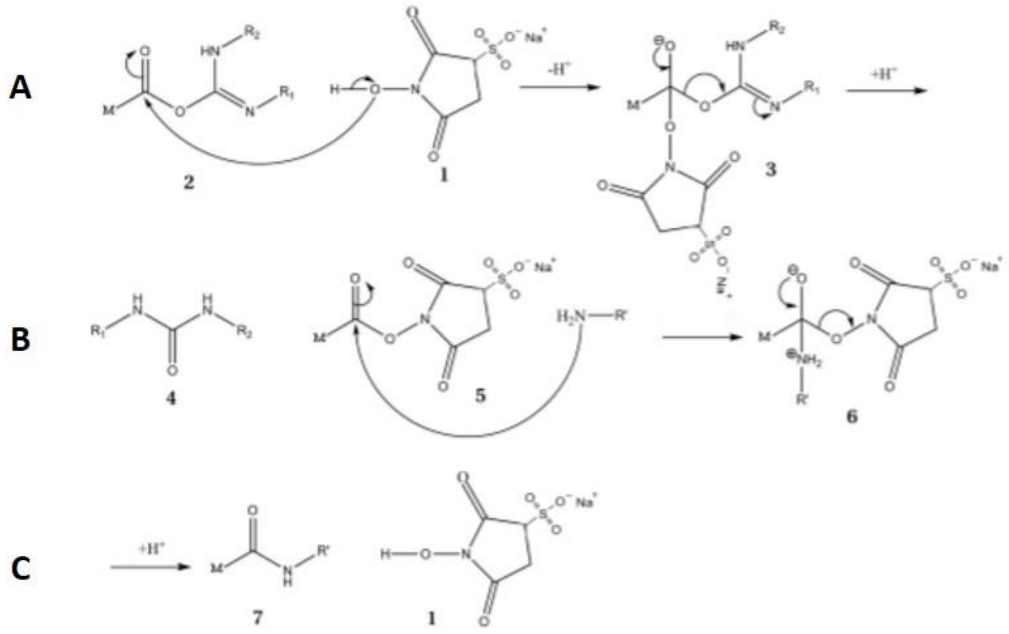

Figure 1.14. The mechanism for sulfo-NHS stabilization of O-acylisourea to prevent undesired side reactions. (A) Sulfo-NHS (1) attacks O-acylisourea (2) and creates a succinimidyl ester (5) and a urea based side product (4) through a reaction intermediate (3). (B, C) The stabilized ester can then be attacked by a primary amine to create the desired amide product (7) through another reaction intermediate (6), regenerating sulfo-NHS in the process [107].

Depending on the reaction conditions, a number of side products can result from this mechanism. Inevitably, soluble urea derivatives will be produced (Figure 1.12, species 5; Figure 1.13, line B; Figure 1.14, species 4) but these are easily removed by dialysis and activated charcoal treatment since they are not associated with the functionalized alginate. Hydrolysis is a major problem for the initial carbodiimide carbocation (e.g. EDC) and O-acylisourea; if they are not quickly attacked by the

appropriate nucleophile, they will hydrolyze and the yield decreases accordingly [108,110,111]. Additionally, if there happens to be a carboxylic acid present on the primary amine (e.g. peptide), EDC can activate the peptide instead and instigate an intramolecular crosslinking reaction [110]. Similarly, since O-acylisourea and the stabilized succinimidyl ester are so reactive to strong nucleophiles, when they are in contact with another carboxylic acid (e.g. from a neighboring monomer), they can react to form an acid anhydride (Figure 1.13, line B) [108,109,112]. Yet this symmetric anhydride is also very reactive and can still result in the desired amide or hydrolyze back into the respective carboxylic acid groups [107,108]. If the polymer backbone or primary amine have multiple amine sources (e.g. arginine in RGD), non-specific conformational binding can result, and this could be problematic for peptide activity with cells.

Notably, O-acylisourea can rearrange due to attack from an intramolecular nitrogen, resulting in the resonance-stabilized and energetically favorable byproduct, N-acylurea (Figure 1.15) [71,108,109,111]. This is particularly problematic relative to the other side reactions since it is covalently bound to the alginate backbone. Furthermore, the carbodiimide has the potential to react with hydroxyl groups present on the alginate backbone, thus forming stable adducts, although it has a strong preference for carboxylate ions. Lastly, additional stable side products could form in the event a hydroxyl group (e.g. from alginate) attacked one of the intermediate species.

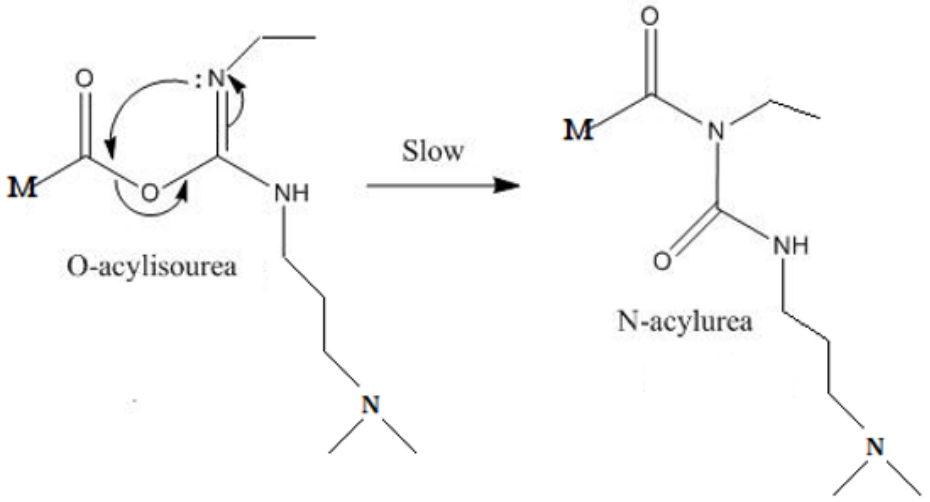

Figure 1.15. The EDC chemistry intermediate O-acylisourea is highly unstable and can rearrange into the stable adduct N-acylurea through a N-O rearrangement. This is the most cited side product from EDC chemistry, as it is stably connected to the polymer [107].

Fortunately, many of these side reactions can be controlled via manipulating pH, reactant concentration, and temperature. For example, to optimize reaction efficiency and minimize side products, it has been recommended to do a two-step reaction, first activating the carboxylic acid with EDC and sulfo-NHS in MES buffer between a pH of 4.5-7.2 and subsequently changing buffers to phosphate buffered saline (PBS) to raise the pH to 7-8 before reacting with the primary amine [106]. This would diminish the chance of non-specific conformational binding with RGD, as arginine's side chain is protonated at physiological pH, ultimately making it less reactive [107]. Additionally, the conversion of O-acylisourea to N-acylurea has been shown to be temperature dependent. Adduct formation can be minimized by

reacting the alginate and EDC at 0°C [107,109,112]. Finally, it has been reported that higher yields can be obtained without overwhelming the reaction mixture with carbodiimide, most likely due to the fact that increased activation has a higher probability of side reactions [71,108,110,111].

It is imperative to calculate the degree of peptide substitution onto alginate, as this dictates the microenvironment observed by cells within the biomaterial [71]. A minimum concentration of RGD is necessary for cells to adhere and interact with the biomaterial, and depending on the ECM that is being mimicked, different peptide types and densities can be desired to better reflect the natural environment. Rowley and co-workers indicated that 1 mg of GRGDY (gly-arg-gly-asp-tyr) per gram of alginate was approximately 2.5 orders of magnitude greater than the minimum ligand spacing identified for cell attachment [71]. This is an approximation based on work from Massia and Hubbell, extrapolating their 2D results into a 3D space under the assumption that the matrix can be modeled as a body-centered cubic unit cell [113].

Therefore, in an effort to calculate the degree of coupling and develop a well characterized system, a number of different techniques have been used depending on the materials and source of primary amine. For instance, radiolabeling peptides, fluorescence, UV-VIS, elemental analysis, protein assays, titration, and NMR have all been implemented in publications [8,61,71,92,107,114,115]. The technique used in a specific situation depends upon the system, as, for example, UV-VIS requires the presence of highly conjugated or colored

substances. As previously mentioned, NMR is a highly accurate quantitative technique that also provides key structural information, such as the concentration of N-acylurea adduct formation [7,107,116–118]. With respect to RGD coupling onto alginate, a wide range of yields have been reported, ranging from approximately 2%-90% despite using similar chemistries [7,8]. This highlights the sensitivity of overall yield to the reaction conditions, as well as the importance of selecting an accurate method of quantifying peptide coupling. Despite this, many publications fail to report the reaction efficiency or simply cite Rowley's study and claim his yields despite potentially changing key factors, such as the peptide used [4,60,64].

1.3 Motivation

The first objective of this thesis is to investigate the reaction efficiency of alginate-RGDSP peptide functionalization and the degree of side product formation as a function of reactant concentration, peptide loading density, and spacer arm length. To these ends, spacer arm lengths of 1 and 12 glycine units will be studied. This will be accomplished by validating a quantitative ^{1}H NMR technique that relies on an internal standard doped into the deuterated solvent for reaction yield analysis.

There is considerable impetus for developing a technique that can be implemented for both qualitative and quantitative analysis of polymer biomaterials. Both ^{1}H and ^{13}C NMR have been utilized extensively to characterize alginate's structure, and some publications have used it to verify successful peptide coupling to the polymer [7,74,87,88,93]. Furthermore, certain research groups have coupled peptides to mannuronan and then enzymatically converted a fraction of the remaining M-units to the full M-G alginate structure [7,75,76]. Utilizing ^{1}H NMR, they have been able to calculate yield, degree of substitution, and assess the changes to mannuronan structure due to chemical modification. Recently, a similar analysis has been extended to the full alginate polymer using specific intrinsic peaks of alginate for calibration [119,120]. Additionally, other research groups have introduced different functional moieties to alginate (e.g. methacrylate groups) and investigated the functionalization yield using ^{1}H NMR via the addition of an internal standard [121–124]. Despite this, peptide coupling in these studies was

still analyzed using other techniques, such as a quantitative assay. Thus to the best of our knowledge, ^{1}H NMR has not been applied to alginate using an internal standard for peptide quantification, which would provide increased versatility in terms of analysis. This is important, as it enables fewer experiments and accurate degree of coupling analysis even when the ligand of interest has peaks that interfere with the anomeric region of the alginate NMR spectrum.

Moreover, questions remain about how the reaction yield and hydrogel properties change when coupling is performed with different peptides. Although Rowley and Mooney's innovative work reported a roughly 20% difference in efficiency when using G_1RGDY versus G_4RGDY, many studies do not relate the degree of coupling or simply cite the yields found in Rowley's first study despite using different peptides [4,61,64,71]. Thus, it is unclear if the altered cellular responses seen in these studies are due to the peptide or other contributing factors, such as a different ligand density presented to the cells. Consequently, this study attempts to determine if there are peptide specific effects on carbodiimide reaction efficiency by expanding upon Rowley's work and studying RGDSP peptides of two different spacer arm lengths, G_1RGDSP and G_{12}RGDSP, over different loading densities and reaction chemistries. These different spacer lengths were chosen due to their biological significance [64].

The second aim of this thesis is to investigate the effect of RGDSP peptide functionalization on alginate hydrogel properties as a function of reactant concentration, degree of peptide substitution, and spacer arm length. To these

ends, rheometry was used in order to generate time, frequency, and strain sweeps, providing insight into viscoelastic behavior, stiffness, fracture point, gel point, and crosslinking time.

To the best of our knowledge, no studies have investigated the effects of the various side reactions that occur in carbodiimide functionalization on hydrogel properties. Here, we attempt to analyze this effect through control experiments where the functionalization process was applied without the introduction of the peptide. Therefore, in conjunction with the peptide functionalized conditions, rheological analysis allows for the structural changes seen via ^{1}H NMR to be correlated with changes in hydrogel mechanical properties and gelation kinetics. Besides having interesting implications from a materials point of view, this allows for the effect of functionalization chemistry on hydrogel performance to be established in a more isolated manner than has been previously reported. Thus, the research presented here provides a more systematic characterization to further elucidate the critical variables that are essential to control in the creation of tissue engineered scaffold microenvironments.

Chapter 2: Materials and Methods

2.1 Materials

PRONOVA UP LVG sodium alginate (minimum of 60% G-content, low viscosity), was purchased from NovaMatrix. The custom peptides G_1RGDSP (gly-arg-gly-asp-ser-pro) and G_{12}RGDSP (gly-gly-gly-gly-gly-gly-gly-gly-gly-gly-gly-gly-arg-gly-asp-ser-pro) were purchased from Biomatik. The peptides were produced in an acetate salt to ensure biological compatibility. Purity and net peptide content information was provided by Biomatik and are summarized in Table 2.1. Peptide solutions were prepared by multiplying the peptide mass by purity and net peptide content percentages in order to ensure accurate concentrations.

Table 2.1. Summary of the purity and net peptide content for each peptide purchased from Biomatik. This information is vital in preparing peptide solutions with accurate concentrations.

Peptide	Purity	Net Peptide Content
G_1RGDSP	99.47%	67.86%
G_{12}RGDSP	99.04%	74.60%

For the functionalization reaction, 2-(N-Morpholino)ethanesulfonic acid hydrate (MES), sodium chloride (NaCl), and N-(3-Dimethylaminopropyl)-N'-ethylcarbodiimide hydrochloride (EDC) were purchased from Sigma Aldrich. Hydroxylamine hydrochloride was purchased from Alfa Aesar. Activated charcoal (50-200 mesh) was purchased from Fisher Scientific. N-hydroxysulfosuccinimide

(sulfo-NHS), ultrapure distilled water, dialysis cassettes (3.5 kDa molecular weight cut-off, MWCO), and Nalgene Rapid-Flow filter units (0.45µm PES membrane) were purchased from ThermoFisher Scientific.

To create alginate hydrogels, calcium carbonate ($CaCO_3$) and D-(+)-Gluconic acid δ-lactone (GDL) were purchased from Sigma Aldrich. Hanks' Balanced Salt Solution (HBSS, no calcium, magnesium, or phenol red) was purchased from ThermoFisher Scientific.

2.2 Methods

2.2.1 Synthesis of Peptide Coupled Alginate

Well-established aqueous carbodiimide chemistry was utilized to functionalize alginate with the RGD peptides of interest. Four different reaction schemes per peptide were used in order to investigate how the functionalization efficiency changes with EDC/sulfo-NHS reactant concentrations, peptide loading density, and peptide spacer arm length. These approaches are summarized in Tables 2.2 and 2.3, below. Note that the reagents listed in the table are based on a reaction using 150 mg of alginate, yet they can be scaled linearly based on the amount of alginate used. The conditions labeled “LA” refer to low activation chemistry that mimics the innovative work performed by Rowley and Mooney [71]. “HA” refers to high activation chemistry in which the amounts of EDC and sulfo-NHS are increased relative to LA chemistry (80% EDC activation by mol vs. 5% activation; 167% sulfo-NHS stabilization by mol vs 50%). The 0.7% and 5% notation refers to the amount of peptide loaded into the reaction by mole percentage with respect to the number of uronic acid monomers initially present. Additionally, controls with no peptide were synthesized for both chemistry conditions. An additional control for the LA chemistry was created, maintaining the level of EDC activation at 5% but increasing the level of sulfo-NHS stabilization proportionately to that which is present in the HA chemistry.

*Table 2.2. Summary of the high activation peptide coupling conditions synthesized in this study. These amounts are based upon reaction with 150 mg of alginate and can be scaled proportionately. *Note that the amount of MES buffer listed is a* volume *given in* milliliters *(sufficient to create a 1% w/v alginate solution based on the batch size).*

Reaction Description		**Amount (µmol)**	
Condition	**Reactant**	**G_1RGDSP**	**G_{12}RGDSP**
HA-C	Alginate (COOH)	810	810
	MES Buffer*	*15*	*15*
	EDC	643	643
	Sulfo-NHS	1135	1135
	Peptide	-	-
	Hydroxylamine HCl	93.3	93.3
HA-0.7%	Alginate (COOH)	810	810
	MES Buffer*	*15*	*15*
	EDC	643	643
	Sulfo-NHS	1135	1135
	Peptide	5.93	5.93
	Hydroxylamine HCl	93.3	93.3
HA-5%	Alginate (COOH)	810	810
	MES Buffer*	*15*	*15*
	EDC	643	643
	Sulfo-NHS	1135	1135
	Peptide	41	41
	Hydroxylamine HCl	93.3	93.3

*Table 2.3. Summary of the low activation peptide coupling conditions synthesized in this study. These amounts are based upon reaction with 150 mg of alginate and can be scaled proportionately. *Note that the amount of MES buffer listed is a* volume *given in* milliliters *(sufficient to create a 1% w/v alginate solution based on the batch size).*

Reaction Description		**Amount (µmol)**	
Condition	**Reactant**	**G_1RGDSP**	**G_{12}RGDSP**
LA-C	Alginate (COOH)	810	810
	MES Buffer*	*15*	*15*
	EDC	40.5	40.5
	Sulfo-NHS	20.3	20.3
	Peptide	-	-
	Hydroxylamine HCl	40.5	40.5
LA-C-NHS	Alginate (COOH)	810	810
	MES Buffer*	*15*	*15*
	EDC	40.5	40.5
	Sulfo-NHS	71.5	71.5
	Peptide	-	-
	Hydroxylamine HCl	40.5	40.5
LA-0.7%	Alginate (COOH)	810	810
	MES Buffer*	*15*	*15*
	EDC	40.5	40.5
	Sulfo-NHS	20.3	20.3
	Peptide	5.93	5.93
	Hydroxylamine HCl	40.5	40.5
LA-5%	Alginate (COOH)	810	810
	MES Buffer*	*15*	*15*
	EDC	40.5	40.5
	Sulfo-NHS	20.3	20.3
	Peptide	40.5	40.5
	Hydroxylamine HCl	40.5	40.5

Thus for the coupling reaction, a 1% w/v alginate stock was prepared in MES buffer (0.3 M NaCl, 0.1 M MES, pH adjusted to 6.5 with NaOH) and allowed to dissolve overnight. Then, using the above reaction scheme, sulfo-NHS, EDC, and peptide, were added to the alginate solution in that order. This step was performed in a glove-bag with low humidity in order to maintain the integrity of the chemicals used. The peptides were dissolved in ultrapure distilled water before they were added to the reaction mixture. All reaction conditions were normalized to the same volume via addition of ultrapure distilled water to ensure identical reactant molarities. The reaction was allowed to proceed for 20 hours before being quenched with hydroxylamine hydrochloride.

The resultant reaction mixture was then purified through extensive dialysis. Ultrapure deionized water (DI water), as generated from a Biolab 3300 RO system (Mar Cor Purification), and dialysis cassettes with a 3.5 kDa MWCO were utilized for this step. A salt gradient was used (0.51 M, 0.43 M, 0.34 M, 0.26 M, 0.17 M, 0.09 M, 0 M, 0 M, 0 M), dissolving the appropriate amount of NaCl into 4 L of DI water. The water was changed every 4-8 hours while salt was present and every 2-4 hours during the pure DI water stages.

The samples were further purified through activated charcoal treatment for 30 minutes. At a minimum, a charcoal mass equal to 50% of the original alginate mass was added to the solution and mixed well using a rocker over the duration of this step. The resultant alginate-charcoal mixture was phase separated through centrifugation, filtered using Nalgene Rapid Flow filtration units, and lyophilized

for a minimum of 3 days. The samples were sealed with Parafilm and stored at -20°C until use.

2.2.2 NMR Characterization

The degree of peptide coupling and reaction side products were analyzed using ^{1}H NMR (Bruker Avance III 500MHz). Lyophilized RGD-coupled alginate was dissolved at a concentration of 20 mg/mL in deuterium oxide (D_2O, 99.9 atom%, Sigma Aldrich) doped with a known concentration of nitrobenzene (Sigma Aldrich). The concentration of nitrobenzene in D_2O was confirmed with UV-VIS and quantitative ^{1}H NMR on a G_1RGDSP sample of known concentration. Once dissolved, a long glass Pasteur pipette was used to transfer the alginate into a NMR tube (Wilmad-LabGlass). The NMR tube was then placed in a 50°C oven for 2 hours, thereby reducing viscosity and ensuring all the alginate had collected at the bottom of the tube. Once this preparation was completed, the sample was loaded into the NMR machine. The following parameters, summarized in Table 2.4, were used during each experiment:

Table 2.4. Summary of the acquisition parameters used in 1H NMR experiments.

Parameter	Value
NS	256
AQ	4.1 s
RG	203
D1	10 s
Temperature	353 K
LB	1 Hz

A water suppression routine was used with a long D1 time in order to ensure adequate relaxation between scans. Once routine data processing was completed (phase adjustment, baseline correction, integration), the ratio of the nitrobenzene standard to select RGD and N-acylurea peaks were compared in order to output the amount of incorporated peptide and reaction byproducts. The relevant calculations are included in Appendix B.

2.2.3 Preparation of Alginate Hydrogels

Protocols for producing alginate hydrogels with homogenous properties through manipulation of the crosslinking kinetics have been well-established and are the basis for this protocol [1,18]. 5% w/v solutions of the lyophilized alginate in HBSS were prepared and allowed to dissolve overnight. Stock solutions of $CaCO_3$ (6% w/v) and GDL (21.4% w/v) were prepared in HBSS. Note that the GDL was not dissolved in HBSS until immediately before use in order to prevent it from hydrolyzing prematurely. In order to make a 0.5 mL hydrogel, 150 mg of 5% w/v alginate stock was added to a 2 mL microcentrifuge tube. Then, the following components were added, in the order and volumes indicated in Table 2.5, below.

*Table 2.5. Summary of the reagents and volumes mixed to create alginate hydrogels. This recipe makes a 0.5 mL gel. *Note that the amount of 5% alginate solution provided in the table is given in* milligrams *since the alginate solution was added by mass in order to circumvent errors due to pipetting a viscous solution.*

Species	Volume (µL)
5% Alginate*	*150*
$CaCO_3$	23
HBSS	307
GDL	20

After the addition of each species, the mixture was carefully mixed with a pipette tip in order to ensure homogeneity while minimizing the addition of air bubbles. The $CaCO_3$-GDL release system ensures slow crosslinking kinetics and thus structurally uniform hydrogels.

2.2.4 Rheological Characterization

The viscoelastic behavior of the hydrogels was analyzed using a TA Instruments ARES-LS2 rheometer (TA Instruments). A cone and plate geometry was used via 25 mm stainless steel conical plate (angle: 0.0994 rad) and a temperature controlled Peltier plate set to 37°C. The protocol for making the hydrogels was followed, and 420 µL of the solution was carefully pipetted onto the center of the Peltier plate. A gap of 0.046 mm was then set, and a low viscosity oil was pipetted around the edge of the cone and plate set-up in order to prevent evaporation of water. A dynamic time sweep was first run at 6.283 rad/s (1Hz) and 1% strain for

13 hours (the time at which the gels reached a stable plateau in modulus). Immediately following this test, a frequency sweep was conducted at 1% strain from 0.1 to 100 rad/s. Finally, a strain sweep was performed at 6.283 rad/s from 0.1-500% strain. Preliminary strain sweeps indicated the linear viscoelastic region (LVR) extended to approximately 4% strain for all conditions, ensuring that the 1% strain used in these studies was not damaging the gels.

2.2.5 Dynamic Light Scattering

Self-organization of G_1RGDSP and G_{12}RGDSP peptides into colloidal particles was assessed by dynamic light scattering using a NanoBrook 90Plus PALS particle sizer (Brookhaven Instruments Corporation) equipped with a He-Ne laser operating at 659 nm. Cuvettes with a 1 mm entrance aperture were used to house the samples, and scattering measurements were performed at a constant temperature of 25°C and a 90° angle. Before testing, samples were dissolved in ultrapure distilled water at different concentrations (3 mg/mL and 5 mg/mL for G_1RGDSP; 3 mg/mL, 5 mg/mL, and 11 mg/mL for G_{12}RGDSP), passed through a 0.45 µm filter to remove dust and large particulates, and sonicated for 5 minutes to break up any aggregates. Each experiment consisted of three scans to ensure no particle aggregation was occurring. A refractive index of 1.6 was estimated for the peptides [125].

Chapter 3: Results and Discussion

3.1 Functionalization Efficiency and Structural Analysis

NMR is an established technique for investigating the structural properties of compounds, and it has been used quantitatively with a high degree of accuracy to assess the abundance of different components within a sample [116–118]. It has also been used extensively for alginate characterization [7,74,87–90,93,119,120,126]. This means NMR is a promising, convenient method for assessing the degree of peptide coupling to alginate while also providing information as to how the functionalization chemistry has affected the alginate structure. The peptide G_1RGDSP was characterized using ^{1}H NMR nearly three decades ago, providing the basis for this analysis [127].

Work has been done to functionalize the mannuronan homopolymer, the M-monomer unit of alginate, with a RGD peptide, and this functionalization efficacy was assessed via ^{1}H NMR based on a ratio of peptide and mannuronan peak areas [7,74]. Recent publications have assessed the degree of coupling (e.g. RGD or methacrylate) on the full alginate polymer using ^{1}H NMR and a similar peak ratio strategy with the anomeric portion of the alginate spectrum [119,120]. A slightly different tactic has been taken by other groups, who have added internal standards to their NMR solutions for the sake of providing a stable basis of protons for the substitution quantification. This has been performed in alginate systems to quantify the degree of derivatization with specific functional groups, such as

methacrylation, although peptide coupling was still quantified using other means, such as external assays [121–124]. In this work, we propose an extension of the use of internal standards within alginate systems by using them as a means of quantifying peptide coupling.

To investigate the effects of peptide substitution, we compare two different reaction schemes with respect to yield and side product formation. Here, yield and efficiency are used synonymously and refer to the percentage of peptide successfully coupled to alginate versus the original amount added. The first chemistry explored is termed “low activation chemistry” (LA), and it refers to the pioneering chemistry used by Rowley and associates to successfully couple RGD to alginate with EDC/sulfo-NHS chemistry [61,71]. To complement the LA control condition, where all steps of the low activation chemistry process were conducted except peptide addition, an additional control was synthesized called LA-C-NHS in which the amount of sulfo-NHS used was increased in order to promote stabilization of reaction intermediates. The second chemistry investigated is a modification of the Rowley chemistry, termed “high activation chemistry” (HA), and it boosts the EDC and sulfo-NHS concentrations to encourage a higher activation level and subsequently higher coupling efficiency.

Additionally, the effects of peptide spacer arm length and peptide loading density on yield and side product formation were explored. Two different RGD peptides were compared, G_1RGDSP and G_{12}RGDSP, at two different loading concentrations, 0.7% and 5% by mole of the total uronic acid monomers available. The 0.7%

loading condition has been shown by previous work in our lab to provide favorable tendon progenitor cell morphological response in alginate hydrogels (data not shown). Therefore, the 5% condition provides complimentary data via insights into the effects of greater peptide loading on the alginate polymer, and subsequently, alginate hydrogels. This also helps to mitigate costs of using expensive custom peptides, as the 5% condition corresponds with a stoichiometric level of loading (for LA chemistry conditions) instead of an excess of peptide relative to the number of activated carboxylate groups.

Table 3.1 summarizes the different conditions investigated. Each condition was labeled under the following notation: reaction scheme (LA or HA), peptide (G1 for G_1RGDSP, G12 for G_{12}RGDSP, or C for controls lacking peptides), and mole ratio of peptide added to the reaction relative to the moles of available carboxylate groups on alginate (0.7% or 5%). Ultimately, the goal of this work was to bracket extreme conditions for the three variables of interest (reactant concentration, spacer arm length, and peptide loading density) in an attempt to further explore the trends of EDC/sulfo-NHS chemistry and to establish the legitimacy of quantitative ^{1}H NMR (qNMR) with an internal standard as a means of analysis for peptide coupled alginate.

Table 3.1. Summary of the different conditions tested via ^1H NMR for quantification of peptide coupling and N-acylurea analysis. Note that all ratios are mol percents.

Condition	EDC:COOH	NHS:EDC	Peptide	RGD:COOH	RGD:EDC
Control	-	-	-	-	-
HA-C	80%	176%	-	-	-
HA-G1-0.7%	80%	176%	G_1RGDSP	0.7%	1%
HA-G1-5%	80%	176%	G_1RGDSP	5%	6%
HA-G12-0.7%	80%	176%	G_{12}RGDSP	0.7%	1%
HA-G12-5%	80%	176%	G_{12}RGDSP	5%	6%
LA-C	5%	50%	-	-	-
LC-C-NHS	5%	176%	-	-	-
LA-G1-0.7%	5%	50%	G_1RGDSP	0.7%	15%
LA-G1-5%	5%	50%	G_1RGDSP	5%	100%
LA-G12-0.7%	5%	50%	G_{12}RGDSP	0.7%	15%
LA-G12-5%	5%	50%	G_{12}RGDSP	5%	100%

^1H NMR was performed on each of the above conditions using D_2O as a solvent. The solutions were doped with nitrobenzene at a concentration of 0.8 mM to act as an internal standard. This route was selected because the ^1H NMR spectrum of alginate is complex, and many prominent peaks shift upon functionalization, either due to the peptide attachment reaction or due to side reactions (see Figure 3.2). Furthermore, peptide peaks overlap with many such alginate peaks, further complicating the analysis. This makes using a specific peak of alginate as an internal standard prone to several sources of error. To address these concerns, we chose to use an internal standard, an additive of known concentration mixed with a known amount of functionalized alginate, to calibrate our measurements.

Nitrobenzene possesses a significantly lower volatility than water (e.g. from the Sigma Aldrich SDS, a value of 0.2 mmHg at 20°C is reported), does not interact with the sample or solvent, and has ^{1}H NMR peaks that are all significantly downfield from alginate and RGD signals. These qualities make it an ideal internal standard for qNMR.

Before using the doped D_2O solution for peptide and side product quantification, the nitrobenzene concentration was validated using UV-Vis and qNMR on a sample of known concentration to ensure accuracy in future experiments. UV-Vis on nitrobenzene solutions dissolved in D_2O was performed at λ=268.5nm [128]. A standard curve, which can be found in Appendix A of this document, predicted a nitrobenzene concentration of 0.81 mM. As a second check, a solution of 6.7 mM G_1RGDSP was prepared in the doped D_2O solvent, and using ^{1}H NMR, the RGD solution concentration was accurately predicted within 0.75% error. This data generated confidence in the accuracy of the solution concentration, and thus 0.81 mM was used as the nitrobenzene concentration in subsequent quantitative ^{1}H NMR experiments. A summary of qNMR calculations can be found in Appendix B. Below, the ^{1}H NMR spectra for nitrobenzene, G_1RGDSP, and N-acylurea, a key side product generated from the EDC/sulfo-NHS chemistry, can be seen in Figure 3.1. The peaks labeled “RGD1” and “RGD2” are likely combinations of different signals and were not assigned to specific protons.

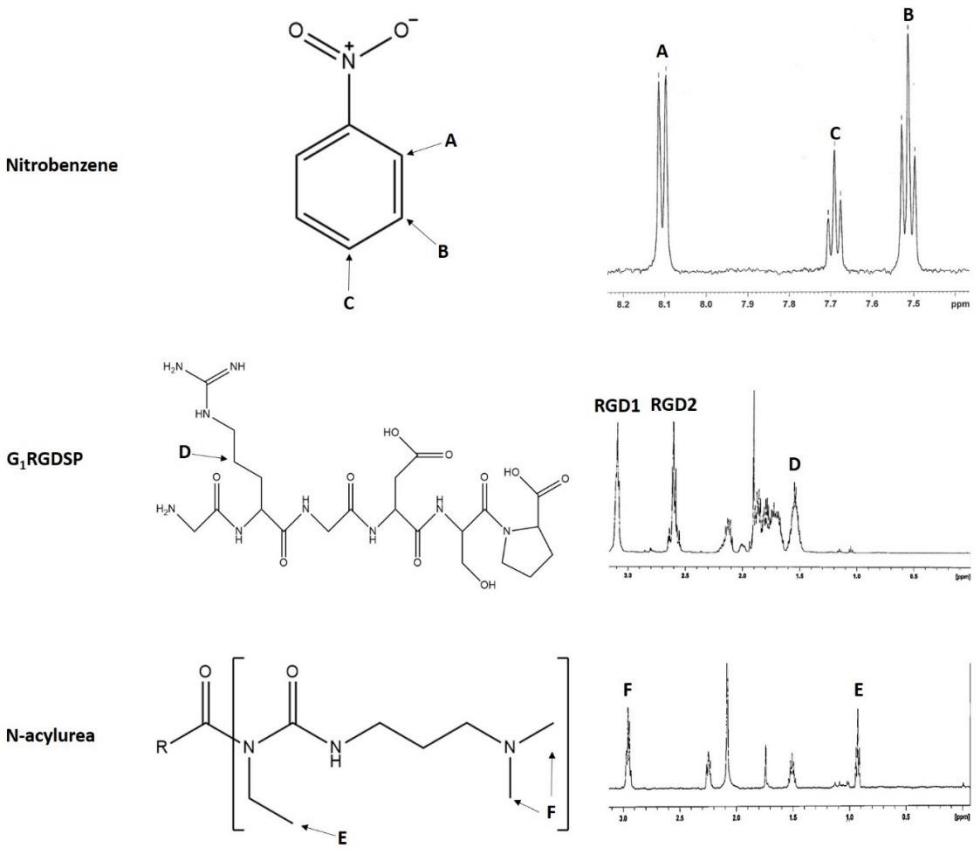

Figure 3.1. Structures of nitrobenzene, G_1RGDSP, and N-acylurea and their corresponding ^{1}H NMR spectra. The relevant peaks for analysis and associated protons have been marked with a letter [7,107,127]. Note that the spectra listed for N-acylurea corresponds to the LA-C condition, and the N-acylurea specific peaks have been labeled accordingly.

Upon satisfactory analysis of nitrobenzene, the 12 conditions described in Table 3.1 were investigated via qNMR for peptide coupling efficiency and N-acylurea formation. All of the spectra were recorded at 353 K and manually phase shifted to set the nitrobenzene peak labeled B (see Figure 3.1) to 7.513 ppm. Representative spectra from the different conditions are shown in Figures 3.2 and

3.3, while the remainder of the spectra can be found in Appendix C. A summary of degrees of coupling can be found in Table 3.2.

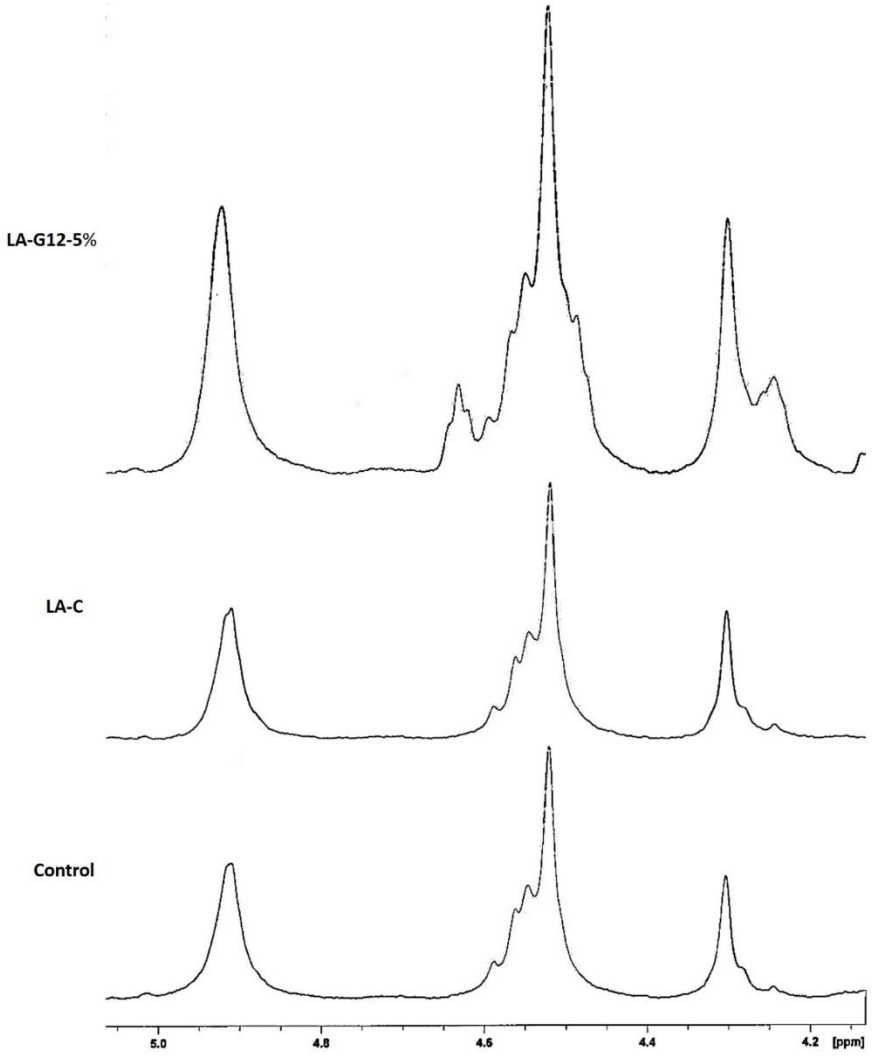

Figure 3.2. The effect of functionalization chemistry (LA-C) and peptide coupling (LA-G12-5%) on the anomeric proton region of the alginate spectrum (Control).

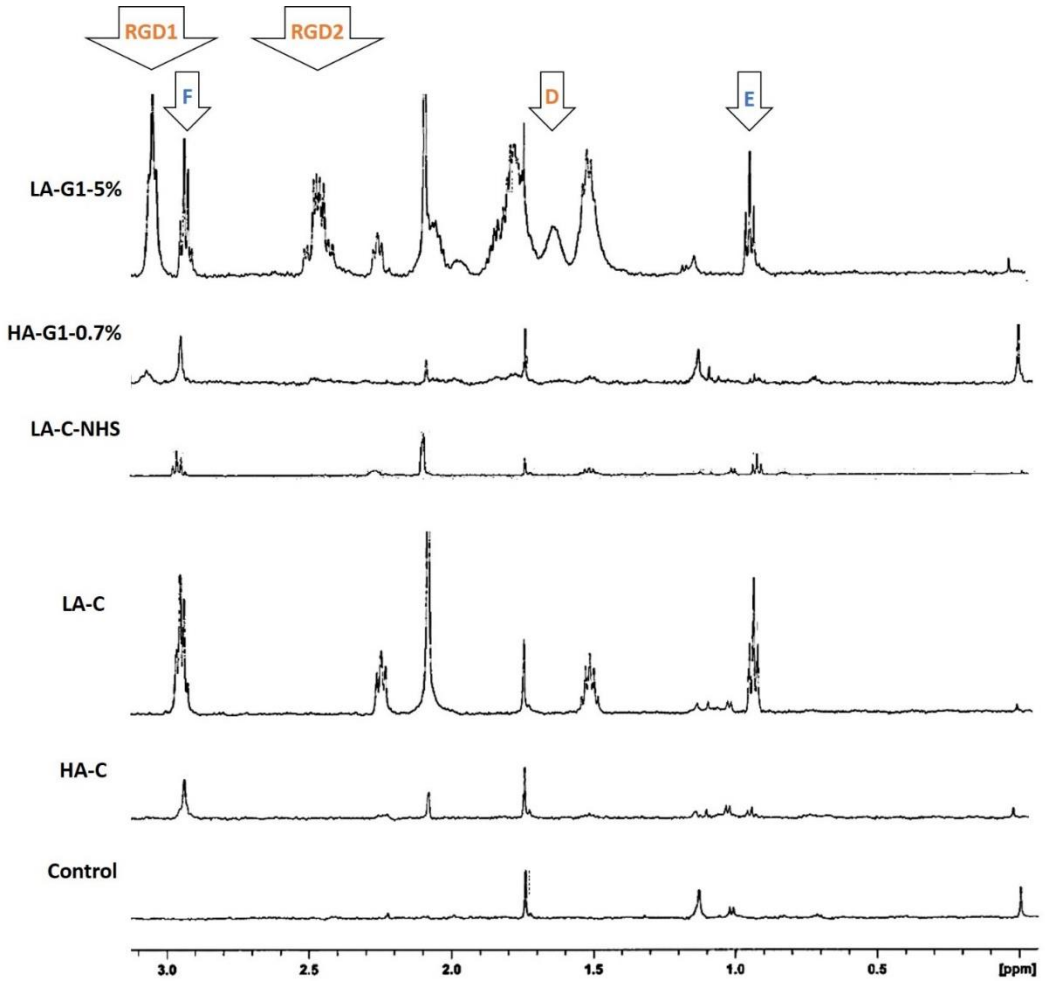

Figure 3.3. The effect of functionalization chemistry (HA-C, LA-C, LA-C-NHS) and peptide coupling (HA-G1-0.7%, LA-G1-5%) on the upfield portion of the alginate (Control) ^{1}H NMR spectrum. The relevant peaks for analysis have been marked with arrows corresponding to the nomenclature in Figure 3.1. The orange labels refer to RGD peaks while blue labels refer to N-acylurea peaks.

As can be seen in Figure 3.2, the ^{1}H NMR spectrum generated for the anomeric proton region of the alginate control (unfunctionalized) is consistent with what has been reported in literature (see Figure 1.9 for structural analysis of unfunctionalized alginate) [87]. There is no difference to the spectrum in the control

chemistry conditions (LA-C, LA-C-NHS, and HA-C), yet there is a significant degree of peak overlap between alginate and peptide peaks for the peptide coupled conditions. This illustrates the utility of using an internal standard for quantification purposes, as if the functionalization process affects the pertinent spectral regions of alginate, accurate integration becomes tricky at best even with advanced deconvolution software. A wide variety of internal standards have been commercially developed, although many additional substances could be used as well as long as they do not interact with the sample or solvent, do not overlap with the relevant portions of the ^{1}H NMR spectrum, are of a known purity, and are not volatile to a significant degree [118]. Therefore, with the proper choice of standard, the internal standard approach provides a high degree of versatility since it enables highly accurate quantification analysis for any type of coupled species to alginate.

Figure 3.3 shows the successive effects of functionalization chemistry and peptide coupling to the upfield portion of the alginate ^{1}H NMR spectrum. Interestingly, it can be seen that a larger degree of side products are coupled to the alginate in the LA-C condition relative to the HA-C. This can be related to the increased amount of sulfo-NHS in the HA-C, as enough sulfo-NHS is added to stabilize over 150% of the activated carboxylic acid groups in the HA-C versus 50% in the LA-C. Importantly, this limits the amount of N-acylurea that can form, as evidenced qualitatively by the significantly reduced peak size of peaks E and F in the HA-C. To confirm this, the LA-C-NHS condition was synthesized, boosting the amount of

sulfo-NHS in the LA-C to match that in the HA-C while maintaining the same EDC activation level. This reduces the amount of N-acylurea present by over two-thirds the original amount, as shown quantitatively in Table 3.2. This observation is as expected from a mechanistic point of view because sulfo-NHS attacks the unstable intermediate O-acylisourea. This removes the problematic urea derivative while maintaining an electrophilic carbon that can be attacked by a primary amine. Therefore, an increased number of sulfo-NHS stabilized reactive intermediates should reduce the amount of N-acylurea that is produced, as is shown here.

With regard to peptide coupling, Figure 3.3 shows two selected conditions, HA-G1-0.7% and LA-G1-5%, representing the conditions with the lowest and highest yields, respectively. The HA-G1-0.7% condition shows slight spectral changes when compared with the functionalized controls, yet these differences are accentuated dramatically in the LA-G1-5% alginate. Figure 3.4 shows a magnified version of the HA-G1-0.7% spectrum to allow for a more accessible comparison of the peaks. Notably, the peak labeled “D” was used for quantitative purposes, and it corresponds to the two gamma protons found in arginine, indicating successful functionalization. This peak is easily integrated using deconvolution algorithms present in most ^{1}H NMR analysis software. While other peptide peaks could be isolated from the alginate and side product peaks, they tended to provide less consistent results or were overlapping peaks consisting of signals from multiple proton sources. Care was not taken to optimize the analysis required to use these peaks quantitatively.

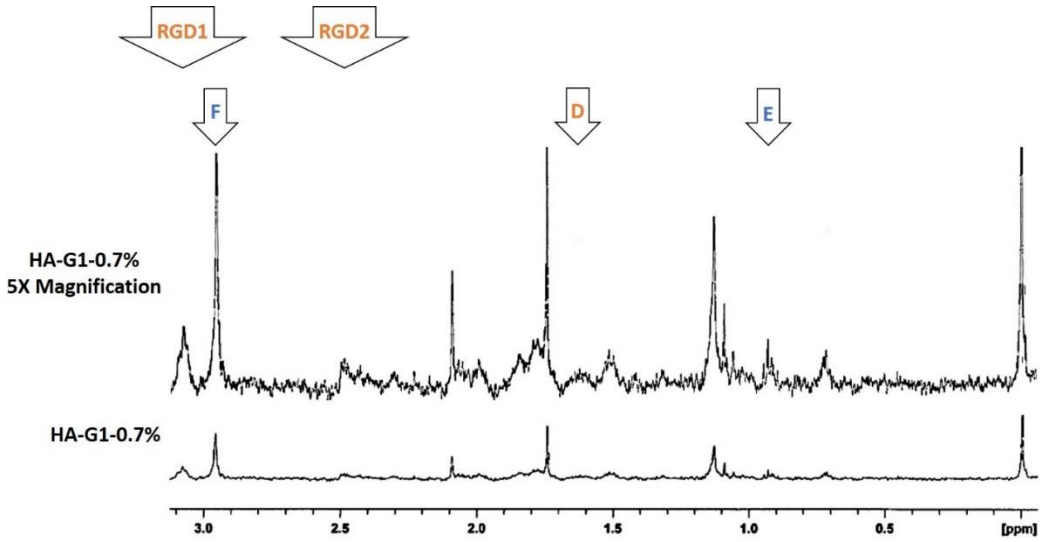

Figure 3.4. A magnified ^{1}H NMR spectrum for the HA-G1-0.7% condition.

Table 3.2 summarizes the peptide coupling percent, reaction efficiency, and mass percent of N-acylurea coupled to the alginate, while Figure 3.5 provides a graphical representation of this data. With respect to efficiency, it is clear that the most significant parameter investigated in this study is the chemistry utilized for the coupling. LA chemistry provided a more optimal reaction in terms of efficiency. Each of the LA conditions had a higher percent yield than their high activation counterparts. Importantly, the LA yields seem to mirror that of the original studies by Rowley, adding further credence to using an internal standard for quantification purposes. When using the peptide G_1RGDY, Rowley found a maximum efficiency of approximately 80%, which is comparable to the 75% efficiency seen in the LA-G1-5% condition [71]. In later studies, when using the peptide G_4RGDY, Rowley reported a drop in the yield to approximately 60%, which is comparable to both LA-G12 conditions in these experiments [61].

Table 3.2. Summary of peptide coupling percentages, percent yields, mass percents, and N-acylurea coupled to the alginate backbone for the different functionalization conditions examined.

Condition	Coupling %	% Yield	RGD Mass %	N-Acylurea Mass %
HA-C	-	-	-	0.06
HA-G1-0.7%	0.05	11	0.17	0.03
HA-G1-5%	0.49	14	1.52	0.01
HA-G12-0.7%	0.12	23	0.8	0.09
HA-G12-5%	1.16	31	7.06	0.03
LA-C	-	-	-	0.72
LA-C-NHS	-	-	-	0.22
LA-G1-0.7%	0.3	61	0.93	1.49
LA-G1-5%	2.53	75	7.37	0.87
LA-G12-0.7%	0.34	62	2.14	1.06
LA-G12-5%	2.18	59	12.43	0.82

Additionally, after an initial peak in activity at around 10% activation, Rowley saw a drop in yield with increasing carboxylic acid activation level [71]. This trend is consistent with the data seen here, where 80% activation with EDC resulted in a significantly diminished yield when compared to 5% activation. This phenomenon, while counterintuitive at first, can likely be explained by the synthesis protocol used. A one-pot synthesis technique was employed, with sulfo-NHS added first, followed by EDC and peptide. Only about 2 minutes were taken between adding the EDC and peptide, and as such, some of the EDC could have activated the carboxylic acid group present on the peptide (e.g. the peptide C-terminus or aspartic acid side chain). This could create strings of peptides, peptides attached to the alginate in unintended orientations, or the peptide could bind to itself due

to an intramolecular reaction with a nucleophile present within the peptide (e.g. the primary amines located at the N-terminus or arginine side chain). Two-thirds of these options incapacitate at least one peptide, and this would probably be exasperated as the level of EDC activation increase. Therefore, an improved chemistry could most likely be produced by finding the optimal time to react the EDC/sulfo-NHS with alginate before adding the peptide. This provides other advantages as well since the optimal level of EDC activation occurs at a different pH from that of amide formation, so a two-step process would enable the opportunity to adjust the pH of the reaction mixture [106].

As previously mentioned, the increase in N-acylurea formation in the LA versus the HA chemistry is likely related to the different ratio of sulfo-NHS:EDC used between the two conditions. Increased sulfo-NHS stabilization is able to reduce the side product formation to less than 0.1% by mass, although it is worth noting that at such a small quantity, the signal to noise ratio is low and thus analysis via NMR is prone to error. That being said, the trend is clear and assesses the benefits of sulfo-NHS stabilization. It would have been interesting to try a peptide coupling condition with LA chemistry and high sulfo-NHS stabilization to investigate the effect on efficiency, although this was not explored further in these experiments.

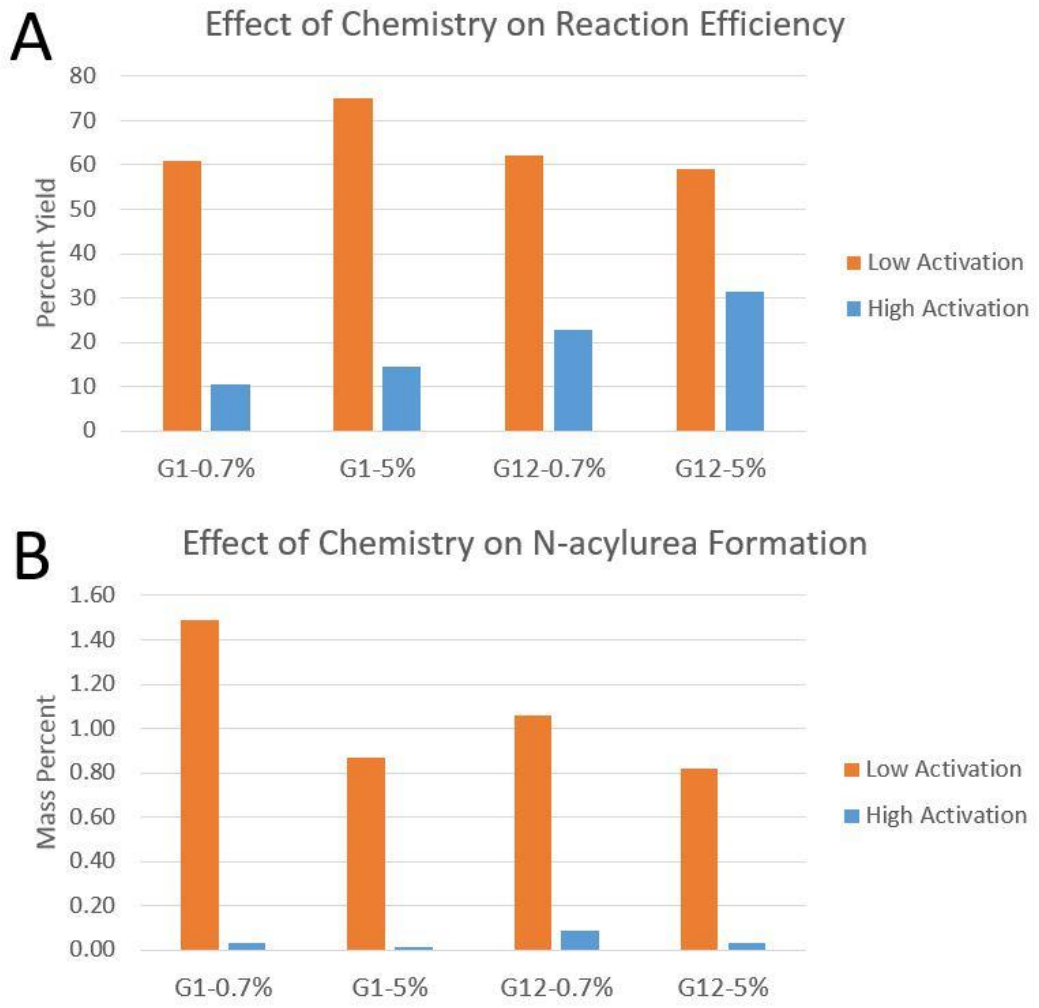

Figure 3.5. Effect of chemistry on reaction efficiency and N-acylurea formation for the 8 different peptide coupling conditions examined.

Overall, there does not seem to be a dramatic change in reaction efficiency with peptide loading concentration. This is consistent with the results reported by Rowley and associates, as they describe a linear relationship between input and incorporated peptide that is consistent over 5 orders of magnitude [71]. Importantly, this trend is reported on a log-log plot, so any minor variations in efficiency between peptide loading concentrations are difficult to discern. With respect to

the data seen in these experiments, three of the four different peptide coupling conditions (HA-G1, HA-G12, and LA-G1) had slightly higher efficiencies at the 5% loading condition, but these increases are slight and are most likely within the error affiliated with NMR processing and batch to batch variation. Here, it is important to note that due to cost and time constraints, each functionalization reaction was performed only once. However, these experiments provide a good foundation for the trends seen and can be validated further if a more precise efficiency is desired at a particular set of conditions.

With respect to N-acylurea formation, higher peptide loading resulted in less N-acylurea formation in all cases. This trend makes sense from a mechanistic point of view, as the reaction with primary amines constitutes a competing reaction to the N-O rearrangement in N-acylurea formation. Therefore, a higher degree of peptide loading should convert more reactive intermediates into amide bonds instead of urea derivatives, as is seen here.

A clear relationship for peptide spacer arm length and peptide coupling efficiency is not as evident. As previously mentioned, at the 5% peptide loading condition, the LA chemistry seemed to mirror Rowley's results, which ranged from spacer arm lengths of one to four glycine units. At 0.7% peptide loading, the reaction yield is virtually identical between the two spacer arm conditions. The HA chemistry exhibited the opposite trend, with the longer spacer arm showing higher efficiency in both loading concentrations. This trend is most likely the product of a number of factors. Interestingly, it was observed that solutions made with G_{12}RGDSP

tended to foam if mixed vigorously, although if mixed carefully, this foaming did not occur. Therefore, we hypothesized that a longer glycine spacer arm makes the peptide act like a surfactant, with the charged RGDSP motif acting as a hydrophilic head and the twelve unit glycine spacer acting as a hydrophobic tail. This would result in the peptide undergoing self-organization into a micelles. To test this conjecture, dynamic light scattering (DLS) was performed at different G_{12}RGDSP concentrations, as is shown in Table 3.3.

Table 3.3. Summary of dynamic light scattering data for the G_{12}RGDSP peptide over three different concentration ranges.

Peptide	Concentration (mg/mL)	Average Diameter (nm)
G_{12}RGDSP	11	164 ± 4
G_{12}RGDSP	5	281 ± 4
G_{12}RGDSP	3	309 ± 11

The diameters reported in Table 3.3 are each the average of three scans conducted at constant temperature. Additionally, the samples were filtered to remove dust and sonicated for 5 minutes before testing in order to ensure any physical aggregates were broken up. DLS calculates a hydrodynamic diameter, which is the diameter of a sphere with equivalent diffusional properties to the particles in solution. Thus if the actual shape of the colloidal particles are unknown, this test can only provide a general sense of size instead of the "true particle diameter." Three different concentrations were used in order to pinpoint the general concentration at which an accurate particle size could be calculated.

When the sample concentration is too high, the particles' Brownian motion will be affected, and this has implications on how the hydrodynamic diameter is calculated.

The average hydrodynamic diameter of G_{12}RGDSP begins to level off around 300 nm. In an unperturbed state, the root mean square (RMS) end-to-end distance of this 17 amino acid peptide can be estimated to be in the range of 2.2-4.7 nm [129]. When converted to a radius of gyration, this corresponds to a distance of approximately 12 nm [130]. Although these calculations are rough approximations, the diameter of gyration would only be 24 nm, which is over an order of magnitude less than that predicted by DLS. Thus the colloidal diameter is much larger than the length of a G_{12}RGDSP peptide, indicating that self-organization is most likely occurring. Although the shape of the resultant colloidal particle remains unknown (e.g. spherical micelle, vesicle bilayer, etc.), this most likely has implications with respect to the availability of the functional groups pertinent to the peptide coupling reaction. Therefore, the colloidal self-assembly of the G_{12}RGDSP peptide, in tandem with additional factors such as EDC activation level, could explain the varying trends seen with respect to reaction efficiency. For example, if a significant side-reaction is the coupling of COOH groups on the peptide with amine groups, such self-assembly would limit access by confining these functional groups to different domains of the micelle (e.g. amine in the core, COOH in the corona). The prevention of these side reactions could lead to the improved yields observed with the G_{12}RGDSP peptide.

To further complement these results, DLS analysis of G_1RGDSP at 3 and 5 mg/mL did not generate a meaningful signal. This, and the fact that the G_1RGDSP solution did not foam, indicates that the smaller peptide did not possess surfactant-like properties and was not forming larger colloidal particles. This further supports the above hypothesis.

In future studies, it would be important to validate these functionalization results with additional replicates, and it would be interesting to see if the shape of the "colloidal peptide" changes as the spacer arm length, spacer arm chemistry, or peptide loading concentration changes (e.g. from spherical micelle to cylindrical micelle, etc.), as this could also affect factors such as reaction efficiency.

All in all, these ^{1}H NMR results speak to the interplay between the many different and competing reactions that occur throughout functionalization [131]. This highlights the nature of the kinetically driven reaction dynamics and provides clues as to how further optimization can occur. As has been made clear from this study and many others, a host of factors have a strong influence on reaction efficacy, including reactant ratios, pH, NaCl molarity, and the specific peptide used [61,71,107]. From this work, it seems that relatively low levels of EDC activation coupled with excess sulfo-NHS stabilization will provide the highest peptide coupling efficiency and the lowest N-acylurea formation. Further optimization has been proposed with respect to changing reaction temperatures and times. It is important to note that this data is only a small piece of the puzzle. Once the ideal reaction conditions have been identified for a specific system, it will be important

to identify how differences in bulk peptide density over a biologically relevant range affect substrate stiffness, as studies have shown cells to be highly sensitive to the mechanical properties of their environment [16]. Regardless, due to the consistency with established literature, this study suggests that using quantitative ^{1}H NMR with an internal standard is an appropriate technique for assessing alginate substitution levels. To the best of our knowledge, we believe we are the first to use this technique in an alginate system for peptide quantification.

While ^{1}H NMR does provide a wealth of structural information, it does not provide a full analysis on its own. For example, unless a difference in chemical shift occurs, the ^{1}H NMR spectrum does not indicate orientation of bound peptide. Therefore, if the RGD peptide attacked the sulfo-NHS stabilized reaction intermediate with a different nucleophile than the N-terminus (e.g. from the arginine or aspartic acid side chains) and thus was bound differently to the alginate, it would be difficult to discern from a simple ^{1}H NMR experiment, although it could have dramatic effects with respect to cell-binding efficacy in biological experiments. Additionally, the reaction is quenched with hydroxylamine hydrochloride, which can attack any unreacted intermediates, resulting in a hydroxamic acid. Similar to the carboxylic acids native to alginate, this simple weak acid is still able to chelate metal ions, yet both of its protons are acidic, making it a poor species to investigate with ^{1}H NMR [132]. One of the mechanistic pathways for the EDC/sulfo-NHS reaction goes through an anhydride intermediate, which also cannot be seen using proton NMR. Alternative spectroscopic methods, such as FTIR, Ramen spectroscopy, or ^{13}C

NMR, would provide both complimentary and corroborating evidence to the NMR analysis done here by providing insight into the relative abundance of particular functional groups that cannot be appropriately analyzed using ^{1}H NMR. Preliminary experiments with FTIR were performed, although they were inconclusive (data not shown).

An additional limitation of quantitative NMR is the high detection limit that this technique possesses. As such, relatively concentrated samples are required to generate a meaningful signal that can be analyzed accurately. As seen in Table 3.2, the HA-0.7% conditions expressed a relatively small degree of coupling, and this resulted in the signal to noise problem shown in Figure 3.4. The peaks of interest, denoted “D” and “E,” are barely above the noise level, ultimately reducing the accuracy of the degree of substitution calculation. Therefore, the values calculated are good estimates of the true degrees of coupling but are likely less accurate than their more highly functionalized counterparts. To enhance the accuracy, more peptide peaks could have been analyzed and subsequently averaged into the coupling calculations. Furthermore, since each chemistry condition was only performed once due to cost and time constraints, batch to batch variation could not be assessed in this study. Finally, it is important to note that during the coupling reaction, the peptide solutions were prepared based on dry peptide weight, but because net peptide content varied from 65-75%, the actual peptide loading level was less than the 0.7% and 5% desired in this study. This was taken into account during efficiency calculations.

3.2 Rheological Analysis of Alginate Hydrogels

At the proper timescales, all materials exhibit solid-like (elastic) and liquid-like (viscous) properties. Rheology is an established technique for studying material viscoelasticity, providing a particularly attractive means of studying hydrogels since they can straddle the line between solid and liquid-like behavior under normal conditions [102,103]. The mechanical properties of alginate hydrogels have been extensively studied, and rheological analysis plays a key role in determining a host of properties relevant to food or biomedical applications [6,8,74,133]. While not an extensive list, rheology can be used either directly or indirectly to find the gel point, time to fully crosslink, frequency dependence, strain response, gel mesh size, creep and hysteresis behavior, and the kinetic profile of the gelation process [8,102]. Therefore, due to the wide variety of tests that can be performed, rheology provides a convenient means of correlating changes in polymer structure with the effects on hydrogel properties.

In this work, the effects of LA and HA chemistry, bulk peptide density, and peptide spacer arm length were examined with respect to the viscoelastic properties of alginate hydrogels. Specifically, time, frequency, and strain sweeps were performed on each of the synthesized conditions in order to provide insight into the gel stiffness, fracture point, gel point, and time necessary to fully crosslink the hydrogels. Ultimately, the goal of this study was to correlate structural changes due to the aforementioned variables, as reported from the ^{1}H NMR analysis in section 3.1, with changes in hydrogel properties. Representative time, frequency,

and strain sweeps from the LA-C-NHS condition are shown in Figure 3.6. The analogous data for each condition is included in Appendix D.

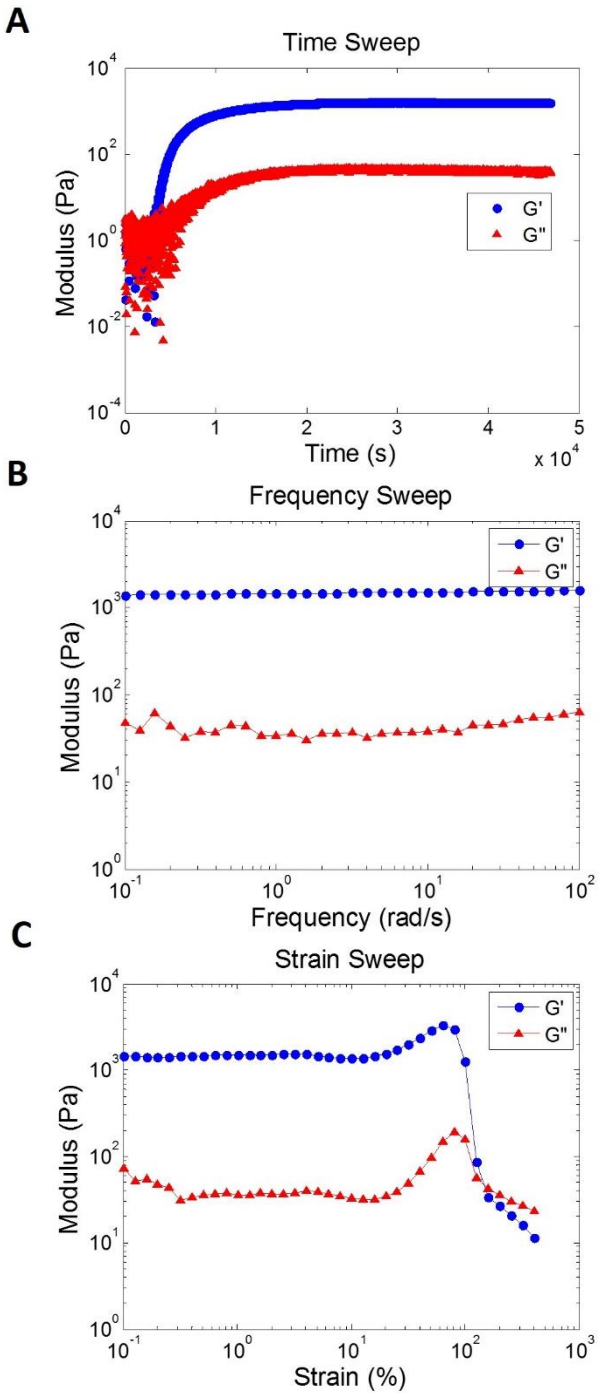

Figure 3.6. Rheological tests performed on alginate hydrogels, where (A) refers to a 13 hour time sweep, (B) refers to a frequency sweep from 0.1 to 100 rad/s, and (C) refers to a strain sweep from 0.1 to 500% strain. These plots are from the LA-C-NHS condition.

Each condition followed the same general behavior as those displayed in Figure 3.6. Figure 3.6A shows a time sweep on a semi-log axis, and it can be broken down into three distinct phases. First, at low times, highly erratic data is seen, indicating a viscous liquid. The loss modulus dominates in liquids, yet as the alginate continues to crosslink, a transition occurs where the storage modulus overtakes the loss modulus. Although not theoretically rigorous, this instant is a decent approximation of the gel point for hydrogels [102,103]. Under certain conditions (e.g. linear flexible polymers), this crossover becomes a very close approximation of the gel point, so following previous work with alginate, this method was used to easily approximate the point at which the polymer network crosslinked sufficiently to be considered a gel [83]. A Matlab script was written to filter out erratic data points from the beginning of the time sweep data to provide better insight into when the G' effectively crossed the G" curve. An example of this filtering can be seen in Appendix D.

The second phase occurs at moderate times, as the G' increases more quickly than the G", indicating progressively more solid-like behavior. Finally, at large times, the moduli exhibit saturation kinetics and stabilize at their respective maximum values, indicative of the final mechanical properties of the hydrogel. This maximum G' value is reported to be the gel's stiffness, and the corresponding time value to this maximum is termed the crosslinking time. Notably, since the G' is over an order of magnitude larger than the G", it can be seen that these gels exhibit primarily solid-like behavior.

Here, it is worth repeating that a $CaCO_3$-GDL system was used in order to control the gelation kinetics. Alginate gels extremely rapidly in the presence of soluble divalent cations (e.g. $CaCl_2$), resulting in non-homogenous gels with gradients in polymer concentration and crosslink density [1]. Yet by using a largely insoluble salt (e.g. $CaCO_3$) that can release calcium ions via controlling the pH (e.g. hydrolysis of GDL), a much slower crosslinking process occurs. This enables the alginate chains to align in a more energetically favorable manner and creates structurally uniform, and thus stronger, gels. The majority of the gels took between 500-600 minutes to fully crosslink, thus exhibiting the desired slow kinetics while creating soft gels that possess biologically relevant stiffness [8]. In the future, the ratio of $CaCO_3$:COOH and $CaCO_3$:GDL could be optimized to provide a balance between gel homogeneity and crosslinking time in order to enhance scaffold compatibility with biological work.

Figure 3.6B shows a frequency sweep over a range of 0.1-100 rad/s, performed immediately after complete gelation (e.g. the experiment reported in Figure 6A). In this experiment, oscillating stress is applied to the gel at increasing frequency. The objective of this test is to determine if the material has viscoelastic properties. Based on the relative magnitudes of G' and G" from the time sweep, it was expected that these gels would respond in a frequency independent manner, as is seen here. This is indicative of a primarily elastic response. The G" tracks the G' quite closely, and this is likely attributable to the water present within the hydrogel. Finally, Figure 3.6C is a strain sweep that ranges from 0.1-500% strain,

performed after the conclusion of the frequency sweep until fracture. The linear viscoelastic region (LVR) extends to approximately 4% strain, after which a significant degree of strain stiffening is seen. This stiffening phenomenon is common in biopolymers and can likely be attributed to a transition from shearing the bulk material to the unfolding of polymer chains, which takes a more significant force input [134]. After a maximum modulus is seen, usually at approximately 80% strain, a precipitous drop-off in mechanical properties occurs. This is indicative of a bulk material failure as the alginate gel is sheared irreparably. A summary of the rheology data acquired from these three tests are shown in Table 3.4 for all conditions.

Table 3.4. Summary of gel stiffness (given by the maximum storage modulus), fracture point (FP, given by the point of bulk gel failure), gel point (GP), and crosslink time (X-link Time) for each condition tested.

Condition	Stiffness (Pa)	FP (Pa)	GP (min)	X-link Time (min)
Control	1020 ± 360	2180 ± 810	55 ± 14	497 ± 38
HA-C	595 ± 76	1040 ± 240	59 ± 9	528 ± 52
HA-G1-0.7%	244 ± 41	483 ± 140	82 ± 7	684 ± 57
HA-G1-5%	460 ± 20	748 ± 230	69 ± 16	669 ± 79
HA-G12-0.7%	231 ± 64	362 ± 85	87 ± 14	628 ± 110
HA-G12-5%	639 ± 64	1130 ± 79	49 ± 11	530 ± 14
LA-C	743 ± 94	1270 ± 420	65 ± 13	448 ± 9
LA-C-NHS	1570 ± 9	3280 ± 220	56 ± 2	513 ± 54
LA-G1-0.7%	781 ± 320	1850 ± 490	59 ± 8	611 ± 66
LA-G1-5%	571 ± 78	1240 ± 210	54 ± 16	533 ± 130
LA-G12-0.7%	679 ± 190	1280 ± 450	50 ± 7	568 ± 110
LA-G12-5%	663 ± 140	1490 ± 34	48 ± 2	611 ± 66

Figure 3.7 shows how gel stiffness and fracture point change with different functionalization chemistries. As expected, the gel stiffness and fracture point data show similar trends. As a note, the LA-C-NHS condition was prepared from a different stock solution of alginate and thus was not compared to the other conditions in the following analyses.

When control conditions (unfunctionalized alginate, HA-C and LA-C) are compared, it can be seen that weaker gels result as more activation is applied. This trend is even more prominent when peptide-functionalized samples prepared with high activation chemistry are compared against those prepared with low activation chemistry. Low activation chemistry leads to visibly higher gel stiffness. This is related with the nature of the functionalization reaction used, and the side reactions involved in EDC/sulfo-NHS chemistry. Carboxylate groups are necessary for cation coordination, yet these same functional groups are removed through the peptide coupling chemistry as the desired amide bond is initiated. Therefore, greater levels of activation will result in fewer remaining carboxylate ions available for coordination and thus weaker gels.

Activated carboxylate groups are highly reactive, capable of generating side products such as N-acylurea, anhydrides, and esters. Not all of the activated groups will result in peptide coupling, but they may still be converted to forms that are unfavorable for complexation. Although the data from the control experiments (e.g. carboxylate groups are activated yet no peptide is added) are within error of each other, the trends indicate that enough structural disruption

occurs to cause a change in mechanical properties. The stiffness of these LA and HA control gels trend lower than that of the unfunctionalized alginate. Furthermore, even though the peptide coupling yield, and hence final peptide density, of the low activation chemistry is higher than that of high activation chemistry, RGD-coupled alginate gels functionalized by the low activation chemistry are stiffer than their high activation counterparts. This means that side reactions that occur in the high activation system also contribute to the prevention of stronger gels by removing carboxyl groups needed for complexation.

Due to the carbodiimde chemistry used in these studies, the activated intermediates can be successfully converted into amide bonds, hydrolyzed back into carboxylic acids, or converted into undesired side products (e.g. N-acylurea, esters). Only hydrolysis regenerates the carboxyl groups that are necessary for coordination purposes, although peptides possess carboxylic acids that could theoretically interact with cations in some capacity as well. Additionally, it is important to reiterate that hydroxylamine hydrochloride is used to quench the reaction after 20 hours, converting any unreacted intermediates into a simple hydroxamic acid. While hydroxamic acids are known to chelate effectively with metal ions, there are important orientation and steric effects to take into account [135]. For example, hydroxamic acids can form N-acids or an O-acids depending on the reaction conditions, and there are a range of resonance stabilized anions based on the particular acid formed; this has implications with respect to how

hydroxamic acids are able to coordinate [132]. Furthermore, while structurally similar to carboxylic acids, the extra nitrogen atom could disrupt the steric organization of polymer chains needed to form specific and strong complexes with calcium ions.

Although the kinetics of reaction intermediate stability were not investigated in this study, a number of studies have explored the mechanism of alginate coordination with metal ions using FTIR. Therefore, subsequent studies could investigate the presence of coupling byproducts (e.g. hydroxamic acids, esters, anhydrides, and N-acylurea) in functionalized alginate and how they impact the efficacy and type of coordination observed [136,137]. This could have a dramatic influence on the bulk mechanical properties, as evidenced by the difference in sterics and coordination between G-blocks, M-blocks, and MG-blocks and how this translates into the G-content largely driving gel stiffness [6,137]. Additionally, it has been shown that raising the pH of the peptide functionalization reaction mixture to greater than 8 will regenerate the carboxyl groups from the sulfo-NHS stabilized intermediates [106]. It would be interesting to try quenching the reaction with this method instead and to compare the resultant gel mechanical properties.

Here, it is worth noting that large error bars are seen on some of the control and low activation conditions. Although outliers were removed using the interquartile range and Tukey fence method, large variation in the data is still seen. This is likely attributed to the fact that these samples were left in solutions of HBSS for a longer amount of time (on the order of 1-2 weeks) than the HA samples before adding

the $CaCO_3$-GDL mixtures to induce gelling. The HA conditions were prepared and tested fresh, and in hindsight, it would have been ideal to test each condition in this manner to prevent the possibility of hydrolysis or bacterial contamination of the alginate chains. That being said, being left for a longer period of time in solution would likely only contribute to decreasing the mechanical properties due to degradation, so the aforementioned trend of decreasing stiffness with increasing activation would likely only be accentuated. Additional variation could result from pipetting the $CaCO_3$ suspension, as despite thorough mixing, it settled quickly. Therefore, small differences in calcium concentration between samples could result and change the degree of crosslinking.

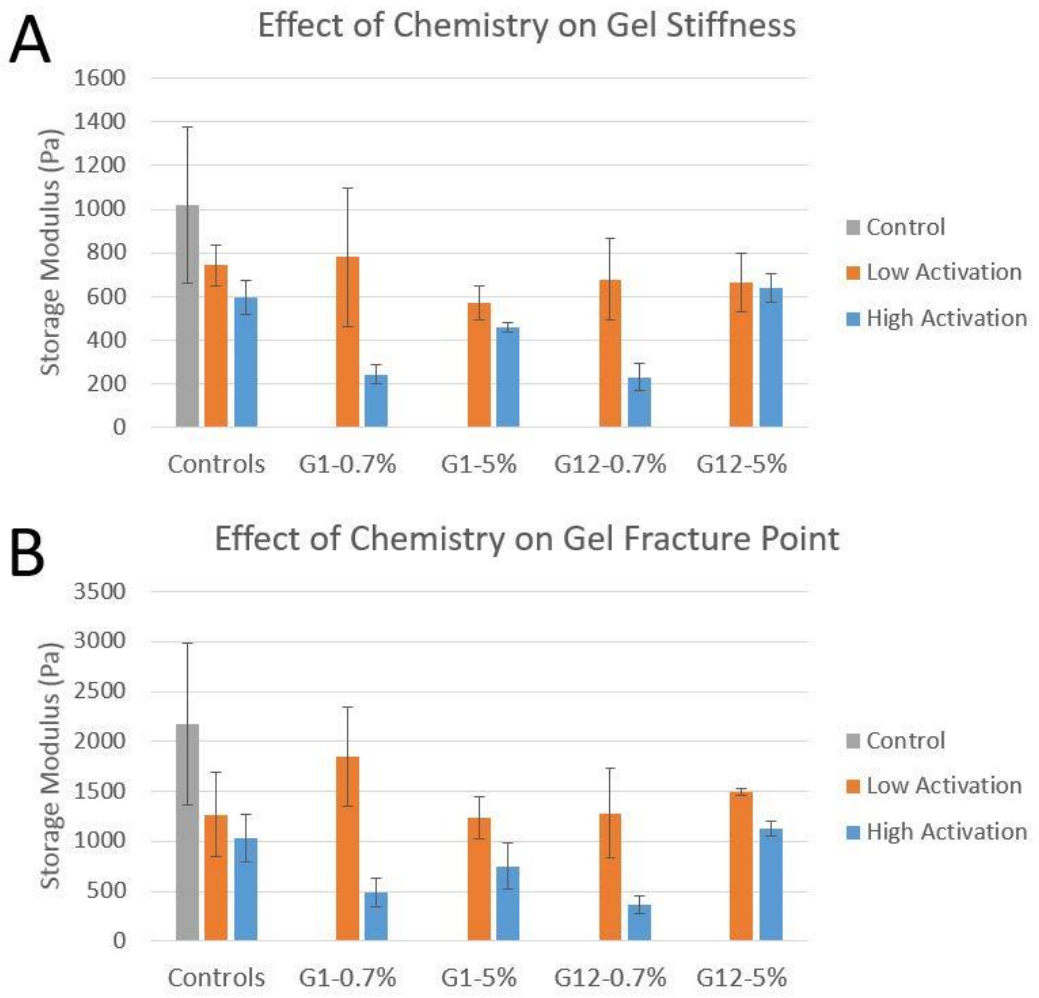

Figure 3.7. (A) Effect of functionalization chemistry on gel stiffness, as identified by the maximum storage modulus obtained via time sweep. (B) Effect of functionalization chemistry on gel fracture point, as identified by the maximum storage modulus obtained via strain sweep, after which bulk gel failure seen.

The data also suggests that coupling peptides to the alginate decreases the mechanical properties relative to the corresponding control conditions. Again, it is difficult to report definitive values from these tests due to the magnitude of the error bars, although the general trend seems to be the same between both

chemistries. This is consistent with what has been reported previously in literature [6,8,79]. A number of theories have been postulated as to why this decrease in modulus occurs, ranging from structural disruptions affecting crosslinking efficacy to differences in hydrophobicity affecting ion exchange [6]. An additional theory provided suggests that the carbodiimide chemistry could result in covalent crosslinking between polymer chains, ultimately impacting network reorganization and causing thermodynamically unfavorable arrangements.

The effects of spacer arm length and peptide loading density are less apparent. Unfortunately, due to the preliminary nature of these experiments with respect to qNMR validation and efficacy assessment of different chemistry formulations, the degrees of peptide coupling and N-acylurea formation are not controlled for between spacer arm conditions. Therefore, it is tricky to make an accurate comparison between corresponding spacer arm lengths since multiple variables are changing. That being said, applying two different loading conditions (0.7% and 5%) does provide a basis for comparing the effect of peptide density on gel mechanical properties. Generally, the data suggests that increased peptide coupling results in stronger mechanical properties for the HA chemistry. This was unexpected, as it was hypothesized that greater peptide coupling would result in weaker mechanics. This can potentially be explained by the aforementioned side reactions argument, indicating that these undesirable byproducts have a greater impact on hydrogel performance than the peptides. For example, less peptide loading could result in a greater concentration of ester or hydroxamic acid

formation thus form weaker gels. A comparable trend cannot be seen for the LA chemistry due to the magnitude of the error bars, placing all conditions within range of each other. Similarly, there appears to be minimal effects of spacer arm length on hydrogel mechanical properties, as with the exception of the HA-G1-5% and HA-G12-5% samples, most conditions are within error of each other.

Next, changes in gelation kinetics were also investigated by tracking the gel point and crosslinking time. These results were obtained from the time sweep experiments and are plotted below in Figure 3.8. Once again, these two factors follow the same tendencies as those observed for gel stiffness and fracture point, although the large margins of error make it challenging to assert any trend conclusively. The control conditions are all comparably within error margins of each other, indicating no significant effect of kinetics due solely to the activation chemistry. Upon addition of peptides, the different conditions tended to take longer to gel and crosslink, with the HA conditions showing a more pronounced increase. This suggests that there is a synergistic disruption of crosslinking kinetics with increased EDC activation and peptide coupling. Compounding upon this argument is that the 0.7% peptide loading conditions tended to take longer to gel and crosslink then their 5% counterparts. Although the majority of these conditions are within error margins of each other, this trend adds more credence to the byproduct-crosslinking disruption hypothesis. Interestingly, previous studies saw no significant effects of RGD on alginate gel point [6]. Finally, spacer arm length did not seem to have a significant effect on kinetics, although the

conditions with a single glycine spacer tended to take slightly longer to gel and crosslink fully.

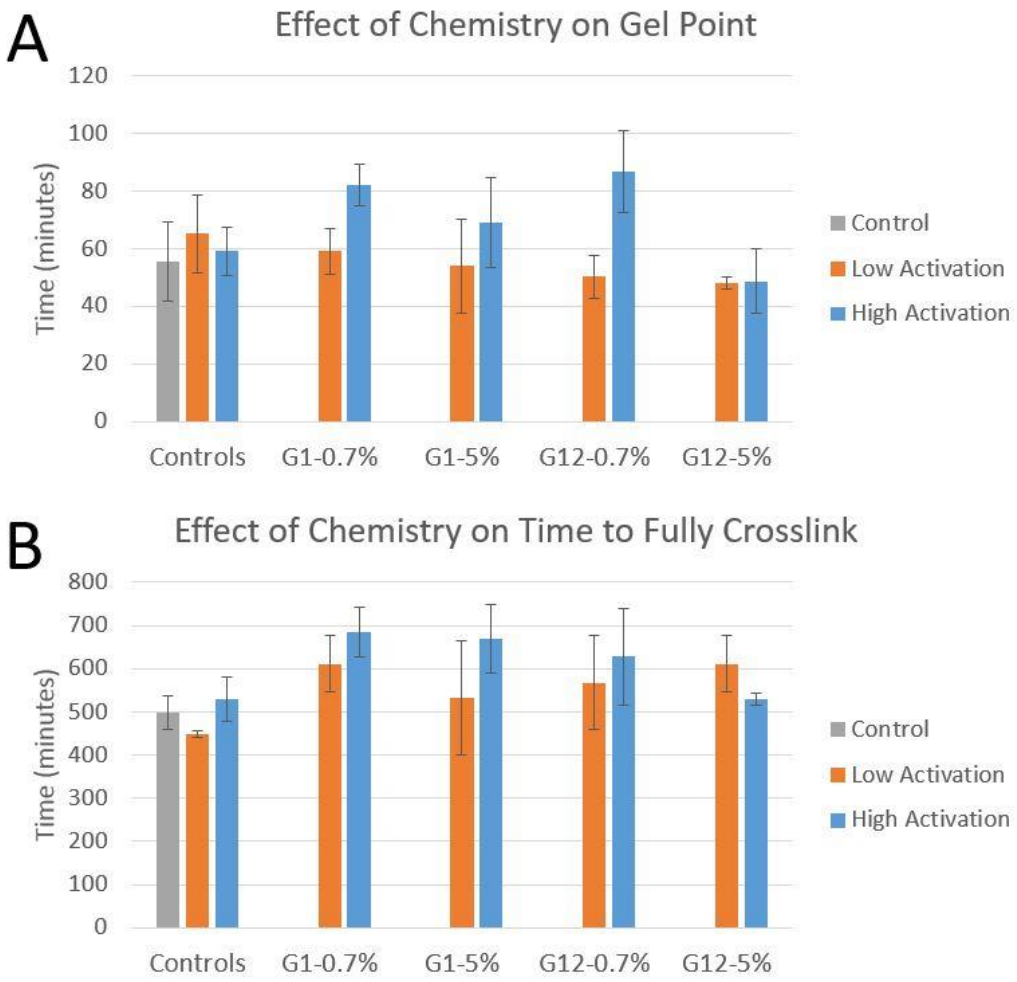

Figure 3.8. (A) Effect of functionalization chemistry on gel point, as identified in time sweep experiments by the crossover point of G' and G" curves. (B) Effect of chemistry on the time to fully crosslink, as identified in time sweep experiments by the point at which G' reached a maximum value.

Overall, this study used rheometry to show the effects of functionalization chemistry, peptide density, and spacer arm length on hydrogel mechanical

properties and gelation kinetics. These gels possess mechanical properties in the range of soft tissues, providing adequate local environments for different cell types, such as neuronal and endothelial cells, as well as embryonic tissues, making them good candidates for further 2D and 3D modeling work [8,46,138]. In tandem with the ^{1}H NMR results, this data suggests a structural disruption of the alginate that inhibits effective coordination with calcium ions. This disruption is likely due to the combination of undesired side products (N-acylurea, esters, and anhydrides) and peptide coupling, as well as the product of the quenching reaction (hydroxamic acids), resulting in weaker gels that take longer to gel and crosslink fully. Therefore, a more extensive investigation using additional spectroscopic methods should be performed to identify the presence of functional groups that could be causing the hypothesized cation coordination interference, whether it be through structural disruption or simply removing sites necessary for cation complexation. Reaction intermediates, such as acid anhydrides, and hydroxamic acids have been identified using FTIR [131,139]. Additionally, different hydroxamated alginates have been synthesized for a variety of applications, such as drug delivery, and characterized using FTIR [140]. Although preliminary FTIR experiments were inconclusive in this study (data not shown), it should be a fairly straightforward method to investigate these conjectures based on previous work cited in the literature. Careful FTIR analysis, Raman spectroscopy, and ^{13}C NMR can be used quantitatively, so these methods could give a sense of the relative abundance of

these species within the alginate and ultimately provide insight into the point at which the concentration of side product causes problematic disruption.

While carbodiimide chemistry is used commonly with different polymers, such as collagen, to create crosslinked networks of varying stiffness, to the best of our knowledge, we are the first to show an effect of the carbodiimide chemistry sans peptide (e.g. HA-C and LA-C conditions) upon alginate hydrogel properties [141]. This has implications in biological work, as this chemistry is clearly changing the alginate in some capacity, ultimately affecting the microenvironment sensed by cells. It is imperative to develop a thorough understanding of the consequences to altering a biomaterial, as this enables researchers to better predict the microenvironmental effects. Additionally, it provides a basis for further optimization as specific features are identified as essential cell-material interaction parameters. This empowers researchers to create scaffolds and 3D models that are able to produce a desired biological response, and most importantly, regenerative solutions to once debilitating problems.

Chapter 4: Conclusions and Future Directions

4.1 Conclusions

This thesis analyzed the effects of carbodiimide chemistry reactant concentrations, ligand loading density, and peptide spacer arm length of G_nRGDSP on reaction yield and hydrogel properties. Of the three primary variables investigated, activation chemistry clearly exhibited the strongest influence on all performance metrics. This highlights the importance of characterization studies and exposes some of the key variables for optimization.

^{1}H NMR was used quantitatively with an added internal standard in order to assess reaction efficiency and byproduct formation. We believe we are the first to use this approach in alginate systems for peptide quantification, and we report highly comparable results to the initial studies by Rowley and associates, ultimately validating this technique. ^{1}H NMR provides a unique versatility with respect to peptide coupling analysis because it simultaneously enables qualitative changes in structure to be compared with quantitative functionalization efficacy calculations. The inclusion of an internal standard allows for increased flexibility within the system, as it permits quantitative analysis even when the ligand of interest has peaks that overlap with the anomeric region of the alginate ^{1}H NMR spectrum.

Low activation chemistry conditions (e.g. 5% activation) exhibited substantially higher peptide coupling yields than their high EDC activation (e.g. 80% activation)

counterparts, with efficiencies between 60-75% versus 11-33%. This can be attributed to the one step synthesis technique used, as EDC most likely reacted with peptide and decreased the yield proportionately. Increasing the level of sulfo-NHS stabilization from 50% to 167% decreased the formation of N-acylurea adducts, as anticipated. Less significant effects were seen with respect to changing peptide loading density. From DLS data, it seems that the G_{12}RGDSP peptide undergoes self-organization into a colloidal species. In tandem with the effects of activation level, this seems to have an effect on the reaction yield, as reaction coupling with G_{12}RGDSP was between 2-3 times more efficient than G_1RGDSP in the high activation chemistry, but this effect was negated in the low activation conditions. Yet since only one functionalization reaction was conducted for each condition, subsequent experiments are required to solidify the trends seen in this investigation.

Rheometry was used to assess the effects of reactant concentration, peptide density, and spacer arm length on hydrogel viscoelastic properties. From time, frequency, and strain sweeps, hydrogel stiffness, fracture point, gel point, and crosslinking time data were obtained. All conditions exhibited saturation-type kinetics through the duration of the time sweep. Primarily elastic behavior was demonstrated upon completion of crosslinking, so all gels were frequency independent. The linear viscoelastic region extended to about 4% strain, after which strain stiffening was seen, followed by a bulk material failure. The fracture point occurred at approximately 80% strain for most conditions.

Again, the carbodiimide reactant ratio proved to be the most significant variable tested in this study. We believe we are the first to decouple the effects of carbodiimide chemistry from the addition of peptides by testing control conditions at each chemistry formulation. In general, increasing activation level tended to decrease hydrogel mechanical properties while synergistically increasing gelation times with peptide coupling. This can likely be attributed to increased structural disruption and thus decreased coordination efficacy with calcium cations, although more studies are needed to explore this hypothesis further.

The trends with respect to spacer arm length and peptide density are less clear due to the magnitude of error bars affiliated with this study, indicating the importance of performing rheometry with fresh, sterile samples.

All in all, the work presented here suggests that the structural modifications to alginate due to carbodiimide chemistry result in altered hydrogel performance. This has key implications in cell-biomaterial interactions and thus on the creation of well characterized synthetic microenvironments that are capable of directing essential cellular processes. For example, beyond gel mechanics (e.g. stiffness or hysteresis effects), the changed hydrogel structure could affect crucial variables for cell survival, such as gel mesh size and thus nutrient transport. Furthermore, additional implications on hydrogel swelling and degradation properties may result, impacting the efficacy of the hydrogel in long term 3D experiments or in *in vivo* work.

4.2 Future Directions

This work aimed to better understand how peptide coupling chemistry affects the structure of functionalized alginate and the mechanical properties of the hydrogels produced from it. Our analysis of the peptide functionalization chemistry showed that higher yields were achieved at lower concentrations of EDC, while side products were minimized at an excess concentration of sulfo-NHS. Our work, however, was limited to a small number of functionalization conditions with no replicates due to the scope and timeline of this study. It would be beneficial to determine the batch to batch variation of these chemistry formulations. Additional studies could identify the optimal concentrations of these reactants in terms of maximizing yield while minimizing byproduct formation. An initial step in this direction would be to increase the amount of sulfo-NHS used in the low activation conditions studied here, and reported in literature, and determine if this would positively impact yield. Taking this a step further, it would be beneficial to study the effects of reactant concentrations more systematically in order to create a set of design rules that provide the means to correlate functionalization chemistry with yield and hydrogel properties. This could provide unique insight in tandem with additional hydrogel characterization experiments, such as mesh size, degradation, swelling, and hysteresis studies.

Another approach to improving the functionalization chemistry would involve modifying the peptide coupling protocol. It has been suggested that a two-step functionalization can result in higher reaction efficiencies since the highest levels

of EDC activation and amide bond formation occur at different pH values [106,107]. While providing the opportunity to create more ideal reaction conditions, this would also allow for the majority of EDC molecules to react with alginate before the peptide is added. This thwarts non-specific reactions with the adhesion ligand from occurring, ultimately increasing the yield. Therefore, it would be beneficial to identify the ideal activation times with EDC and sulfo-NHS before adding the peptide in order to maximize yield while minimizing byproduct formation. Additionally, the quenching reaction, where the unreacted active esters are converted to stable species, can be modified. In this work, quenching was performed by adding hydroxylamine hydrochloride, which generates a hydroxamic acid functional group. Alternatively, carboxylic acids can be regenerated from sulfo-NHS stabilized reaction intermediates by changing pH [106]. Future work could explore how this change would affect the subsequent hydrogel mechanical property and gelation kinetics data.

Consistent with what was previously reported by Rowley, it appears that spacer arm length plays a role in determining reaction efficiency [61,71]. The DLS data indicates that G_{12}RGDSP peptides are self-organizing in solution to some capacity, so future studies could investigate how the size and shape of these micelles impact reaction efficiency. Similarly, it would also be interesting to assess the impact of spacer arm length, chemistry, and ligand concentration on colloidal organization (e.g. shape and size). For example, molecules possessing different hydrophilicities (e.g. PEG or more hydrophilic amino acids, such as serine) could be used as spacer

arms instead of glycine, and the effect on colloidal organization could be investigated. Lastly, there will likely be an optimally sized spacer arm length that maintains high efficiency and biological relevancy while minimizing steric hindrance effects of bulky peptide side groups [107]. Thus, finding the appropriate spacer arm length for different applications and cell types will likely be beneficial.

While the proposed quantitative NMR analysis is highly informative, it can be further improved upon additional studies. It would be advantageous to analyze multiple peaks for RGD and N-acylurea, as this would allow for increased accuracy even at low signal to noise ratios. Additionally, since a number of functional groups cannot be adequately studied via ^{1}H NMR, such as anhydrides, esters, and simple hydroxamic acids, additional spectroscopic techniques should be employed in order to provide a clearer picture as to the structural effects of carbodiimide chemistry on alginate. This will allow for the effects of structural disruption on hydrogel properties to be more completely assessed. FTIR, ^{13}C NMR, and Raman spectroscopy have all been used to study alginate, as well as other carbodiimide chemistry systems, providing a foundation for this analysis [126,131,136,142]. Ultimately, this would enable correlations of calcium coordination efficacy, carboxylate ion removal, and gel mechanics to be determined.

While many of the results presented here provide interesting data from a materials science point of view, introducing cells into the hydrogels could alter many of the reported trends. For example, studies have described the effects of cell concentration on the tensile and compressive moduli of RGD-modified

alginate hydrogels [79]. One such study found that a higher tensile modulus was seen when cells were added to peptide functionalized alginate gels rather than unfunctionalized alginate. This increase in mechanical properties was attributed to cell-material crosslinking at the ligand sites. Therefore, as the effects of peptide coupling on the alginate material are more fully understood, it will be important to provide additional characterization studies to understand how cells alter the three dimensional scaffolding matrix they grow in over time. This could occur through a variety of processes, such the aforementioned cellular crosslinking, as well as through matrix deposition and remodeling. This has major implications on the microenvironments that cells sense and creates more impetus for designing materials that cells can interact with on a fundamental level [96].

Additionally, it will be important to improve the gelation kinetics such that once cells are added, a sufficiently crosslinked gel can be achieved during incubation before the gels are placed into media. If the gels are not sufficiently crosslinked before being placed in media, they will likely degrade at a faster rate due to increased calcium transport. Thus, it will be much harder to control the mechanical properties of the gels due to the interplay between continued crosslinking and increased cation diffusion in conjunction with the presence of cellular alterations. Consequently, the levels of $CaCO_3$ and GDL must be optimized to provide sufficiently fast gelation without compromising gel homogeneity or creating a biologically harmful local pH. This could also be achieved by using smaller $CaCO_3$ particles, as increased surface area facilitates faster dissolution

rates and increased likelihood of acidic attack in $CaCO_3$-GDL systems [97]. Additionally, it will be important to assess the length of time these 3D culture systems can be incubated sans media without reducing cell viability. This data would be complimented well by swelling, degradation, and mechanics studies after different periods of time in media. Although similar studies have been conducted, this information would change from system to system and thus must be investigated [18].

Appendix

Appendix A

UV-Vis was performed on the 0.8 mM solution of nitrobenzene in D_2O in order to validate its concentration for quantitative ^1H NMR experiments. The standard curve generated is produced below, in Figure A.1. After dilution adjustment, the average absorbance of the 0.8 mM sample was 5.26 AU. Using the equation of best fit through the relevant points on the standard curve, the solution concentration is shown to be 0.807 mM in nitrobenzene.

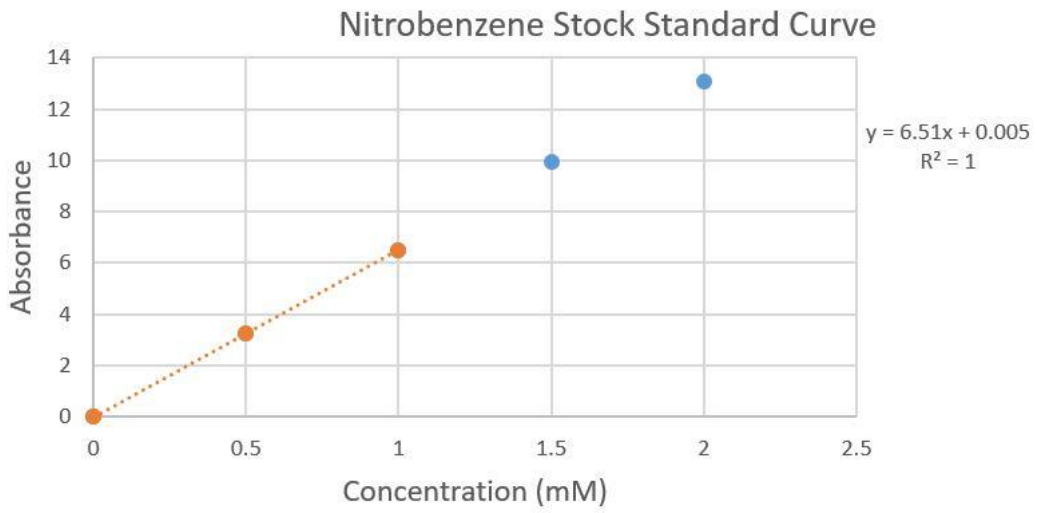

Figure A.9. Standard Curve developed by UV-Vis in order to validate the nitrobenzene concentration doped into D_2O. Samples from 0 mM to 2 mM were made from a 40 mM stock solution.

Appendix B

The degree of coupling of RGD and N-acylurea to alginate can be quantified using ^{1}H NMR on the basis that the signal intensity is directly proportional to the number of protons responsible for generating a particular peak [117]. Below, a sample calculation for the LA-G1-0.7% condition is shown in order to illustrate how reaction efficiency and yield analyses were performed.

Assumptions:

- MW (alginate) ≈ 200,000 g/mol
- MW (repeat unit, alginate) ≈ 185.139 g/mol

QNMR Theory:

$$\frac{n_x}{n_y} = \frac{I_x}{I_y} \times \frac{N_y}{N_x}$$

- n_x = molarity of component x
- I_x = integrated peak area for component x
- N_x = number of protons that peak corresponds to

Sample Calculation:

1. 1H NMR spectrum analysis
    - Nitrobenzene
        - Peak: 7.513 ppm
        - Concentration: 0.807 mM

- Peak area: 2.415
- Number of protons: 2

- RGD
  - Peak: 1.646 ppm
  - Concentration: Unknown
  - Peak area: 0.952
  - Number of protons: 2

$$\frac{n_{NB}}{n_{RGD}} = \frac{2.415}{0.952} \times \frac{2}{2} = 2.54$$

$$2.54 = \frac{M_{NB}}{M_{RGD}} = \frac{0.807\ mM}{M_{RGD}} \rightarrow M_{RGD} = 0.318\ mM$$

2. Find degree of coupling:
   - 1.08 mL of a 20 mg/mL alginate-RGD sample was prepared
   - Note: the calculation for the mass of N-acylurea is not shown, although it is analogous to what is shown here
   - RU refers to alginate monomer repeat unit

$$Mass\ of\ RGD = \frac{0.318\ \mu mols}{mL} \times 1.08\ mL \times \frac{1\ mol}{10^6\ \mu mol} \times \frac{587.613\ g}{1\ mol} \times \frac{1000\ mg}{1\ g}$$

$$= 0.202\ mg\ RGD$$

$$Mols\ of\ RGD = \frac{0.318\ mmol}{1\ L} \times \frac{1\ L}{1000\ mL} \times \frac{1000\ \mu mols}{1\ mmol} \times 1.08\ mL$$

$$= 0.343\ \mu mols\ RGD$$

$$Mass\ of\ alginate = Total\ mass - Mass\ RGD - Mass\ N - Acylurea$$

$$= 21.6\ mg - 0.202\ mg - 0.322\ mg = 21.076\ mg\ alginate$$

$$Mols\ of\ alginate$$

$$= 21.076\ mg\ \times \frac{1\ g}{1000\ mg} \times \frac{1\ mol}{200{,}000\ g} \times \frac{10^6\ \mu mol}{1\ mol}$$

$$= 0.105\ \mu mol$$

$$Degree\ of\ Polymerization = \frac{200{,}000\ g}{1\ mol} \times \frac{1\ mol}{185.139\ g\ RU} = 1080.269$$

$$Mols\ of\ COOH\ groups = \frac{0.105\ \mu mol\ alginate}{1} \times 1081 = \ 113.9\ \mu mol$$

$$DC = \frac{0.343\ \mu mol\ RGD}{113.9\ \mu mol\ COOH} = 0.003 \rightarrow 0.3\%\ coupling\ to\ alginate$$

3. Find reaction yield:

- Theoretical RGD coupling to alginate at 100% yield: 0.00496

$$Yield = \frac{0.00301}{0.00496} = 0.61 = 61\%$$

Appendix C

The ^{1}H NMR spectrum for each condition synthesized is shown below. Note that only the relevant portion for alginate and the RGD peptides are shown.

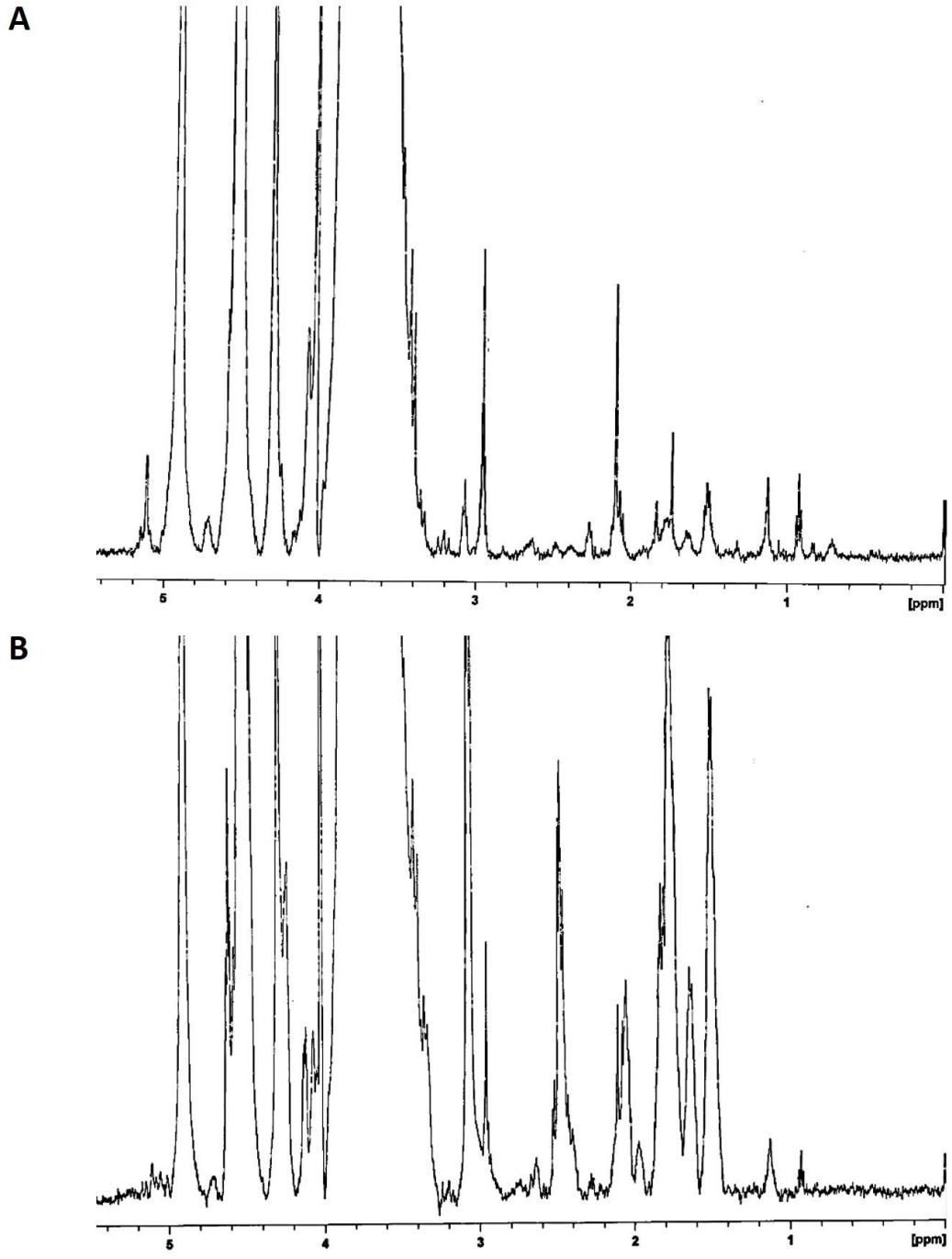

Figure A.10. ^{1}H NMR spectra from the HA-G12-0.7% (A) and HA-G12-5% (B) conditions.

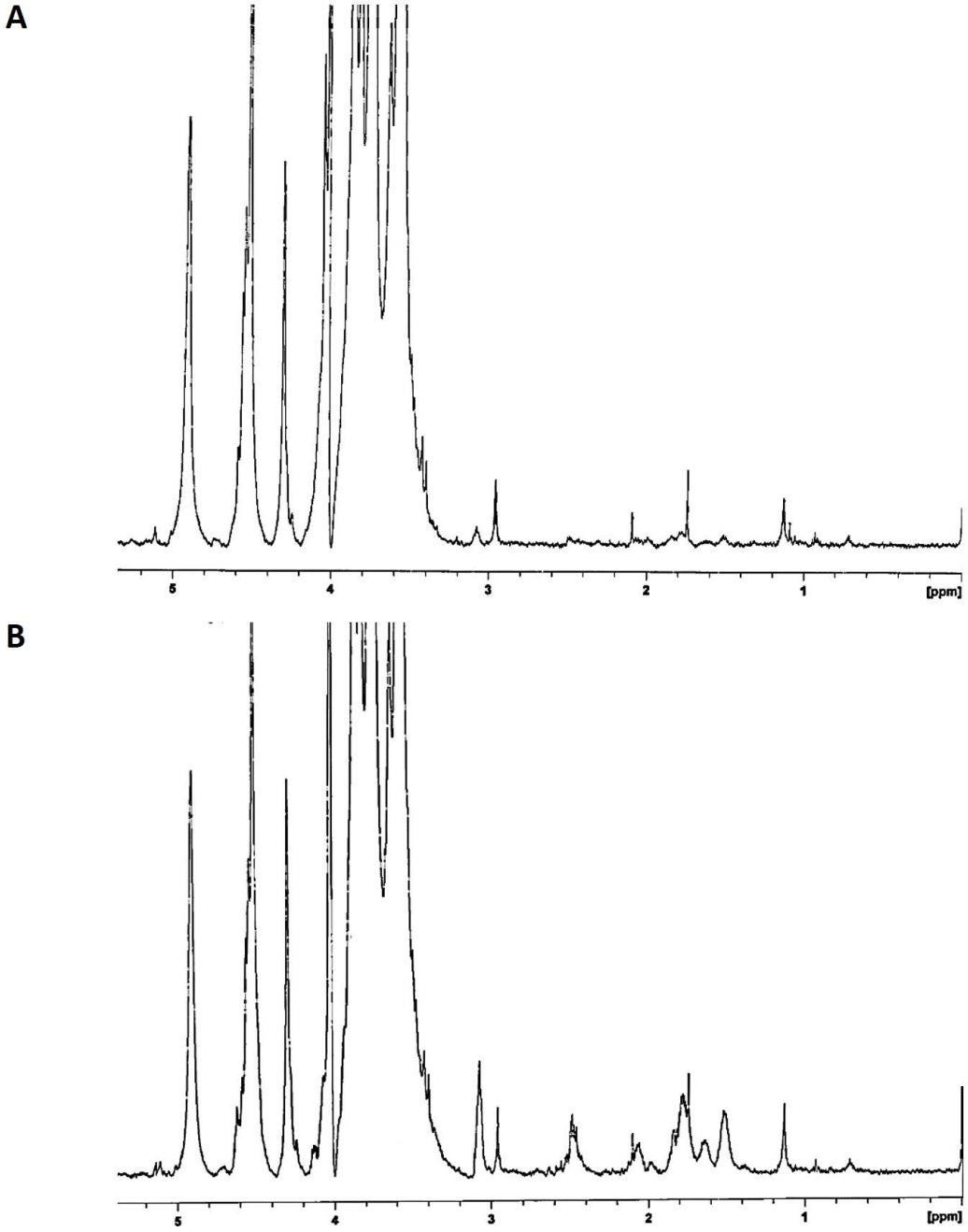

Figure A.11. ^{1}H NMR spectra from the HA-G1-0.7% (A) and HA-G1-5% (B) conditions.

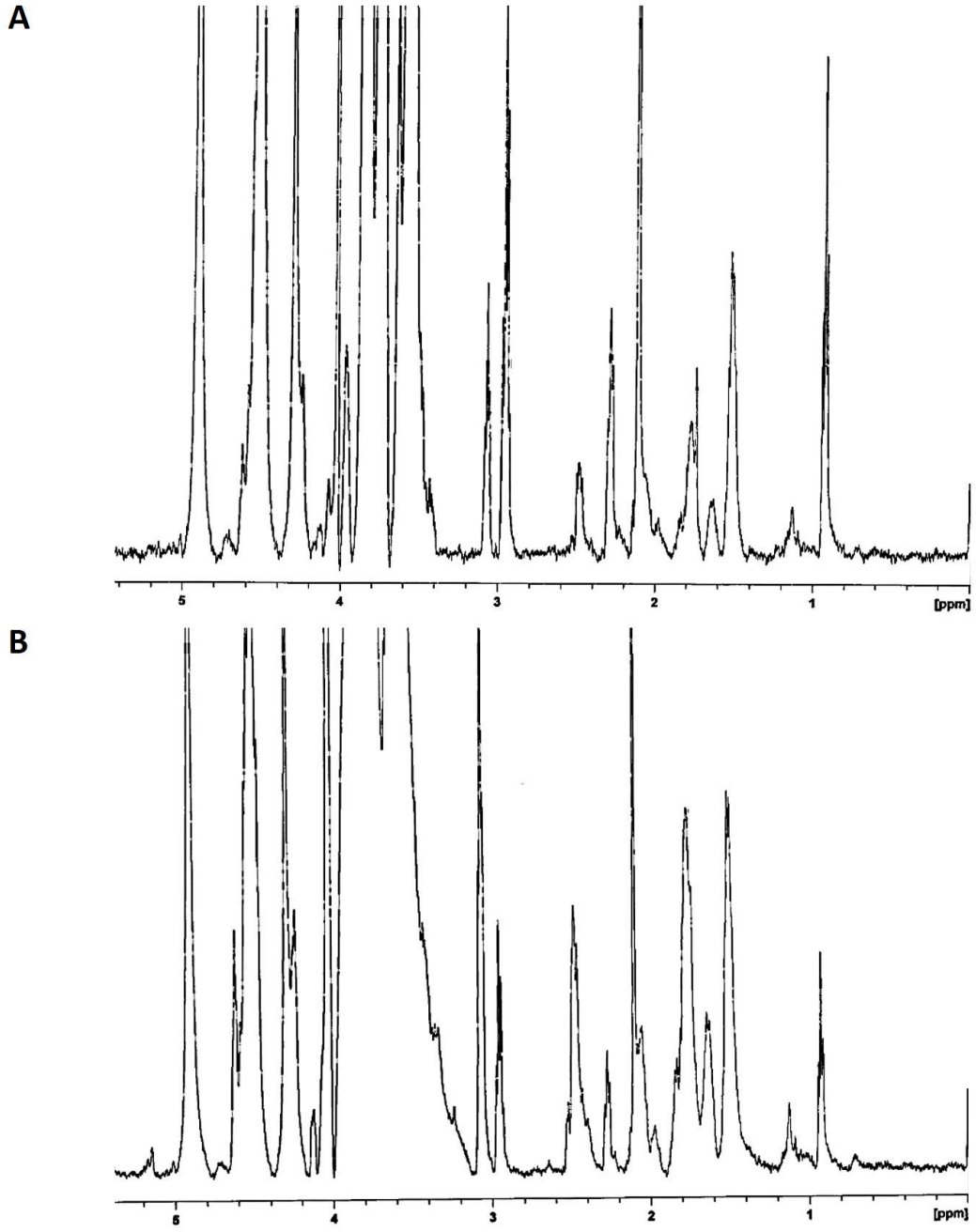

Figure A.12. ^{1}H NMR spectra from the LA-G12-0.7% (A) and LA-G12-5% (B) conditions.

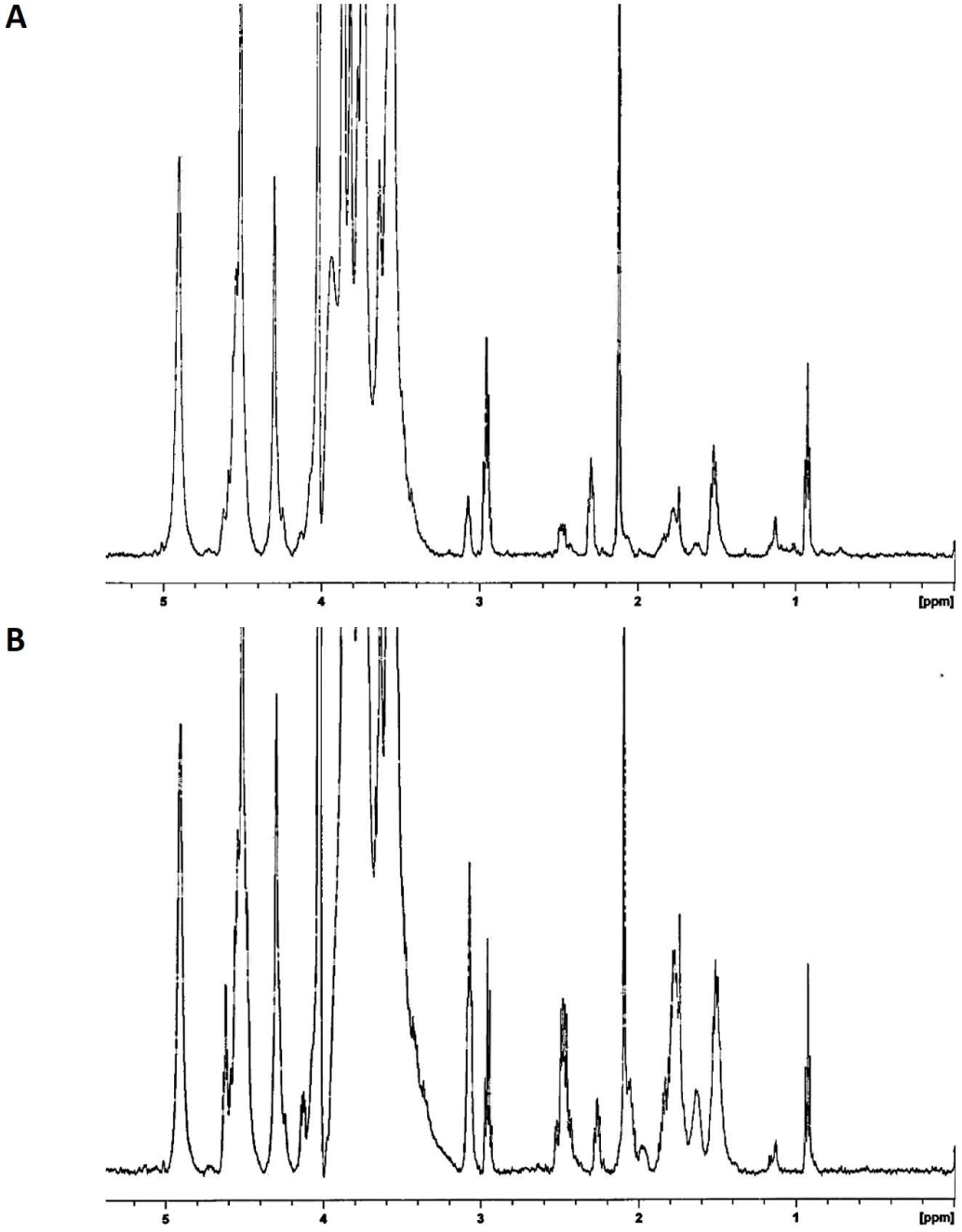

Figure A.13. ^{1}H NMR spectra from the LA-G1-0.7% (A) and LA-G1-5% (B) conditions.

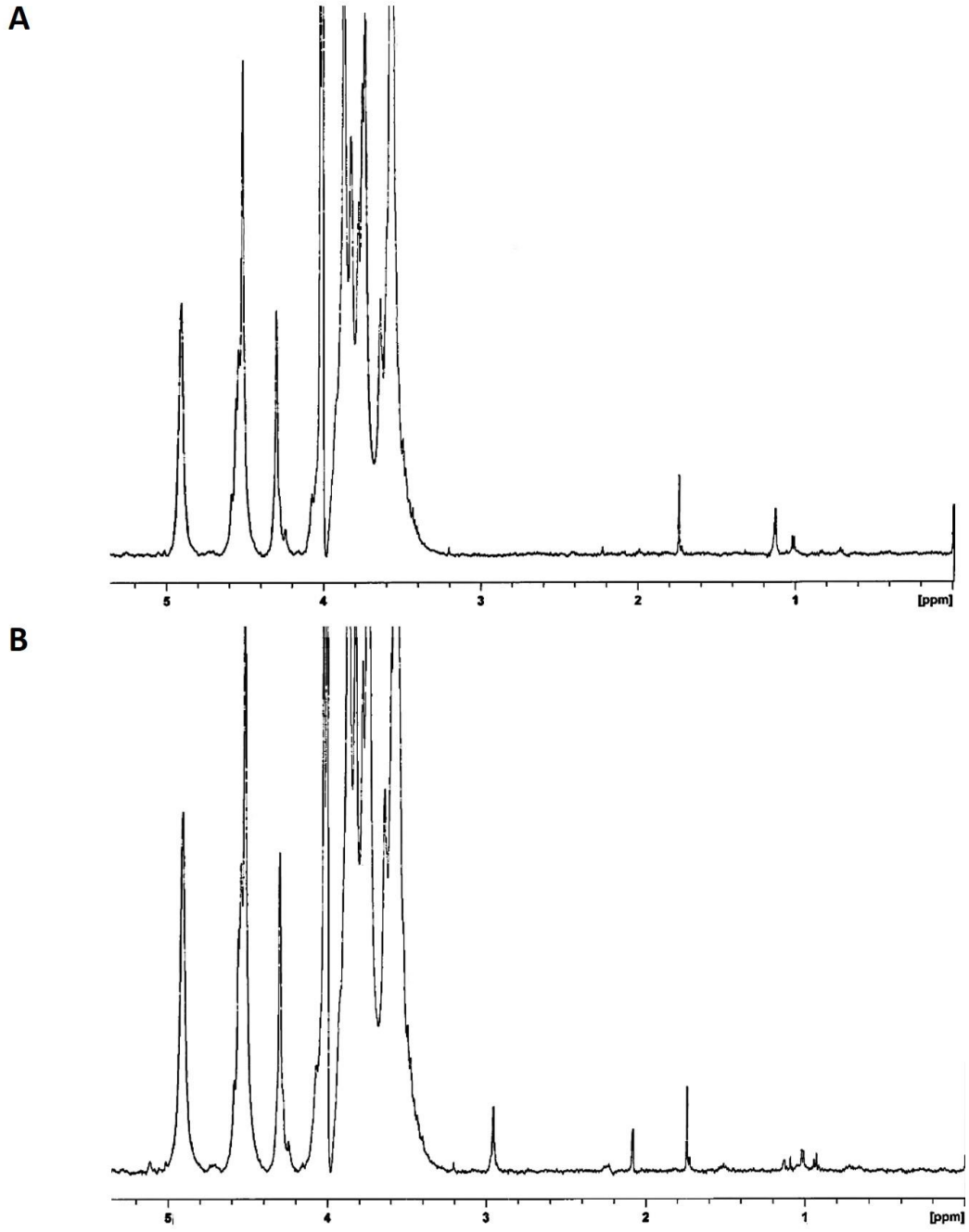

Figure A.14. ^{1}H NMR spectra from the unfunctionalized control (A) and HA-C (B) conditions.

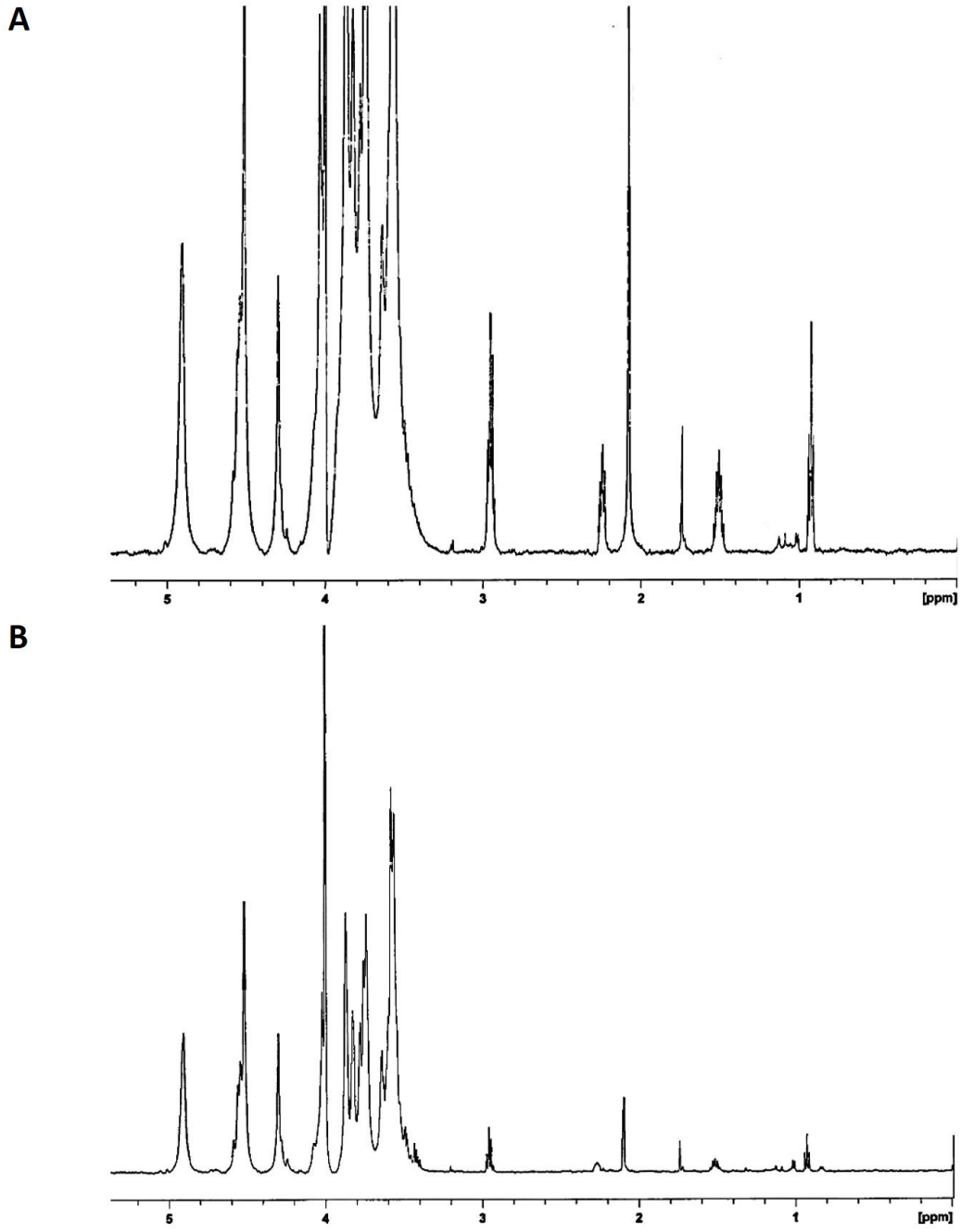

Figure A.15. ^{1}H NMR spectra from the LA-C (A) and LA-C-NHS (B) conditions.

Appendix D

An example of the Matlab filtering function as applied to the erratic pre-gel rheometry data is shown below. Additionally, representative time, strain, and frequency sweeps are graphically displayed for each condition, showing the similarity of general viscoelastic behavior amongst all condition.

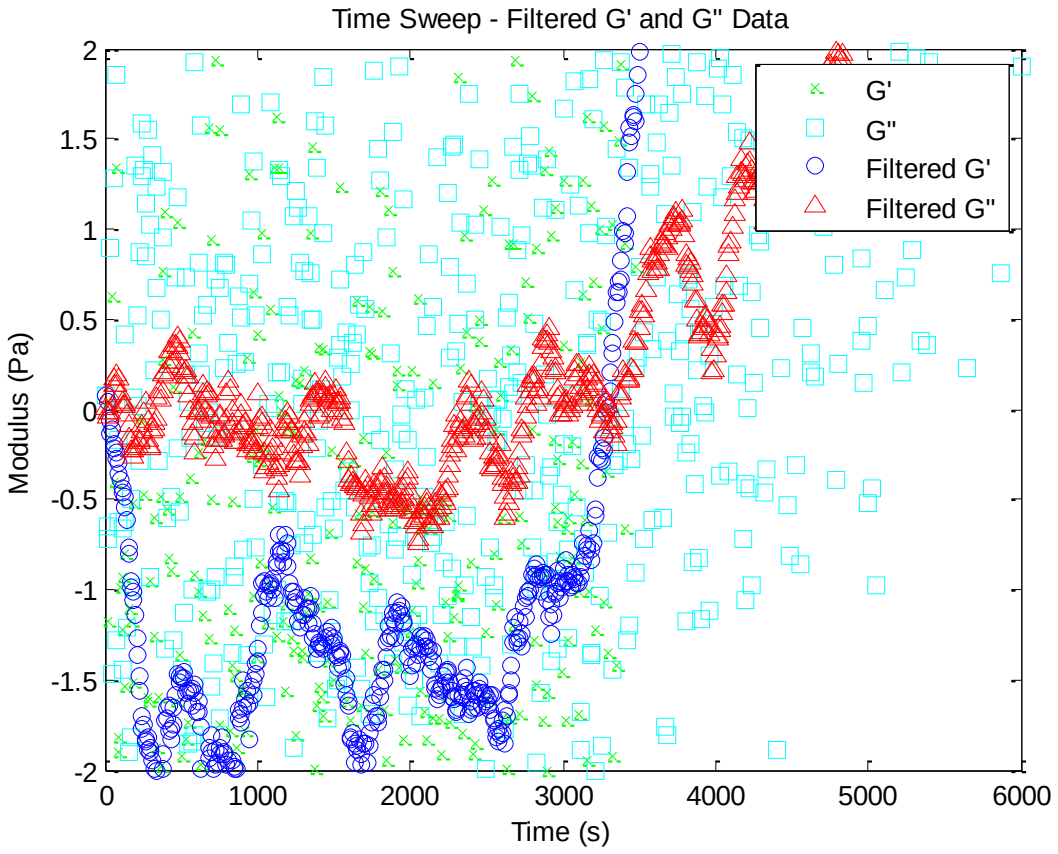

Figure A.16. The beginning of a time sweep for the LA-C-NHS condition. The true G' and G" data are shown, as are the filtered data. The crossover point of the filtered G' and G" curves is indicative of the gel point.

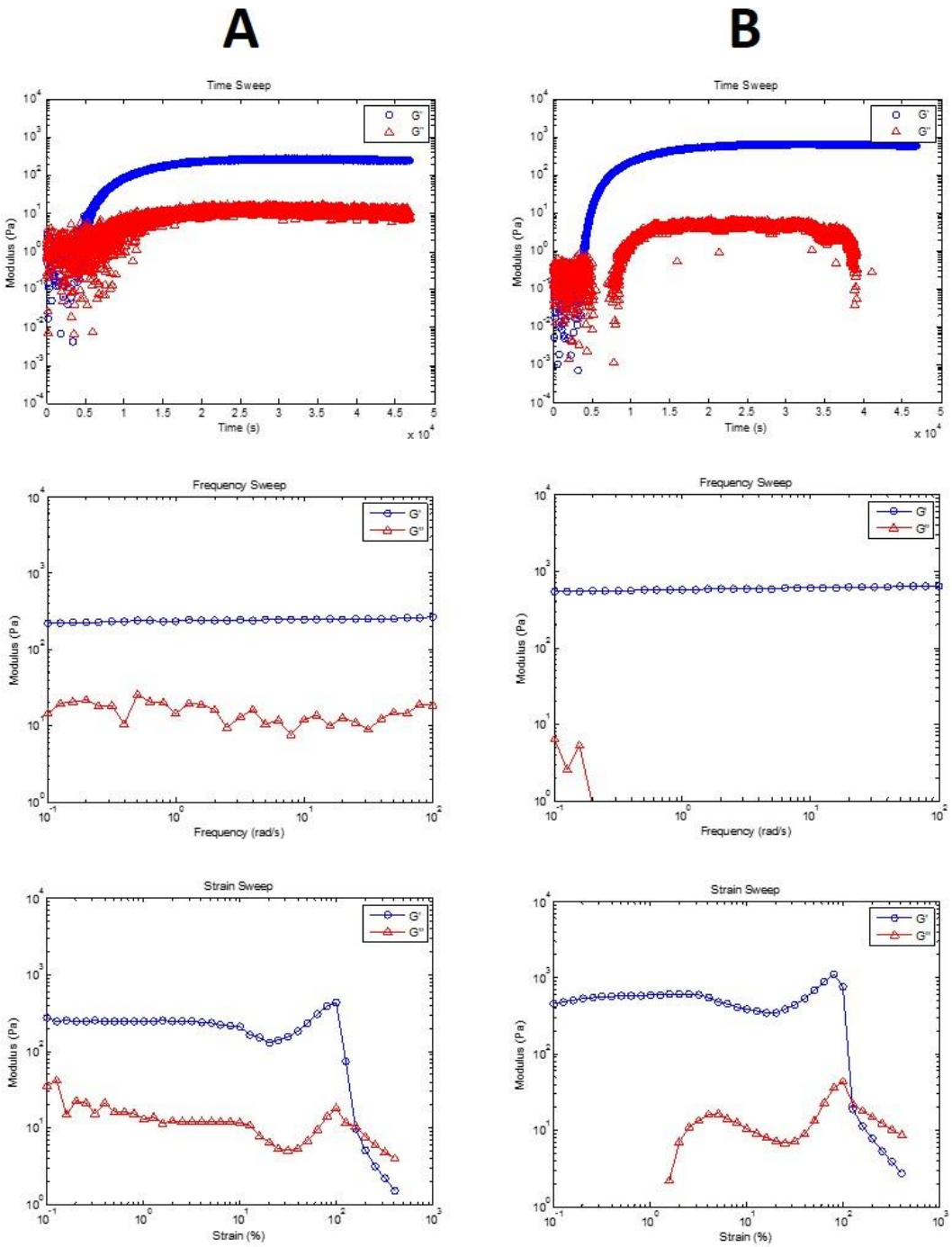

Figure A.17. Representative time (top), frequency (middle) and strain (bottom) sweeps for the HA-G12-0.7% (A) and HA-G12-5% (B) conditions.

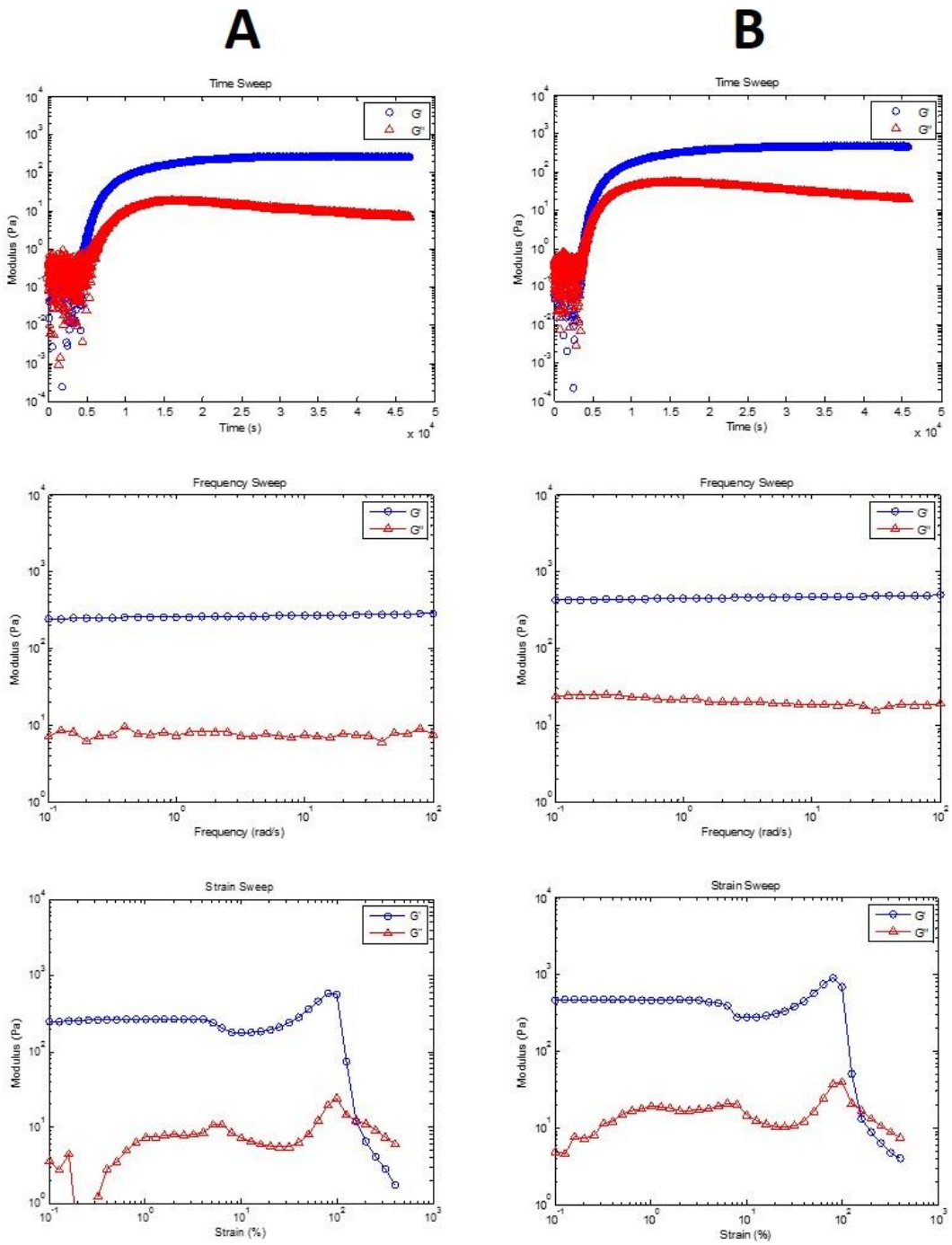

Figure A. 18. Representative time (top), frequency (middle) and strain (bottom) sweeps for the HA-G1-0.7% (A) and HA-G1-5% (B) conditions.

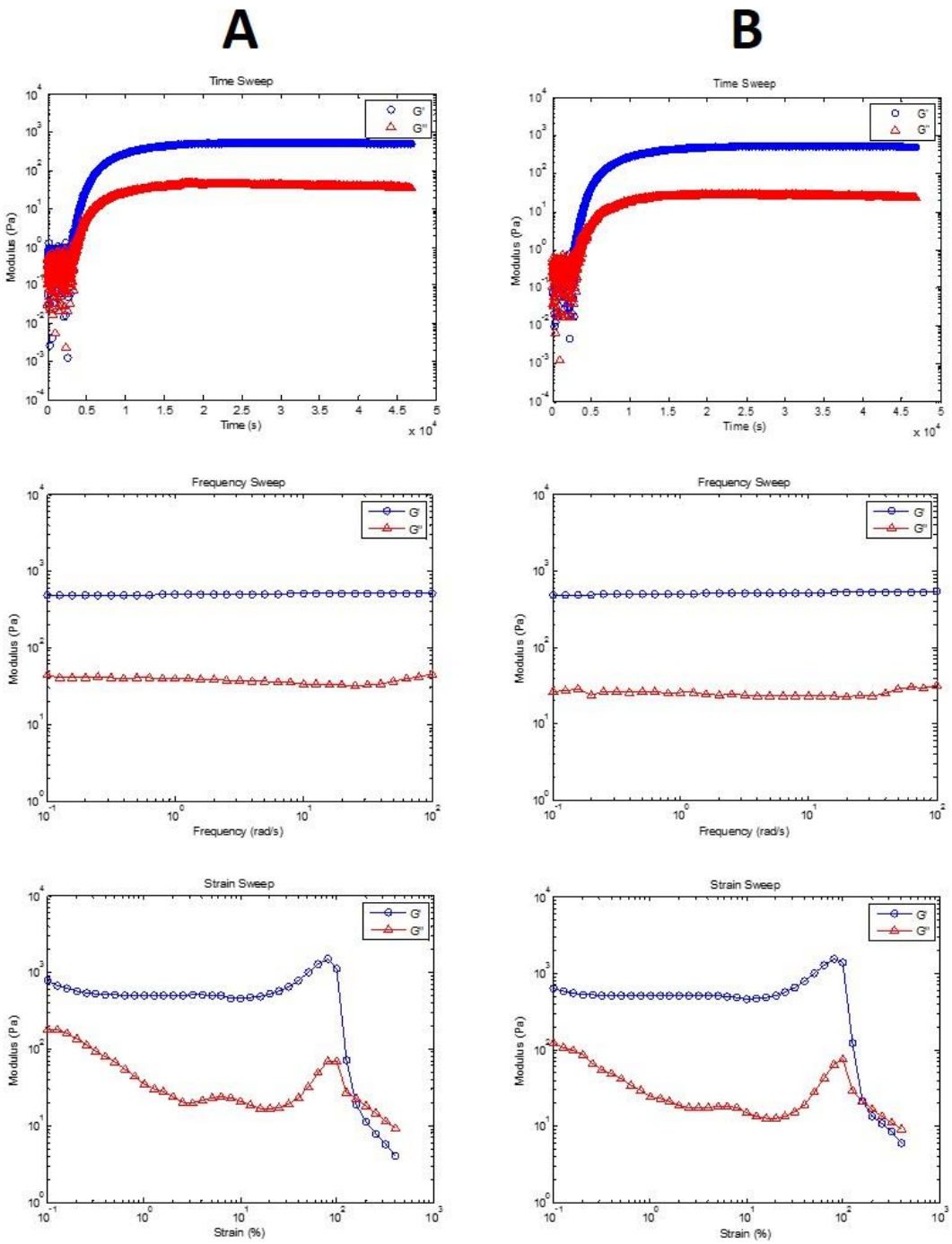

Figure A.19. Representative time (top), frequency (middle) and strain (bottom) sweeps for the LA-G12-0.7% (A) and LA-G12-5% (B) conditions.

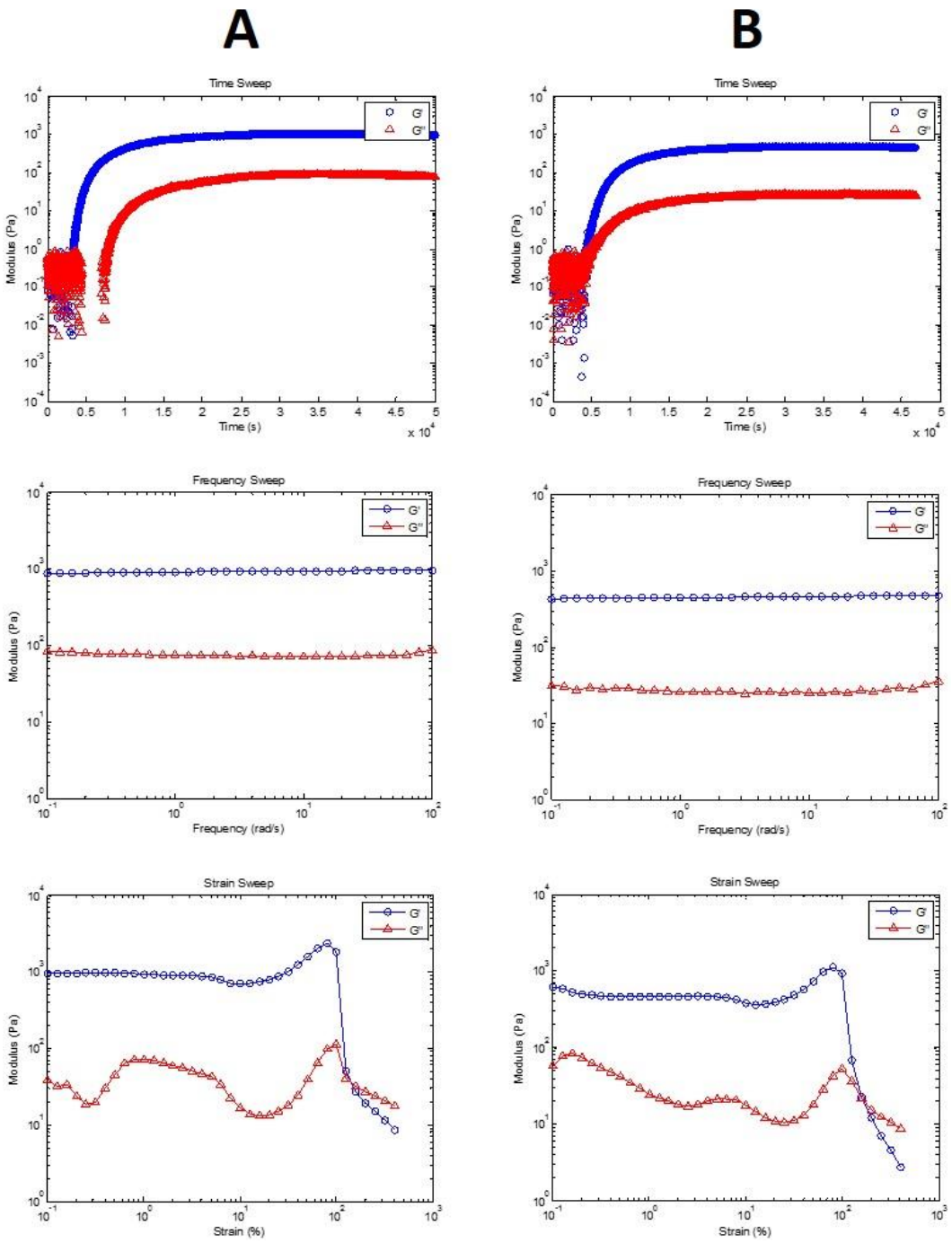

Figure A.20. Representative time (top), frequency (middle) and strain (bottom) sweeps for the LA-G1-0.7% (A) and LA-G1-5% (B) conditions.

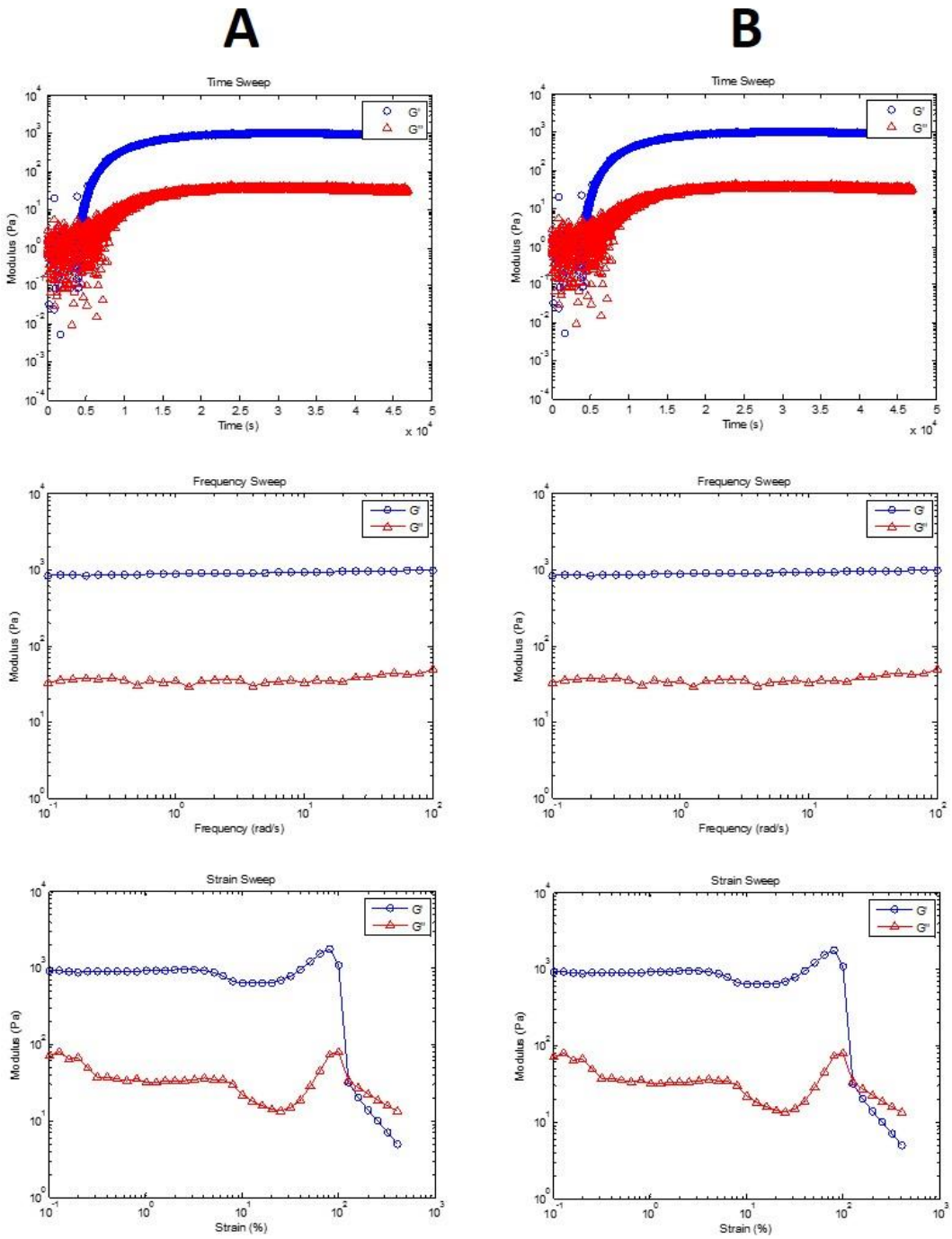

Figure A.21. Representative time (top), frequency (middle) and strain (bottom) sweeps for the unfunctionalized control (A) and HA-C (B) conditions.

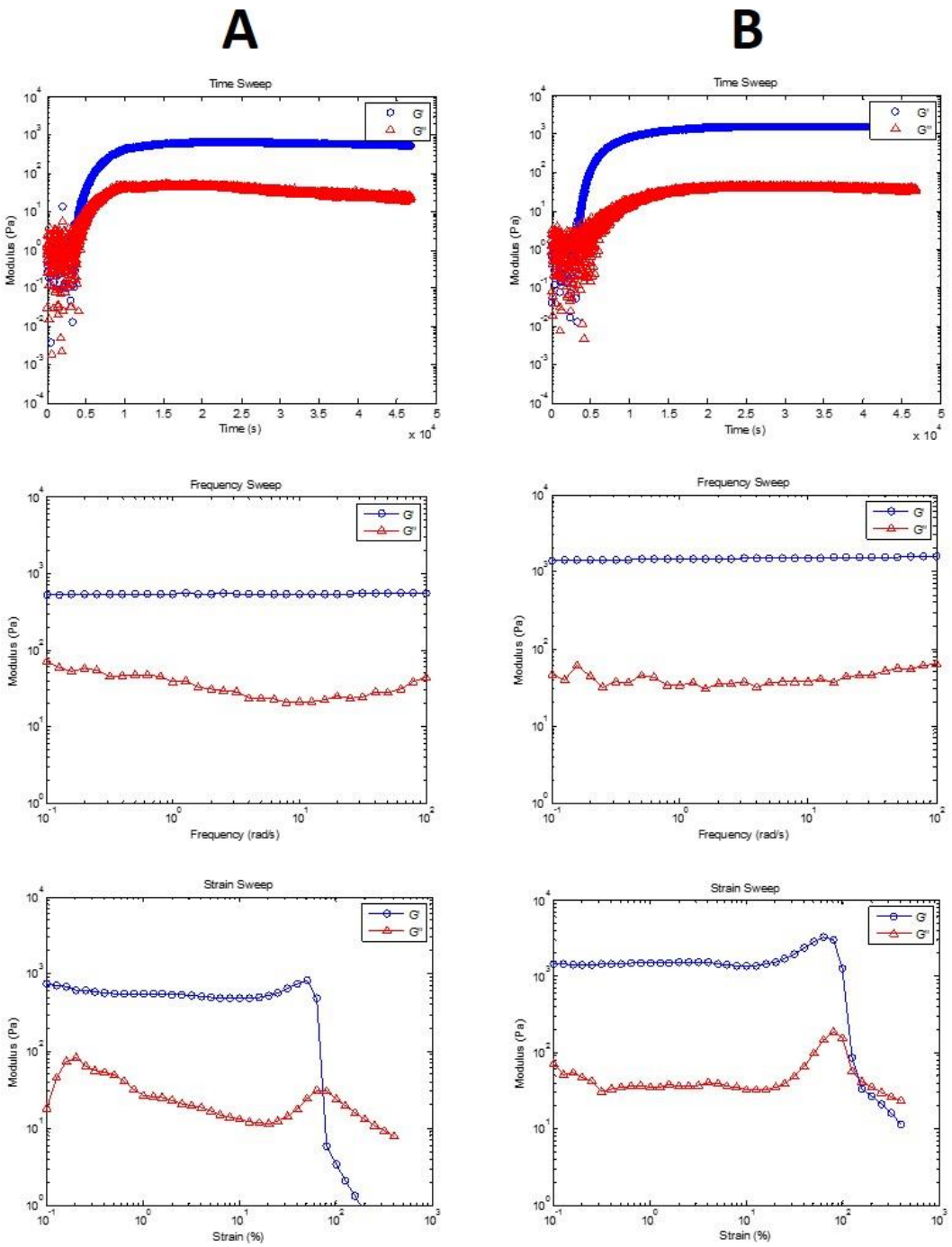

Figure A.22. Representative time (top), frequency (middle) and strain (bottom) sweeps for the LA-C (A) and LA-C-NHS (B) conditions.

References

1. Kuo, C. K. & Ma, P. X. Ionically crosslinked alginate hydrogels as scaffolds for tissue engineering: Part 1. Structure, gelation rate and mechanical properties. *Biomaterials* **22,** 511–521 (2001).

2. Even-Ram, S., Artym, V. & Yamada, K. M. Matrix Control of Stem Cell Fate. *Cell* **126,** 645–647 (2006).

3. Lee, K. Y. & Mooney, D. J. Alginate : properties and biomedical applications. *Prog. Polym. Sci.* **37,** 106–126 (2012).

4. Mehta, M., Madl, C. M., Lee, S., Duda, G. N. & Mooney, D. J. The collagen I mimetic peptide DGEA enhances an osteogenic phenotype in mesenchymal stem cells when presented from cell-encapsulating hydrogels. *J. Biomed. Mater. Res. Part A* n/a–n/a (2015). doi:10.1002/jbm.a.35497

5. Kurtz, A. & Oh, S.-J. Age related changes of the extracellular matrix and stem cell maintenance. *Prev. Med. (Baltim).* **54 Suppl,** S50–6 (2012).

6. Drury, J. L., Dennis, R. G. & Mooney, D. J. The tensile properties of alginate hydrogels. *Biomaterials* **25,** 3187–3199 (2004).

7. Sandvig, I. *et al.* RGD-peptide modified alginate by a chemoenzymatic strategy for tissue engineering applications. *J. Biomed. Mater. Res. - Part A* 896–906 (2014). doi:10.1002/jbm.a.35230

8. Maia, F. R., Fonseca, K. B., Rodrigues, G., Granja, P. L. & Barrias, C. C. Matrix-driven formation of mesenchymal stem cell–extracellular matrix microtissues on soft alginate hydrogels. *Acta Biomater.* **10,** 3197–3208 (2014).

9. Dhandayuthapani, B., Yoshida, Y., Maekawa, T. & Kumar, D. S. Polymeric Scaffolds in Tissue Engineering Application: A Review. *Int. J. Polym. Sci.* **20101,** 1–19 (2011).

10. Atala, A., Kasper, F. K. & Mikos, A. G. Engineering Complex Tissues. *Sci. Transl. Med.* **4,** 160rv12–160rv12 (2012).

11. Mannoor, M. S. *et al.* 3D printed bionic ears. *Nano Lett.* **13,** 2634–2639 (2013).

12. Altman, G. H. *et al.* Silk matrix for tissue engineered anterior cruciate ligaments. *Biomaterials* **23,** 4131–4141 (2002).

13. Seliktar, D. Designing Cell-Compatible Hydrogels for Biomedical Applications. **336,** 13–17 (2012).

14. Ma, Z., Kotaki, M., Inai, R. & Ramakrishna, S. Potential of nanofiber matrix as tissue-engineering scaffolds. *Tissue Eng.* **11,** 101–9 (2005).

15. Kim, B. & Mooney, D. J. Extracellular Matrices for Tissue Engineering. **16,** 373–378 (1998).

16. Engler, A. J., Sen, S., Sweeney, H. L. & Discher, D. E. Matrix Elasticity Directs Stem Cell Lineage Specification. *Cell* **126,** 677–689 (2006).

17. Langer, R. & Tirrell, D. A. Designing materials for biology and medicine. *Nature* **428,** 487–92 (2004).

18. Kuo, C. K. & Ma, P. X. Maintaining dimensions and mechanical properties of ionically crosslinked alginate hydrogel scaffoldsin vitro. *J. Biomed. Mater. Res. Part A* **84A,** 899–907 (2008).

19. Drury, J. L. & Mooney, D. J. Hydrogels for tissue engineering: Scaffold design variables and applications. *Biomaterials* **24,** 4337–4351 (2003).

20. Lutolf, M. P. & Hubbell, J. a. Synthetic biomaterials as instructive extracellular microenvironments for morphogenesis in tissue engineering. *Nat. Biotechnol.* **23,** 47–55 (2005).

21. Brandl, F., Sommer, F. & Goepferich, A. Rational design of hydrogels for tissue engineering: Impact of physical factors on cell behavior. *Biomaterials* **28,** 134–146 (2007).

22. Partlow, B. P. *et al.* Highly tunable silk biomaterials. *Adv. Funct. Mater.* **24,** 4615–4624 (2014).

23. Malafaya, P. B., Silva, G. A. & Reis, R. L. Natural-origin polymers as carriers and scaffolds for biomolecules and cell delivery in tissue engineering applications. *Adv. Drug Deliv. Rev.* **59,** 207–233 (2007).

24. S, K. V., D, B. K. & S, R. S. Natural Polymers – A Comprehensive Review. *Int. J. Res. Pharm. Biomed. Sci.* **3,** 1597–1613 (2012).

25. Barnes, C. P., Pemble, C. W., Brand, D. D., Simpson, D. G. & Bowlin, G. L. Cross-linking electrospun type II collagen tissue engineering scaffolds with carbodiimide in ethanol. *Tissue Eng.* **13,** 1593–605 (2007).

26. Place, E. S., George, J. H., Williams, C. K. & Stevens, M. M. Synthetic polymer scaffolds for tissue engineering. *Chem. Soc. Rev.* **38,** 1139–1151 (2009).

27. Gunatillake, P. A., Adhikari, R. & Gadegaard, N. Biodegradable synthetic polymers for tissue engineering. *Eur. Cells Mater.* **5,** 1–16 (2003).

28. Rezwan, K., Chen, Q. Z., Blaker, J. J. & Boccaccini, A. R. Biodegradable and bioactive porous polymer/inorganic composite scaffolds for bone tissue engineering. *Biomaterials* **27,** 3413–3431 (2006).

29. Frantz, C., Stewart, K. M. & Weaver, V. M. The extracellular matrix at a glance. *J. Cell Sci.* **123,** 4195–4200 (2010).

30. Singh, P., Carraher, C. & Schwarzbauer, J. E. Assembly of Fibronectin Extracellular Matrix. *Annu. Rev. Cell Dev. Biol.* **26,** 397–419 (2010).

31. Humphrey, J. D., Dufresne, E. R. & Schwartz, M. A. Mechanotransduction and extracellular matrix homeostasis. *Nat. Rev. Mol. Cell Biol.* **15,** 802–812 (2014).

32. Bonnans, C., Chou, J. & Werb, Z. Remodelling the extracellular matrix in development and disease. *Nat. Rev. Mol. Cell Biol.* **15,** 786–801 (2014).

33. Mouw, J. K., Ou, G. & Weaver, V. M. Extracellular matrix assembly: a multiscale deconstruction. *Nat. Rev. Mol. Cell Biol.* **15,** 771–785 (2014).

34. Gieni, R. S. & Hendzel, M. J. Mechanotransduction from the ECM to the genome: Are the pieces now in place? *J. Cell. Biochem.* **104,** 1964–1987 (2008).

35. Cox, T. R. & Erler, J. T. Remodeling and homeostasis of the extracellular matrix: implications for fibrotic diseases and cancer. *Dis. Model. Mech.* **4,** 165–78 (2011).

36. Hynes, R. O. & Naba, A. Overview of the matrisome-An inventory of extracellular matrix constituents and functions. *Cold Spring Harb. Perspect. Biol.* **4,** 1–16 (2012).

37. Ricard-Blum, S. The Collagen Family. *Cold Spring Harb. Perspect. Biol.* **3,** 1–19 (2011).

38. Fratzl, P. 1 Collagen: Structure and Mechanics, an Introduction 11. 1998–2000 (1998).

39. Karp, G. *Cell and Molecular Biology: Concepts and Experiments*. (Wiley, 2009).

40. Kielty, C. M. Elastic fibres in health and disease. *Expert Rev. Mol. Med.* **8,** 1–23 (2006).

41. Sophia Fox, A. J., Bedi, A. & Rodeo, S. A. The basic science of articular cartilage: structure, composition, and function. *Sports Health* **1,** 461–8 (2009).

42. Kim, S. H., Turnbull, J. & Guimond, S. Extracellular matrix and cell signalling: The dynamic cooperation of integrin, proteoglycan and growth factor receptor. *J. Endocrinol.* **209,** 139–151 (2011).

43. Glass, Z. A., Schiele, N. R. & Kuo, C. K. Informing tendon tissue engineering with embryonic development. *J. Biomech.* **47,** 1964–1968 (2014).

44. Wang, J. H. C., Guo, Q. & Li, B. Tendon biomechanics and mechanobiology - A minireview of basic concepts and recent advancements. *J. Hand Ther.* **25,** 133–141 (2012).

45. Hockaday, L. A., Saeger, M. D., Karanja, F. W. & Kuo, C. K. *Mechanobiology of Embryonic and Adult Tendons*. *Tendon Regeneration* (Elsevier Inc., 2015). doi:10.1016/B978-0-12-801590-2.00003-X

46. Schiele, N. R., Marturano, J. E. & Kuo, C. K. Mechanical factors in embryonic tendon development: potential cues for stem cell tenogenesis. *Curr. Opin. Biotechnol.* **24,** 834–40 (2013).

47. Ruoslahti, E. Brain extracellular matrix. *Glycobiology* **6,** 489–492 (1996).

48. Silver, F. H., Freeman, J. W. & Seehra, G. P. Collagen self-assembly and the development of tendon mechanical properties. *J. Biomech.* **36,** 1529–1553 (2003).

49. Pankov, R. & Yamada, K. M. Fibronectin at a glance. *J. Cell Sci.* **115,** 3861–3863 (2002).

50. Schwarzbauer, J. E. & DeSimone, D. W. Fibronectins, their fibrillogenesis, and in vivo functions. *Cold Spring Harb. Perspect. Biol.* **3,** 1–19 (2011).

51. Muro, a F. *et al.* Regulation of fibronectin EDA exon alternative splicing: possible role of RNA secondary structure for enhancer display. *Mol. Cell. Biol.* **19,** 2657–2671 (1999).

52. Pierschbacher, M. D. & Ruoslahti, E. Cell attachment activity of fibronectin can be duplicated by small synthetic fragments of the molecule. *Nature* **309,** 30–33 (1984).

53. Barczyk, M., Carracedo, S. & Gullberg, D. Integrins. *Cell Tissue Res.* **339,** 269–280 (2010).

54. Ruoslahti, E. Rgd and Other Recognition Sequences for Integrins. *Annu. Rev. Cell Dev. Biol* **12,** 697–715 (1996).

55. Schaffner, P. & Dard, M. M. Structure and function of RGD peptides involved in bone biology. *Cell. Mol. Life Sci.* **60,** 119–132 (2003).

56. Boudreau, N. J. & Jones, P. L. Extracellular matrix and integrin signalling: the shape of things to come. *Biochem. J.* **339 (Pt 3,** 481–488 (1999).

57. Li, R., Hoess, R. H., Bennett, J. S. & DeGrado, W. F. Use of phage display to probe the evolution of binding specificity and affinity in integrins. *Protein Eng.* **16,** 65–72 (2003).

58. Bellis, S. L. Advantages of RGD peptides for directing cell association with biomaterials. *Biomaterials* **32,** 4205–10 (2011).

59. Cavalcanti-Adam, E. A., Aydin, D., Hirschfeld-Warneken, V. C. & Spatz, J. P. Cell adhesion and response to synthetic nanopatterned environments by steering receptor clustering and spatial location. *HFSP J.* **2,** 276–85 (2008).

60. Lee, K. Y. *et al.* Nanoscale Adhesion Ligand Organization Regulates Osteoblast Proliferation and Differentiation. *Nano Lett.* **4,** 1501–1506 (2004).

61. Rowley, J. A. & Mooney, D. J. Alginate type and RGD density control myoblast phenotype. *J. Biomed. Mater. Res.* **60,** 217–223 (2002).

62. Bae, M.-S., Lee, K. Y., Park, Y. J. & Mooney, D. J. RGD Island Spacing Controls Phenotype of Primary Human Fibroblasts Adhered to Ligand-Organized Hydrogels. *Macromol. Res.* **15,** 469–472 (2007).

63. Park, K.-H. *et al.* Synthesis of Arg-Gly-Asp (RGD) sequence conjugated thermo-reversible gel via the PEG spacer arm as an extracellular matrix for a pheochromocytoma cell (PC12) culture. *Biosci. Biotechnol. Biochem.* **68,** 2224–9 (2004).

64. Lee, J. W. J. J. W. *et al.* The effect of spacer arm length of an adhesion ligand coupled to an alginate gel on the control of fibroblast phenotype. *Biomaterials* **31,** 5545–5551 (2010).

65. Hern, D. L. & Hubbell, J. a. Incorporation of adhesion peptides into nonadhesive hydrogels useful for tissue resurfacing. *J. Biomed. Mater. Res.* **39,** 266–276 (1998).

66. Dhoot, N. O., Tobias, C. a, Fischer, I. & Wheatley, M. a. Peptide-modified alginate surfaces as a growth permissive substrate for neurite outgrowth. *J. Biomed. Mater. Res. A* **71,** 191–200 (2004).

67. Guo, L. *et al.* Promotion of microvasculature formation in alginate composite hydrogels by an immobilized peptide GYIGSRG. *Sci. China Chem.* **55,** 1781–1787 (2012).

68. Hennessy, K. M. *et al.* The effect of collagen I mimetic peptides on mesenchymal stem cell adhesion and differentiation, and on bone formation at hydroxyapatite surfaces. *Biomaterials* **30,** 1898–1909 (2009).

69. Yamada, K. M. Adhesive recognition sequences. *J. Biol. Chem.* **266,** 12809–12812 (1991).

70. Pawar, S. N. & Edgar, K. J. Alginate derivatization: A review of chemistry, properties and applications. *Biomaterials* **33,** 3279–3305 (2012).

71. Rowley, J. A., Madlambayan, G. & Mooney, D. J. Alginate hydrogels as synthetic extracellular matrix materials. *Biomaterials* **20,** 45–53 (1999).

72. Smidsrod, O. & Skjåk-Bræk, G. Alginate as immobilization matrix for cells. *Trends Biotechnol.* **8,** 71–78 (1990).

73. Standard Guide for Characterization and Testing of Alginates as Starting Materials Intended for Use in Biomedical and Tissue- Engineered Medical Product Applications. *Astm* 1–8 (2014). doi:10.1520/F2103-01R07E02.materials.

74. Donati, I., Draget, K. I., Borgogna, M., Paoletti, S. & Skjäk-Bræk, G. Tailor-made alginate bearing galactose moieties on mannuronic residues: Selective modification achieved by a chemoenzymatic strategy. *Biomacromolecules* **6,** 88–98 (2005).

75. Mørch, Y. a, Donati, I., Strand, B. L. & Skjåk-Braek, G. Molecular engineering as an approach to design new functional properties of alginate. *Biomacromolecules* **8,** 2809–14 (2007).

76. Mørch, Ý. A., Holtan, S., Donati, I., Strand, B. L. & Skjåk-Bræk, G. Mechanical properties of C-5 epimerized alginates. *Biomacromolecules* **9,** 2360–2368 (2008).

77. Rokstad, A. M. *et al.* Cell-compatible covalently reinforced beads obtained from a chemoenzymatically engineered alginate. *Biomaterials* **27,** 4726–4737 (2006).

78. Mørch, Ý. A. Novel alginate microcapsules for cell therapy. (Norweigian University of Science and Technology, 2008).

79. Drury, J. L., Boontheekul, T. & Mooney, D. J. Cellular cross-linking of peptide modified hydrogels. *J. Biomech. Eng.* **127,** 220–228 (2005).

80. Yen, C. N. *et al.* Use of porous alginate sponges for substantial chondrocyte expansion and matrix production: Effects of seeding density. *Biotechnol. Prog.* **24,** 452–457 (2008).

81. Qian, Z. *et al.* Chitosan-alginate sponge: Preparation and application in curcumin delivery for dermal wound healing in rat. *J. Biomed. Biotechnol.* **2009,** (2009).

82. Kong, H. J., Hsiong, S. & Mooney, D. J. Nanoscale cell adhesion ligand presentation regulates nonviral gene delivery and expression. *Nano Lett.* **7,** 161–166 (2007).

83. Bonino, C. a., Samorezov, J. E., Jeon, O., Alsberg, E. & Khan, S. a. Real-time in situ rheology of alginate hydrogel photocrosslinking. *Soft Matter* **7,** 11510 (2011).

84. Lawrie, G. *et al.* Interactions between alginate and chitosan biopolymers characterized using FTIR and XPS. *Biomacromolecules* **8,** 2533–2541 (2007).

85. Li, P., Dai, Y., Zhang, J., Wang, A. & Wei, Q. Chitosan-Alginate Nanoparticles as a Novel Drug Delivery System for Nifedipine. *Int. J. Biomed. Sci.* **4,** 221–228 (2008).

86. Jensen, H. M., Larsen, F. H. & Engelsen, S. B. in *Natural Products From Marine Algae: Methods and Protocols* **1308,** 347–363 (2015).

87. Standard Test Method for Determining the Chemical Composition and Sequence in Alginate by Proton Nuclear Magnetic Resonance (1 H NMR). *Astm* **10,** 1–5 (2012).

88. Santi, C. *et al.* NMR Analysis of Non Hydrolyzed Samples of Sodium Alginate. *12th Int. Electron. Conf. Synth. Org. Chem.* 1–5 (2008). at <http://www.usc.es/congresos/ecsoc/12/hall_f_PSC/f1002/f1002.pdf>

89. Grasdalen, H., Larsen, B. & Smidsrod, O. A P.M.R. Study of the Composition and Sequence of Uronate Residues in Alginates. *Carbohydr. Res.* **68,** 23–31 (1979).

90. Grasdalen, H. High-field, 1H NMR spectroscopy of alginate sequential structure and linkage conformations. *Carbohydr. Res.* **118,** 255–260 (1983).

91. Lu, J. *et al.* Impact of hydrolysis conditions on the detection of mannuronic to guluronic acid ratio in alginate and its derivatives. *Carbohydr. Polym.* **122,** 180–8 (2015).

92. Donati, I. *et al.* Galactose-substituted alginate: Preliminary characterization and study of gelling properties. *Biomacromolecules* **4,** 624–631 (2003).

93. Montanucci, P. *et al.* Insights in Behavior of Variably Formulated Alginate-Based Microcapsules for Cell Transplantation. **2015,** (2014).

94. Comaposada, J., Gou, P., Marcos, B. & Arnau, J. Physical properties of sodium alginate solutions and edible wet calcium alginate coatings. *LWT - Food Sci. Technol.* **64,** 212–219 (2015).

95. Fonseca, K. B. *et al.* Enzymatic, physicochemical and biological properties of MMP-sensitive alginate hydrogels. *Soft Matter* **9,** 3283 (2013).

96. Fonseca, K. B., Bidarra, S. J., Oliveira, M. J., Granja, P. L. & Barrias, C. C. Molecularly designed alginate hydrogels susceptible to local proteolysis as three-dimensional cellular microenvironments. *Acta Biomater.* **7,** 1674–1682 (2011).

97. Ingar Draget, K., Ostgaard, K. & Smidsrod, O. Homogeneous alginate gels: A technical approach. *Carbohydr. Polym.* **14,** 159–178 (1990).

98. Draget, K. I., Ostgaard, K. & Smidsrød, O. Alginate-based solid media for plant tissue culture. *Appl. Microbiol. Biotechnol.* **31,** 79–83 (1989).

99. Bouhadir, K. H. *et al.* Degradation of partially oxidized alginate and its potential application for tissue engineering. *Biotechnol. Prog.* **17,** 945–950 (2001).

100. Boontheekul, T., Kong, H. J. & Mooney, D. J. Controlling alginate gel degradation utilizing partial oxidation and bimodal molecular weight distribution. *Biomaterials* **26,** 2455–2465 (2005).

101. Zhang, G. Evaluating the viscoelastic properties of biological tissues in a new way. *J. Musculoskelet. Neuronal Interact.* **5,** 85–90 (2005).

102. Choi, B. *et al. Introduction to In Situ Forming Hydrogels for Biomedical Applications*. *Series in BioEngineering* (2015). doi:10.1007/978-981-287-152-7

103. Kavanagh, G. M. & Ross-Murphy, S. B. Rheological characterization of polymer gels. *Prog. Polym. Sci.* **23,** 533–562 (1998).

104. Ross-Murphy, S. B. Rheological characterization of polymer gels and networks. *Polym. Gels Networks* **2,** 229–237 (1994).

105. Ahearne, M., Yang, Y., El Haj, A. J., Then, K. Y. & Liu, K.-K. Characterizing the viscoelastic properties of thin hydrogel-based constructs for tissue engineering applications. *J. R. Soc. Interface* **2,** 455–63 (2005).

106. Pierce Premium Grade Sulfo-NHS.

107. McDonagh, B. H. Optimalised Carbodiimide Chemistry for RGD-coupled Alginate. (Norwegian University of Science and Technology, 2012).

108. Nakajima, N. & Ikada, Y. Mechanism of amide formation by carbodiimide for bioconjugation in aqueous media. *Bioconjug. Chem.* **6,** 123–130 (1995).

109. Iwasawa, T., Wash, P., Gibson, C. & Rebek Jr., J. Reaction of an Introverted Carboxylic Acid with Carbodiimide. *Tetrehedron* **63,** 6506–6511 (2007).

110. Grabarek, Z. & Gergely, J. Zero-length crosslinking procedure with the use of active esters. *Anal. Biochem.* **185,** 131–135 (1990).

111. Sehgal, D. & Vijay, I. K. A method for the high efficiency of water-soluble carbodiimide-mediated amidation. *Analytical biochemistry* **218,** 87–91 (1994).

112. Montalbetti, C. A. G. N. & Falque, V. Amide bond formation and peptide coupling. *Tetrahedron* **61,** 10827–10852 (2005).

113. Massia, S. P. & Hubbell, J. A. An RGD spacing of 440 nm is sufficient for integrin alpha v beta 3-mediated fibroblast spreading and 140 nm for focal contact and stress fiber formation. *J. Cell Biol.* **114,** 1089–1100 (1991).

114. Masuelli, M. A., Membranas, L. De, Aplicada, I. D. F., Química, F. De & Farmacia, B. Mark-Houwink Parameters for Aqueous-Soluble Polymers and Biopolymers at Various Temperatures. *J. Polym. Biopolym. Phys. Chem.* **2,** 37–43 (2014).

115. Polyak, B., Geresh, S. & Marks, R. S. Synthesis and characterization of a Biotin-Alginate Conjugate and Its Application in a Biosensor Construction. *Biomacromolecules* **5,** 389–396 (2004).

116. Bharti, S. K. & Roy, R. Quantitative 1H NMR spectroscopy. *TrAC Trends Anal. Chem.* **35,** 5–26 (2012).

117. Malz, F. & Jancke, H. Validation of quantitative NMR. *J. Pharm. Biomed. Anal.* **38,** 813–23 (2005).

118. Pauli, G. F., Jaki, B. U. & Lankin, D. C. Quantitative 1H NMR: Development and Potential of a Method for Natural Products Analysis. *J. Nat. Prod.* **68,** 133–149 (2005).

119. Dalheim, M. *et al.* Efficient functionalization of alginate biomaterials. *Biomaterials* **80,** 146–156 (2016).

120. Desai, R. M., Koshy, S. T., Hilderbrand, S. A., Mooney, D. J. & Joshi, N. S. Versatile click alginate hydrogels crosslinked via tetrazine-norbornene chemistry. *Biomaterials* **50,** 30–37 (2015).

121. Jeon, O., Bouhadir, K. H., Mansour, J. M. & Alsberg, E. Photocrosslinked alginate hydrogels with tunable biodegradation rates and mechanical properties. *Biomaterials* **30,** 2724–2734 (2009).

122. Jeon, O., Alt, D. S., Ahmed, S. M. & Alsberg, E. The effect of oxidation on the degradation of photocrosslinkable alginate hydrogels. *Biomaterials* **33,** 3503–3514 (2012).

123. Jeon, O., Powell, C., Solorio, L. D., Krebs, M. D. & Alsberg, E. Affinity-based growth factor delivery using biodegradable, photocrosslinked heparin-alginate hydrogels. *J. Control. Release* **154,** 258–266 (2011).

124. Jeon, O., Powell, C., Ahmed, S. M. & Alsberg, E. Biodegradable, photocrosslinked alginate hydrogels with independently tailorable physical properties and cell adhesivity. *Tissue Eng. Part A* **16,** 2915–2925 (2010).

125. McMEEKIN, T. L., Groves, M. L. & Hipp, N. J. Refractive Indices of Amino Acids, Proteins, and Related Substances. **44,** 54–66 (1964).

126. Grasdalen, H., Larsen, B. & Smisrod, O. 13C-n.m.r. studies of monomeric composition and sequence in alginate. *Carbohydr. Res.* **89,** 179–191 (1981).

127. Mickos, H., Bahr, J. & Luning, B. The Three-Dimensional Structure of the RGD Adhesion Sequence of Fibronectin; NMR Studies of the Peptides RGDS and GRDSP. *Acta Chem. Scand.* **44,** 161–164 (1990).

128. Szpakowska, M. & Czaplicka, I. Spectrophotometric Investigations of Nitrobenzene Liquid Membrane Oscillator with Hexadecyltrimethylammonium Bromide. *Ars Separatoria Acta* **2,** 64–70 (2003).

129. Creighton, T. E. *Proteins: Structures and Molecular Properties*. (W. H. Freeman, 1993).

130. Young, R. J. & Lovell, P. A. *Introduction to Polymers, Third Edition*. (CRC Press, 2011).

131. Sam, S. *et al.* Semiquantitative study of the EDC/NHS activation of acid terminal groups at modified porous silicon surfaces. *Langmuir* **26,** 809–814 (2010).

132. Kakkar, R. in *Hydroxamic Acids: A Unique Family of Chemicals with Multiple Biological Activities* 19–53 (2013). doi:10.1007/978-3-642-38111-9

133. Fernández Farrés, I. & Norton, I. T. Formation kinetics and rheology of alginate fluid gels produced by in-situ calcium release. *Food Hydrocoll.* **40,** 76–84 (2014).

134. Jaspers, M. *et al.* Ultra-responsive soft matter from strain-stiffening hydrogels. *Nat. Commun.* **5,** 5808 (2014).

135. Marmion, C. J., Parker, J. P. & Nolan, K. B. *Hydroxamic Acids: An Important Class of Metalloenzyme Inhibitors*. *Comprehensive Inorganic Chemistry II (Second Edition): From Elements to Applications* **3,** (Elsevier Ltd., 2013).

136. Sartori, C., Finch, D. S., Ralph, B. & Gilding, K. Determination of the cation content of alginate thin films by FTi.r. spectroscopy. *Polymer (Guildf).* **38,** 43–51 (1997).

137. Papageorgiou, S. K. *et al.* Metal-carboxylate interactions in metal-alginate complexes studied with FTIR spectroscopy. *Carbohydr. Res.* **345,** 469–473 (2010).

138. Marturano, J. E., Arena, J. D., Schiller, Z. a, Georgakoudi, I. & Kuo, C. K. Characterization of mechanical and biochemical properties of developing embryonic tendon. *Proc. Natl. Acad. Sci. U. S. A.* **110,** 6370–6375 (2013).

139. Sałdyka, M. & Mielke, Z. Infrared Matrix Isolation Studies and Ab Initio Calculations of Formhydroxamic Acid. *J. Phys. Chem. A* **106,** 3714–3721 (2002).

140. Raut, N. S., Deshmukh, P. R., Umekar, M. J. & Kotagale, N. R. Zinc cross-linked hydroxamated alginates for pulsed drug release. *Int. J. Pharm. Investig.* **3,** 194–202 (2013).

141. Ahmad, Z. *et al.* Effect of 1-ethyl-3-(3-dimethylaminopropyl) carbodiimide and N-hydroxysuccinimide concentrations on the mechanical and biological characteristics of cross-linked collagen fibres for tendon repair. *Regen. Biomater.* **2,** 77–85 (2015).

142. Campos-Vallette, M. M. *et al.* Characterization of sodium alginate and its block fractions by surface-enhanced Raman spectroscopy. *J. Raman Spectrosc.* **41,** 758–763 (2010).